Universidade do Minho
Escola de Engenharia

Sílvia Clara Mesquita da Silva Reis

Development and characterization of sensors fabricated from polymer based magnetoelectric nanocomposites

março de 2017

UMinho | 2017

Sílvia Clara Mesquita da Silva Reis **Development and characterization of sensors fabricated from polymer based magnetoelectric nanocomposites**

Universidade do Minho
Escola de Engenharia

Sílvia Clara Mesquita da Silva Reis

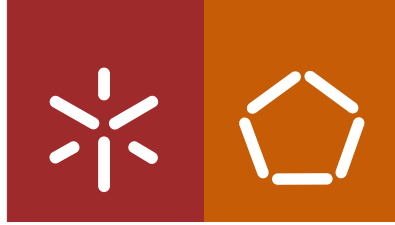# Development and characterization of sensors fabricated from polymer based magnetoelectric nanocomposites

Tese de Doutoramento em Engenharia Electrónica
e de Computadores

Trabalho realizado sob a orientação do
Professor Doutor José Gerardo Rocha
do
Professor Doutor Senentxu Lanceros-Mendez
e do
Doutor Pedro Martins

março de 2017

DECLARAÇÃO

Nome: Sílvia Clara Mesquita da Silva Reis

Endereço electrónico: silvinha_reis@hotmail.com

Título tese: Development and characterization of sensors fabricated from polymer based magnetoelectric nanocomposites

Orientadores: Professor Doutor José Gerardo Rocha, Professor Doutor Senentxu Lanceros-Mendez e Doutor Pedro Martins

Ano de conclusão: 2017

Designação do Doutoramento: Programa Doutoral em Engenharia Electrónica e de Computadores

Universidade do Minho, 29 / 03 / 2017

Assinatura: _Silva Clara Mesquita da Silva Reis_

STATEMENT OF INTEGRITY

I hereby declare having conducted my thesis with integrity. I confirm that I have not used plagiarism or any form of falsification of results in the process of the thesis elaboration.

I further declare that I have fully acknowledged the Code of Ethical Conduct of the University of Minho.

University of Minho, _29. 03. 2017_____

Full name: _Sílvia Clara Mesquita da Silva Reis_____

Signature: _Sílvia Clara Mesquita da Silva Reis_____

To Leonor and Clara

Acknowledgments

To Professor Gerardo, my supervisor, I would like to express my gratitude for encouraging me to continue my academic career, for all friendship and support he always gave me. To Professor Senentxu, my co-supervisor, is difficult to say in words how much I thank you, for all the courage you always gave me to never give up, for the opportunity to work in this fantastic group, for everything I learn from you – the scientific knowledge, the work methodology, how to be a leader – and mainly for your friendship. To Doctor Pedro Martins, my co-supervisor, for all the friendship, advices and support during this journey.

I wish to extend my thanks to Professor José Manuel Barandiarán, Professor Jon Gutierrez, Andoni and Iñaki for the kind reception and the great time I have experienced during my stay in Basque Country University.

To my friends of the Electroactive Smart Materials group I would like to thank all the good times we spent together, all the friendship and mutual aid. To the Magnetoelectric group thanks for all the help, effort and support. My friends Marco, Pedro, Nelson and Renato thanks for all our meetings and pleasant discussions. Without you, none of this would have been possible. I wish to extend my thanks to Vítor Correia for all the support and friendship.

To my family for the love that you always gave me. A very special thanks to my parents for everything that you have done and continuing doing for me, for the unconditional love, support and motivation you always gave to me.

Lastly, but most important, I wish to thank to João, for your love, courage, advices, unconditional support, for being present at good and difficult times and for all the help in this journey, and to my little ones, Leonor and Clara, for encouraging me to be a better person, for all the joy that comes with every smile and even for every night without sleep.

Abstract

Sensors are increasingly used in many applications areas, integrated in structures, industrial machinery, or in the environment, contributing to improve the society level of well-being. It is expected that sensorization will play on of the most relevant roles in the fourth industrial revolution, and allow, together with mechanization and informatization, a full automation. Particularly, magnetic sensors allow measurements, without physical contact, of parameters such as direction, presence, rotation, angle, or current, in addition to magnetic field. In this way, for most applications, such sensors offer a safe, non-invasive and non-destructive measurement, as well as provide a reliable and almost maintenance-free technology.

Industry demands for smaller, cheaper and low-powered magnetic sensors, motivating the exploration of new materials and different technologies, such as polymer-based magnetoelectric (ME) composites. These composites are flexible, versatile, lightweight, low cost, easy to model in complicated shapes, and typically involve a low-temperature fabrication process, being in this way, a solution for innovative magnetic sensor device applications. Therefore, the main objective of this thesis is the development of polymer-based ME sensors to be incorporated into technological devices.

Thus, the ME effect is increasingly being considered an attractive alternative for magnetic field and current sensing, being able to sense static and dynamic magnetic fields.

In order to obtain a wide-range ME response, a nanocomposite of $Tb_{0.3}Dy_{0.7}Fe_{1.92}$ (Terfenol-D)/$CoFe_2O_4$/poly(vinylidene fluoride-trifluoroethylene) (P(VDF-TrFE)) was produced and their morphological, piezoelectric, magnetic and magnetoelectric properties investigated. The obtained composites reveals a high piezoelectric response ($\approx$-18 pC$\cdot$N^{-1}) that is independent of the weight ratio between the fillers. In turn, the magnetic properties of the composites are influenced by the composite composition. It was found that the magnetization saturation values decrease with increasing $CoFe_2O_4$ content (from 18.5 to 13.3 emu$\cdot$g^{-1}) while the magnetization and coercive field values increase (from 3.7 to 5.5 emu$\cdot$g^{-1} and from 355.7 to 1225.2 Oe, respectively) with increasing $CoFe_2O_4$ content. Additionally, the films show a wide-range dual-peak ME response at room temperature with the ME coefficient increasing with increasing weight content of Terfenol-D, from 18.6 mV$\cdot$cm$^{-1}\cdot$Oe^{-1} to 42.3 mV$\cdot$cm$^{-1}\cdot$Oe^{-1}.

The anisotropic ME effect on a $Fe_{61.6}Co_{16.4}Si_{10.8}B_{11.2}$ (FCSB)/poly(vinylidene fluoride) (PVDF)/FCSB laminate composite has been used for the development of a

magnetic field sensor able to detect both magnitude and direction of ac and dc magnetic fields. The accuracy (99% for both ac and dc sensors), linearity (92% for the dc sensor and 99% for the ac sensor), sensitivity (15 and 1400 mV·Oe^{-1} for the dc and ac fields, respectively), and reproducibility (99% for both sensors) indicate the suitability of the sensor for applications.

A dc magnetic field sensor based on a PVDF/Metglas composite and the corresponding readout electronic circuits for processing the output ME voltage were developed. The ME sensing composite presents an electromechanical resonance frequency close to 25.4 kHz, a linear response (r^2=0.997) in the 0–2 Oe dc magnetic field range, and a maximum output voltage of 112 mV (ME voltage coefficient α_{33} of ≈30 V·cm^{-1}·Oe^{-1}). By incorporating a charge amplifier, an ac–rms converter and a microcontroller with an on chip analog-to-digital converter (ADC), the ME voltage response is not distorted, the linearity is maintained, and the ME output voltage increases to 3.3 V ($\alpha_{33effective}$=1000 V·cm^{-1}·Oe^{-1}). The sensing device, including the readout electronics, has a maximum drift of 0.12 Oe with an average total drift of 0.04 Oe, a sensitivity of 1.5 V·Oe^{-1} (15 kV·T^{-1}), and a 70 nT resolution. Such properties allied to the accurate measurement of the dc magnetic field in the 0–2 Oe range makes this polymer-based device very attractive for applications, such as Earth magnetic field sensing, digital compasses, navigation, and magnetic field anomaly detectors.

A dc current sensor device based on a ME PVDF/Metglas composite, a solenoid, and the corresponding electronic instrumentation were developed. The ME sample exhibits a maximum α_{33} of 34.48V·cm^{-1}·Oe^{-1}, a linear response (r^2=0.998) and a sensitivity of 6.7 mV·A^{-1}. With the incorporation of a charge amplifier, a precision ac/dc converter and a microcontroller, the linearity is maintained (r^2=0.997), the ME output voltage increases to a maximum of 2320 mV and the sensitivity is increased to 476.5 mV·A^{-1}. Such features indicate that the fabricated ME sensing device is suitable to be used in non-contact electric current measurement, motor operational status checking, and condition monitoring of rechargeable batteries, among others.

In this way, polymer-based ME composites proved to be suitable for magnetic field and current sensor applications.

Resumo

Os sensores estão a ser cada vez mais utilizados em diversas áreas, integrados em estruturas, máquinas industriais ou projetos ambientais, contribuindo para melhorar o nível de bem-estar e eficiência da nossa sociedade. Espera-se que a "sensorização" contribua decisivamente para a quarta revolução industrial, e que permita, em conjunto com a mecanização e a informatização, uma completa automação. Em particular, os sensores magnéticos permitem medir parâmetros como a direção, presença, rotação, ângulo ou corrente, para além do campo magnético, tudo isto sem qualquer contacto físico. Assim, para a maioria das aplicações, estes sensores oferecem uma medição segura, não invasiva e não destrutiva, para além de garantirem uma tecnologia confiável e de escassa manutenção.

A indústria procura e exige sensores magnéticos mais pequenos, mais baratos e de baixo consumo, daí a motivação para explorar novos materiais e diferentes tecnologias, tais como os compósitos magnetoelétricos (ME) baseados em polímeros. Estes compósitos são flexíveis, versáteis, leves, de baixo custo, fáceis de se modelar em formas complexas e tipicamente envolvem um processo de fabricação a baixa temperatura, constituindo uma solução fiável e de qualidade para os sensores magnéticos. É da constatação deste potencial que surge este estudo e o objetivo desta tese: o desenvolvimento de sensores ME de base polimérica.

O efeito ME é cada vez mais considerado como uma alternativa credível para a medição de campo magnético e da intensidade da corrente elétrica, podendo detetar campos magnéticos estáticos e dinâmicos.

De modo a obter uma gama mais alargada de resposta ME, produziram-se nanocompósitos de $Tb_{0.3}Dy_{0.7}Fe_{1.92}$ (Terfenol-D)/$CoFe_2O_4$/poli(fluoreto de vinilideno trifluor-etileno) (P(VDF-TrFE) e as suas propriedades morfológicas, piezoelétricas, magnéticas e magnetoelétricas foram investigadas. Os compósitos obtidos revelam uma elevada resposta piezoelétrica ($\approx$-18 pC$\cdot$N^{-1}) que é independente da percentagem de cada material magnetoestrictivo. Por sua vez, as propriedades magnéticas são influenciadas pela composição dos compósitos. Verificou-se que a magnetização de saturação diminuí com o aumento da percentagem de $CoFe_2O_4$ (de 18.5 para 13.3 emu$\cdot$g^{-1}) enquanto que a magnetização e o campo coercivo aumentam (de 3.7 para 5.5 emu$\cdot$g^{-1} e de 355.7 para 1225.2 Oe, respetivamente) com o aumento da percentagem em massa de $CoFe_2O_4$.

O efeito ME anisotrópico num compósito $Fe_{61.6}Co_{16.4}Si_{10.8}B_{11.2}$ (FCSB)/ poli(fluoreto de vinilideno) (PVDF)/FCSB laminado foi utilizado para desenvolver um sensor de campo magnético capaz de detetar tanto a magnitude como a direção de campos magnéticos ac e dc. A exatidão (99% para ambos os sensores ac e dc), linearidade (92% para o sensor dc e 99% para o ac), sensibilidade (15 e 1400 mV·Oe^{-1} para o sensor dc e ac, respetivamente) e reprodutibilidade (99% para ambos os sensores) indicam a aptidão destes sensores para aplicações avançadas.

Desenvolveu-se ainda um sensor de campo magnético dc baseado num compósito ME de PVDF/Metglas, bem como a correspondente eletrónica de leitura para processar a tensão de saída ME. O compósito ME apresenta uma ressonância eletromecânica de aproximadamente 25.4 kHz, uma resposta linear (r^2=0.997) para uma gama de campos magnéticos dc entre 0–2 Oe e uma tensão de saída máxima de 112 mV (coeficiente ME $\alpha_{33}\approx30$ V·cm^{-1}·Oe^{-1}). Ao incorporar um amplificador de carga, um conversor ac–rms e um microcontrolador com um conversor analógico-digital (ADC), a tensão ME não é distorcida, a linearidade manteve-se e a tensão ME aumentou para 3.3 V ($\alpha_{33efectivo}$=1000 V·cm^{-1}·Oe^{-1}). O sensor, incluindo a eletrónica de leitura, obteve um desvio máximo de 0.12 Oe com um desvio total médio de 0.04 Oe, uma sensibilidade de 1.5 V·Oe^{-1} (15 kV·T^{-1}) e 70 nT de resolução. Tais propriedades aliadas à medida exata do campo magnético dc entre 0–2 Oe tornam este dispositivo indicado para aplicações como sensores de campo magnético terrestre, compassos digitais, navegação e detetores de anomalia no campo magnético.

Foi ainda possível desenvolver e otimizar um sensor de corrente baseado num compósito ME de PVDF/Metglas, num solenoide e na correspondente eletrónica de instrumentação. A amostra ME exibe um α_{33} máximo de 34.48V·cm^{-1}·Oe^{-1}, uma resposta linear (r^2=0.998) e uma sensibilidade de 6.7 mV·A^{-1}. Com a incorporação de um amplificador de carga, um conversor ac/dc de precisão e um microcontrolador, a linearidade manteve-se, a tensão ME aumentou para um máximo de 2320 mV e a sensibilidade subiu para 476.5 mV·A^{-1}. Estas propriedades tornam este sensor ME apropriado para a medição de corrente elétrica sem contato, para a verificação do estado de funcionamento de motores e para monitorização da condição de baterias recarregáveis, entre outros.

Concluindo-se deste modo que os compósitos de ME com base em polímeros provaram ser adequados para aplicações na medição de campos magnéticos e intensidade de corrente elétrica.

Contents

List of figures

List of tables

List of symbols

C_f	Capacitor
d_{ij}	Piezoelectric coefficient
E_Y	In-plane Young's modulus
f_r	Resonance frequency
f_{HPF}	High-pass filter cutting frequency
H_{ac}	AC magnetic field
H_C	Coercive field
H_{dc}	DC magnetic field
I_{ac}	AC current
M_R	Remanent magnetization
M_S	Saturation magnetization
n	Harmonic mode order
q_{ij}	Piezomagnetic coefficient
r^2	Correlation coefficient
R_f	Resistor
t	Thickness
V_{ME}	Magnetoelectric voltage
wt %	Weight content
α_{ij}	Magnetoelectric coefficient
$\Delta\vec{E}$	Variation of the electric field
$\Delta\vec{H}$	Variation of the magnetic field
$\Delta\vec{M}$	Variation of the magnetization
$\Delta\vec{P}$	Variation of the electrical polarization
ΔV	Induced magnetoelectric voltage
ε_r	Permittivity
λ_S	Saturation magnetostriction
λ_{ij}	Magnetostrictive coefficient
μ_r	Permeability
ρ	Density
χ	Magnetic susceptibility

List of abbreviations

2G	Second-generation
3G	Third-generation
ac	Alternating current
ADC	Analog-to-digital converter
AGND	Analog ground
AMR	Anisotropic magnetoresistance
AR	Axial-ratio
BNC	Bayonet Neill–Concelman
bps	Bits per second
C–C	Circumferentially magnetized–circumferentially poled
CAD	Computer-aided design
CFO	$CoFe_2O_4$
CMOS	Complementary metal-oxide-semiconductor
COM	Communication port
CP	Circularly polarized
dc	Direct current
DMF	N,N-dimethylformamide
DSP	Digital signal processor
EDS	Energy-dispersive X-ray microanalysis
FCSB	$Fe_{61.6}Co_{16.4}Si_{10.8}B_{11.2}$
FS	Full-scale input
FSO	Full-scale output
FTDI	Future Technology Devices International
GMI	Giant magnetoimpedance
GMR	Giant magnetoresistance
GND	Digital ground
HPF	High pass filter
ICSP	In-circuit serial programming
LF	Low frequency
LSB	Less significant byte
LSCO	$La_{1-x}Sr_xCoO_3$
LSMO	$La_{1-x}Sr_xMnO_3$

LTE	Long-term evolution
ME	Magnetoelectric
MEMS	Microelectromechanical systems
MFC	Macro fibre composite
MIPS	Million instructions per second
MPM	Magnetostrictive–piezoelectric–magnetostrictive
MSB	Most significant byte
MSMA	Magnetic shape memory alloy
NDE	Non-destructive evaluation
P(VDF-TrFE)	Poly(vinylidene fluoride-trifluoroethylene)
PCB	Printed circuit board
PLL	Phase Locked Loop
PMN-PT	$Pb(Mg_{1/3}Nb_{2/3})O_3–PbTiO_3$
PMP	Piezoelectric–magnetostrictive–piezoelectric
PVC	Polyvinyl chloride
PVDF	Poly(vinylidene fluoride)
PZT	$Pb(Zr_xTi_{1-x})O_3$
RF	Radio frequency
rms	Root mean square
SEM	Scanning electron microscope
SMD	Surface-mounted device
SNR	Signal-to-noise ratio
SQUID	Superconducting quantum interference devices
SWR	Standing-wave ratio
TD	Terfenol-D
Terfenol-D	$Tb_xDy_{1-x}Fe_2$ (x~0.3)
UART	Universal asynchronous receiver/transmitter
USB	Universal serial bus
VSM	Vibrating sample magnetometer
UXO	Unexploded ordnance
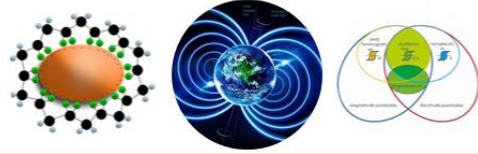
1 Introduction

This chapter introduces the main topics of this thesis, the objectives and the methodology of the work. It begins with a framework, where it is shown the importance of sensors, emphasizing the magnetic ones, and the need to fabricate sensors from polymer-based magnetoelectric materials. The objectives of the present work are identified and the used methodology to achieve them presented. Finally, the structure of the thesis is also presented.
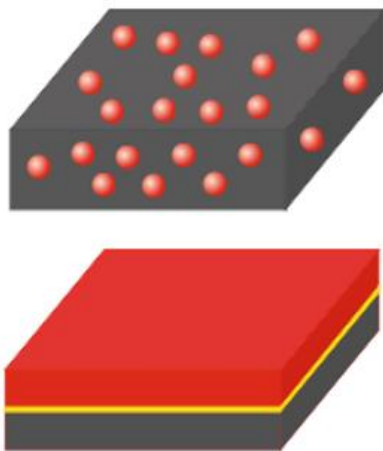
1.1 Framework

Over the last decades, sensors have gained space in many application areas, from home to industrial applications, passing through health, environmental or even military applications [1, 2]. Sensorization is essential for the fourth industrial revolution, taking place after mechanization, where steam engine, the combustion engine and the electric motor were invented, and informatization, that emerged with the computer and the internet [3]. With sensors, humans are learning to artificially expand their senses, they convert a physical or chemical signal into an electrical signal, allowing, together with mechanization and informatization, a full automation [3, 4]. Sensors monitor everything that surrounds daily life and contribute to improve the level of well-being of society [2, 4].

Particularly, magnetic sensors have been widely used for over 2000 years, being the first applications for direction finding or navigation, using the Earth's magnetic field as a tool [5]. Nowadays, measuring the magnetic field is not always the final and desired goal, being also used for measuring other parameters, such as direction, presence, rotation, angle, or current [5, 6]. Moreover, these parameters are determined by detecting the presence, strength or/and direction of magnetic fields, not only from the Earth but also from magnets, fields produced by electric currents, and even biomagnetic fields from the neuronal activity of the brain [4]. Magnetic sensors can measure such parameters without physical contact, so for most applications, they offer a safe, non-invasive and non-destructive measurement, as well as provide a reliable and maintenance-free technology [5, 7].

Magnetic field sensing can be used in different application areas, such as industrial, automotive, military, medical, geophysics, and materials mechanics [8, 9]. In industrial and automotive environment, magnetic field sensors are used mainly for position, angle and rotation-speed sensing [10, 11]. Regarding the automotive sector they also allow navigation of vehicles with respect to Earth magnetic field, as well as detect and recognize vehicles for traffic control [6, 12]. In the military sector they are used to detect unexploded ordnance (UXO) and submarines, besides track autonomous missiles or intelligent ammunition during the flight [9, 13]. Medical applications require magnetic field sensors of high resolution and high sensitivity, since biomagnetic signals range, approximately, from 50 to 10^6 fT at a frequency range from dc to several hundred Hertz. The main sources

of these fields are neurons in the brain, muscle tissues in the heart and magnetic impurities distributed throughout the lungs [14, 15]. Moreover, magnetic trackers are used to navigate catheters inside the body [6]. In geophysical prospection, the Earth magnetic field measurements are used to study the magnetic field orientation of a rock or core sample, providing information as how the rock was formed. Furthermore, magnetic field sensing allows mineralogical survey and archaeological prospecting [6, 14, 16]. Magnetic sensing can also be used for mechanics of materials essays through non-destructive evaluation (NDE) techniques. Eddy current tests have been used for many years to detect cracks and flaws in conductive materials. In this way, it is possible to detect stress or corrosion in reinforcing rods used in bridges or buildings and do an assessment of the expected life of mechanical components [14, 17].

Despite all these vast and broad applications, industry demands for smaller, cheaper and lower power magnetic sensors [6]. Sensors with all these characteristics were one of the motivations to explore new materials and different technologies. Polymer-based magnetoelectric (ME) composites can be an innovative tool for that exploration once they are flexible, versatile, lightweight, low cost, easy to model in complicated shapes and typically involve a low-temperature fabrication process, being in this way, a solution for magnetic sensors applications [18].

ME materials are characterized by the variation of the electrical polarization $(\vec{P})$ in the presence of a varying applied magnetic field $(\vec{H})$ – called direct ME effect:

$$\Delta \vec{P} = \alpha \Delta \vec{H} \tag{1.1}$$

or as the variation of the induced magnetization $(\vec{M})$ in the presence of a varying applied electrical field $(\vec{E})$ – called converse ME effect:

$$\Delta \vec{M} = \alpha \Delta \vec{E} \tag{1.2}$$

where α is the ME coefficient [19-21].

This effect is present in materials through two different principles: directly, through the coupling of magnetic moments and electric dipoles, in single-phase ME materials [22-24], or indirectly, by the elastic coupling between piezoelectric and magnetostrictive phases, in ME composites [21, 22, 25].
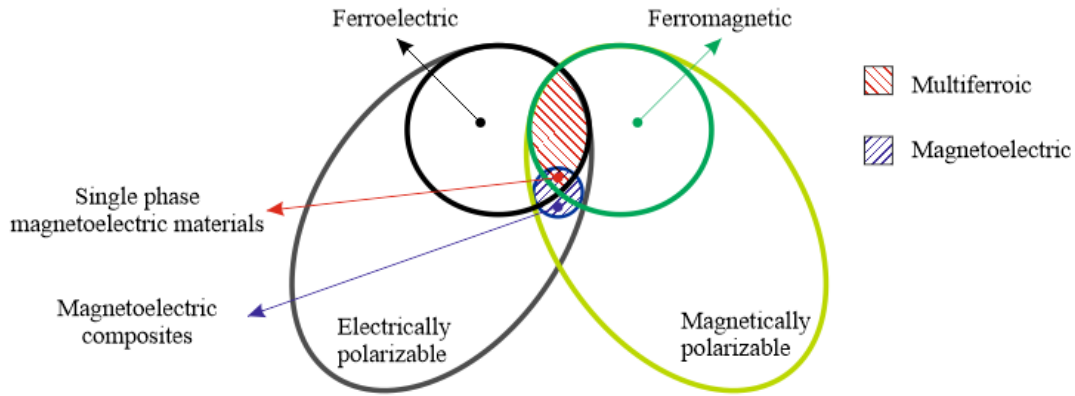
Figure 1.1. Relationship between ferroic, multiferroic and magnetoelectric materials.

Single-phase ME materials (Figure 1.1) are part of a wider group, called multiferroic materials, which possesses at least two of the primary ferroic properties – ferroelectricity, ferromagnetism and ferroelasticity [22, 23]. Single-phase ME materials, typically, show rather low Curie or Néel temperatures, and exhibit a weak ME coupling at room temperature [24, 26], hindering, in this way, their incorporation into technological applications [20, 26].

In ME composites, neither of the constituents phases show ME properties, but the stress and elastic mediated coupling interaction between the phases can produce a strong ME effect. Thus, when a magnetic field is applied to the composite, a strain is induced in the magnetostrictive phase, which is transmitted to the piezoelectric phase, leading to a change in electrical polarization. Therefore, the ME effect in composites is extrinsic, strongly depending on the microstructure and coupling interaction across the magnetostrictive and piezoelectric interfaces. These composites produce, in comparison with single-phases materials, a large ME response at room temperature [20, 21, 25].

ME composites can be classified according to the type of composed materials. Different approaches are found in the literature based on one of two fundamental type of piezoelectric materials, either constituted by a piezoelectric ceramic or polymeric, together with a magnetostrictive element [21]. Although ceramic-based ME composites show a higher ME coefficient than polymer-based ME composites, such composites may become fragile and are limited by deleterious reactions at the interface regions, resulting in low electrical resistivity and high dielectric losses. Furthermore, they are dense and brittle, which can lead to fatigue and failure during operation [21, 27, 28]. The use of piezoelectric polymers, such as poly(vinylidene fluoride) (PVDF) and its copolymers, can solve some of ceramic-based composites limitations, since they are flexible, show large

electrical resistivity and small losses. Besides that, they can be easily fabricated by conventional low-temperature processes into a variety of forms [20, 21, 27]. In this way, they are being more suitable than ceramic-based composites for incorporation into devices.

According to Martins *at al*. [21], polymer-based ME composites can be classified as nanocomposites, *polymer as a binder* or laminated composites (Figure 1.2).
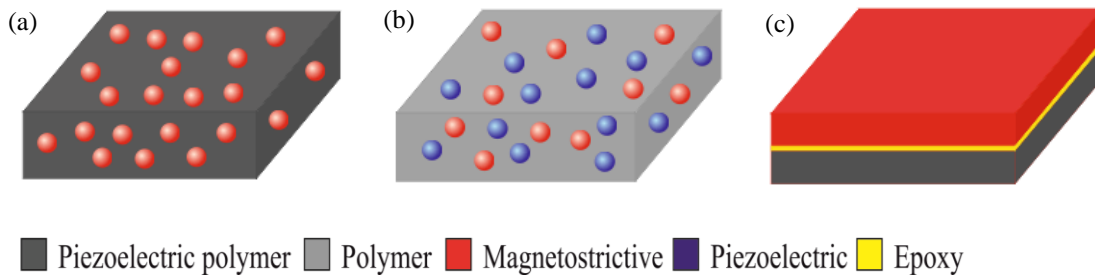
Figure 1.2. Types of polymer-based ME materials: (a) nanocomposites, (b) *polymer as a binder*, and (c) laminated composites.

Nanocomposites are formed by nanoparticles of a magnetostrictive material within a piezoectric polymer. Their main advantage is the easy fabrication process, as the mechanical properties of the polymer are preserved for sufficiently small nanoparticle weight fractions [29]. The optimum dc magnetic field is high, making them suitable for high-field dc magnetic field sensors. However, they exhibit a low ME coefficient, when compared with laminate composites [21].

In *polymer as a binder* composites, the polymer is not used as the piezoelectric phase of the ME composite, but as a binder for the piezoelectric and magnetrostrictive particles, keeping them together and providing the stress coupling between the piezoelectric and magnetostrictive phases [21]. Despite the flexibility, easy shaping and simple fabrication of *polymer as a binder* ME materials, all of these features are inferior to those of the particulate nanocomposites [21, 30]. Nevertheless, their ME coefficient is slightly higher than the one exhibited by ME nanocomposites [21].

Laminate composites are formed by a piezoelectric polymer layer glued to a magnetostrictive layer by an epoxy resin. Laminate polymer-based ME materials, exhibit the highest ME coefficient, within the reported ME composites [31]. They reveal low optimum dc magnetic field, facilitating the application miniaturization [21, 32]. However, their fabrication process is not trivial, owing to the fact that they need to be glued.

Polymer-based ME composites are ready for technological applications, their ME coefficient value and the wide range of magnetic fields at which they respond, allow a

variety of device applications. Some of the promising applications include ac and dc magnetic field sensors, current sensors, actuators, filters, antennas, multiple-state memories and energy harvesting devices, among others [21, 25, 33]. For some of these applications, polymer-based ME composites, due to their unique characteristics such as flexibility, versatility and low cost, can be an advantage [21, 33]. The present thesis demonstrates the viability of polymer-based ME composites in ME applications.

1.2 Objectives

In the present thesis, polymer-based ME composites will be produced, characterized and optimized, to reach the ultimate goal, the development of ME sensors. It is expected that these sensors will optimize the products and applications developed by AVEL-electrónica, lda., or even, open up new business areas for the company. Therefore, the objectives of this work are:

1. Development of a system for ME materials characterization, taking into account, the study of particulate nanocomposites, which have high optimum dc magnetic field, and laminate composites, which have low optimum dc magnetic field. Moreover, low dc magnetic field system will be optimized to allow anisotropic tests in order to evaluate the magnetic field direction.

2. Development of new polymer-based ME nanocomposite formed by two types of magnetostrictive particles and able to respond to a wide-range of magnetic fields.

3. Implement a ME sensor able to detect magnitude and direction of ac and dc magnetic fields and study important characteristics for the sensors applicability, such as sensitivity, linearity, and accuracy.

4. Implement a dc magnetic field sensor; design, optimize and fabricate electronic circuits for processing the ME output voltage, and develop a user interface.

5. Implement a dc current sensor.

1.3 Methodology

The research work is divided in several main tasks, which complement each other, and indicates the followed methodology. Firstly, two systems for ME materials characterization were developed, one for low dc magnetic fields and another for high dc magnetic fields. Moreover, to study the direction of magnetic field, a specified sample

holder, which allows to rotate the sample 360º in relation to the applied magnetic field, was developed.

Afterwards, the work focus on the production and characterization of ME composites. Materials optimization is different when it relates to particulate nanocomposites or laminate composites. Magnetoelectric composites were fabricated in order to develop composites able to respond to a wider range of magnetic fields. Laminates were prepared in order to develop anisotropic magnetic field and current sensors, both with the corresponding readout electronics.

For the preparation of nanocomposites, it was taken into account the concentration, magnetostriction and hysteresis of nanoparticles, their good dispersion and distribution on the polymer matrix, and the best coupling between nanoparticles and polymer. The optimization of laminate ME composites took into consideration the bonding layer, sizes, structure and geometries of the composite.

Characterization techniques were applied to study the composites morphology, piezoelectric, magnetic and magnetoelectric properties, among others.

At the same time, magnetic field and current sensors were developed. The essential characteristics for sensors development were evaluated, including sensitivity, linearity and accuracy. The possibility to measure the direction of the magnetic field, in addition to its magnitude, was evaluated. Once the feasibility of ME composites as sensors has been proven, signal processing of the ME output voltage was carried out and a C# application was developed for user interface.

1.4 Structure

This thesis provides a comprehensive and logic description of the work achieved during the PhD period. It is divided in eight chapters, being five of them based on published or submitted scientific papers.

The first chapter introduces the theme with a brief framework, showing the importance of sensors and polymer-based ME materials. Moreover, the main objectives, the used methodology and the thesis structure are presented.

The chapter 2, concerns with the state of the art, showing the main applications of polymer-based ME materials: sensors, actuators, energy harvester devices, antennas and memories.

Chapter 3 describes the measuring systems developed for ME materials characterization. The options are presented, the system implementation is shown and validated.

Chapter 4 reports on the piezoelectric, magnetic and ME properties of a wide-range polymer-based nanocomposite.

Chapters 5 and 6 describe the implementation of magnetic field sensors based on polymer-based ME laminate composites.

The seventh chapter describes the implementation of a dc current sensor.

Finally, chapter 8 reports some final considerations, presents the conclusions and the suggestions for future work.

1.5 References

[1]   I. F. Akyildiz, W. Su, Y. Sankarasubramaniam, and E. Cayirci, "Wireless sensor networks: A survey," *Computer Networks,* vol. 38, pp. 393-422, 2002.

[2]   J. Yick, B. Mukherjee, and D. Ghosal, "Wireless sensor network survey," *Computer Networks,* vol. 52, pp. 2292-2330, 2008.

[3]   J. H. Huijsing, "Smart Sensor Systems: Why? Where? How?," in *Smart Sensor Systems*, G. C. M. Meijer, Ed., ed: John Wiley & Sons, Ltd, 2008, pp. 1-21.

[4]   J. S. Wilson, *Sensor Technology Handbook*: Elsevier Inc., 2005.

[5]   M. J. Caruso, T. Bratland, C. H. Smith, and R. Schneider, "A new perspective on magnetic field sensing," *Sensors (Peterborough, NH),* vol. 15, pp. 34-46, 1998.

[6]   P. Ripka, "Sensors based on bulk soft magnetic materials: Advances and challenges," *Journal of Magnetism and Magnetic Materials,* vol. 320, pp. 2466-2473, 2008.

[7]   A. E. Mahdi, L. Panina, and D. Mapps, "Some new horizons in magnetic sensing: High-Tc SQUIDs, GMR and GMI materials," *Sensors and Actuators, A: Physical,* vol. 105, pp. 271-285, 2003.

[8]   J. Lenz and A. S. Edelstein, "Magnetic sensors and their applications," *IEEE Sensors Journal,* vol. 6, pp. 631-649, 2006.

[9]   A. L. Herrera-May, L. A. Aguilera-Cortés, P. J. García-Ramírez, and E. Manjarrez, "Resonant magnetic field sensors based on MEMS technology," *Sensors,* vol. 9, pp. 7785-7813, 2009.

[10]   K. M. H. Lenssen, D. J. Adelerhof, H. J. Gassen, A. E. T. Kuiper, G. H. J. Somers, and J. B. A. D. Van Zon, "Robust giant magnetoresistance sensors," *Sensors and Actuators, A: Physical,* vol. 85, pp. 1-8, 2000.

[11]   C. P. O. Treutler, "Magnetic sensors for automotive applications," *Sensors and Actuators, A: Physical,* vol. 91, pp. 2-6, 2001.

[12]   J. Včelák, P. Ripka, and A. Zikmund, "Precise Magnetic Sensors for Navigation and Prospection," *Journal of Superconductivity and Novel Magnetism,* vol. 28, pp. 1077-1080, 2015.

[13]   A. Sheinker, B. Ginzburg, N. Salomonski, P. A. Dickstein, L. Frumkis, and B. Z. Kaplan, "Magnetic anomaly detection using high-order crossing method," *IEEE Transactions on Geoscience and Remote Sensing,* vol. 50, pp. 1095-1103, 2012.

[14] R. L. Fagaly, "Superconducting quantum interference device instruments and applications," *Review of Scientific Instruments,* vol. 77, 2006.

[15] K. Sternickel and A. I. Braginski, "Biomagnetism using SQUIDs: Status and perspectives," *Superconductor Science and Technology,* vol. 19, 2006.

[16] M. Mandea and M. Purucker, "Observing, modeling, and interpreting magnetic fields of the solid earth," *Surveys in Geophysics,* vol. 26, pp. 415-459, 2005.

[17] T. Dogaru and S. T. Smith, "Giant magnetoresistance-based eddy-current sensor," *IEEE Transactions on Magnetics,* vol. 37, pp. 3831-3838, 2001.

[18] M. Alnassar, A. Alfadhel, Y. P. Ivanov, and J. Kosel, "Magnetoelectric polymer nanocomposite for flexible electronics," *Journal of Applied Physics,* vol. 117, 2015.

[19] G. Srinivasan, "Magnetoelectric composites," in *Annual Review of Materials Research* vol. 40, ed, 2010, pp. 153-178.

[20] J. Ma, J. Hu, Z. Li, and C. W. Nan, "Recent progress in multiferroic magnetoelectric composites: From bulk to thin films," *Advanced Materials,* vol. 23, pp. 1062-1087, 2011.

[21] P. Martins and S. Lanceros-Méndez, "Polymer-based magnetoelectric materials," *Advanced Functional Materials,* vol. 23, pp. 3371-3385, 2013.

[22] W. Eerenstein, N. D. Mathur, and J. F. Scott, "Multiferroic and magnetoelectric materials," *Nature,* vol. 442, pp. 759-765, 2006.

[23] M. Fiebig, "Revival of the magnetoelectric effect," *Journal of Physics D: Applied Physics,* vol. 38, 2005.

[24] W. Prellier, M. P. Singh, and P. Murugavel, "The single-phase multiferroic oxides: From bulk to thin film," *Journal of Physics Condensed Matter,* vol. 17, 2005.

[25] C. W. Nan, M. I. Bichurin, S. Dong, D. Viehland, and G. Srinivasan, "Multiferroic magnetoelectric composites: Historical perspective, status, and future directions," *Journal of Applied Physics,* vol. 103, 2008.

[26] D. R. Patil, A. D. Sheikh, C. A. Watve, and B. K. Chougule, "Magnetoelectric properties of ME particulate composites," *Journal of Materials Science,* vol. 43, pp. 2708-2712, 2008.

[27] K. J. Loh and D. Chang, "Zinc oxide nanoparticle-polymeric thin films for dynamic strain sensing," *Journal of Materials Science,* vol. 46, pp. 228-237, 2011.

[28] S. Jiansirisomboon, K. Songsiri, A. Watcharapasorn, and T. Tunkasiri, "Mechanical properties and crack growth behavior in poled ferroelectric PMN-PZT ceramics," *Current Applied Physics,* vol. 6, pp. 299-302, 2006.

[29] P. Martins, X. Moya, L. C. Phillips, S. Kar-Narayan, N. D. Mathur, and S. Lanceros-Mendez, "Linear anhysteretic direct magnetoelectric effect in Ni 0.5Zn0.5Fe2O4/poly(vinylidene fluoride-trifluoroethylene) 0-3 nanocomposites," *Journal of Physics D: Applied Physics,* vol. 44, 2011.

[30] P. Martins, A. Lasheras, J. Gutierrez, J. M. Barandiaran, I. Orue, and S. Lanceros-Mendez, "Optimizing piezoelectric and magnetoelectric responses on CoFe2O4/P(VDF-TrFE) nanocomposites," *Journal of Physics D: Applied Physics,* vol. 44, 2011.

[31] M. Silva, S. Reis, C. S. Lehmann, P. Martins, S. Lanceros-Mendez, A. Lasheras*, et al.*, "Optimization of the magnetoelectric response of poly(vinylidene fluoride)/epoxy/vitrovac laminates," *ACS Applied Materials and Interfaces,* vol. 5, pp. 10912-10919, 2013.

[32]   J. Zhai, S. Dong, Z. Xing, J. Li, and D. Viehland, "Giant magnetoelectric effect in Metglas/polyvinylidene-fluoride laminates," *Applied Physics Letters,* vol. 89, 2006.

[33]   J. F. Scott, "Applications of magnetoelectrics," *Journal of Materials Chemistry,* vol. 22, pp. 4567-4574, 2012.

2 State of the art

A state of the art indicating the main applications of polymer-based magnetoelectric materials is presented. Applications in the area of sensors, actuators, energy harvesting devices, antennas and memories based on polymer-based magnetoelectric materials are presented and discussed.
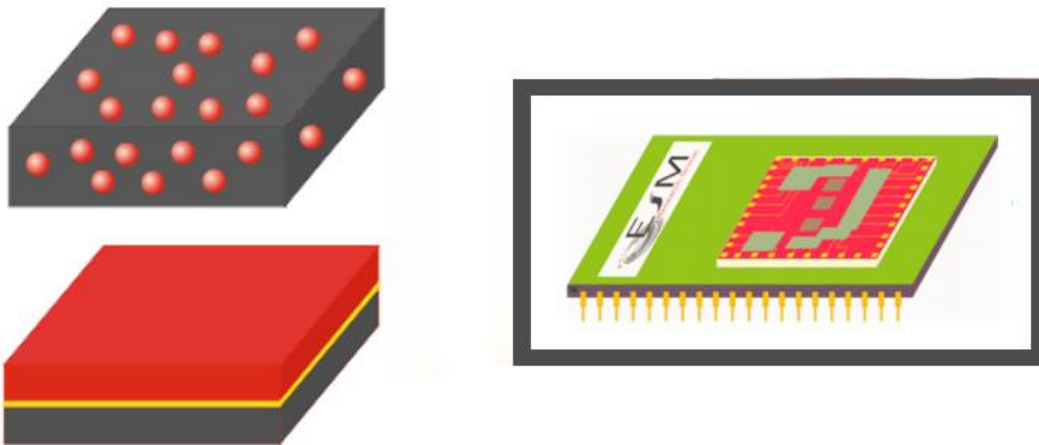
2.1 Introduction

Throughout the years, efforts have been made to improve the magnetoelectric (ME) coefficient in polymer-based composites, and these efforts have been directed toward the preparation techniques of samples, the choice of materials, and the different structures and thicknesses of the samples. Initially, the technique used to fabricate composites was conventional sintering; however, in order to suppress interdiffusion and chemical reaction of the constituents and to improve the quality of the composites, hot pressing has also been used [1]. Different types of materials can be used in the fabrication of ME composites, that is, hard materials such as piezoelectric ($Pb(Zr_xTi_{1-x})O_3$ (PZT) and $BaTiO_3$) and piezomagnetic ($NiFe_2O_4$, $CoFe_2O_4$, $La_{1-x}Sr_xMnO_3$ (LSMO), and $La_{1-x}Sr_xCoO_3$ (LSCO)) ceramics; soft materials, for piezomagnetics Metglas and Terfenol-D ($Tb_xDy_{1-x}Fe_2$ (x~0.3)); or piezoelectric polymers such as poly(vinylidene fluoride) (PVDF) or poly(vinylidene fluoride-trifluoroethylene) (P(VDF-TrFE)).

The use of polymer-based nanocomposites is the most recent approach to obtain highly flexible and nonbrittle ME composites [2, 3]. In comparison to ceramic ME composites, polymer composites can be easily fabricated by conventional low-temperature processing into a variety of forms, such as thin sheets, films, or moulded shapes, and can exhibit suitable mechanical properties for flexible and large-area applications [2].

Polymer-based ME materials have been investigated to find applications in magnetic field sensors (Figure 2.1), actuators, energy-harvesting devices, filters, oscillators, miniature antennas, memories and biomedical devices, among others [4-6].
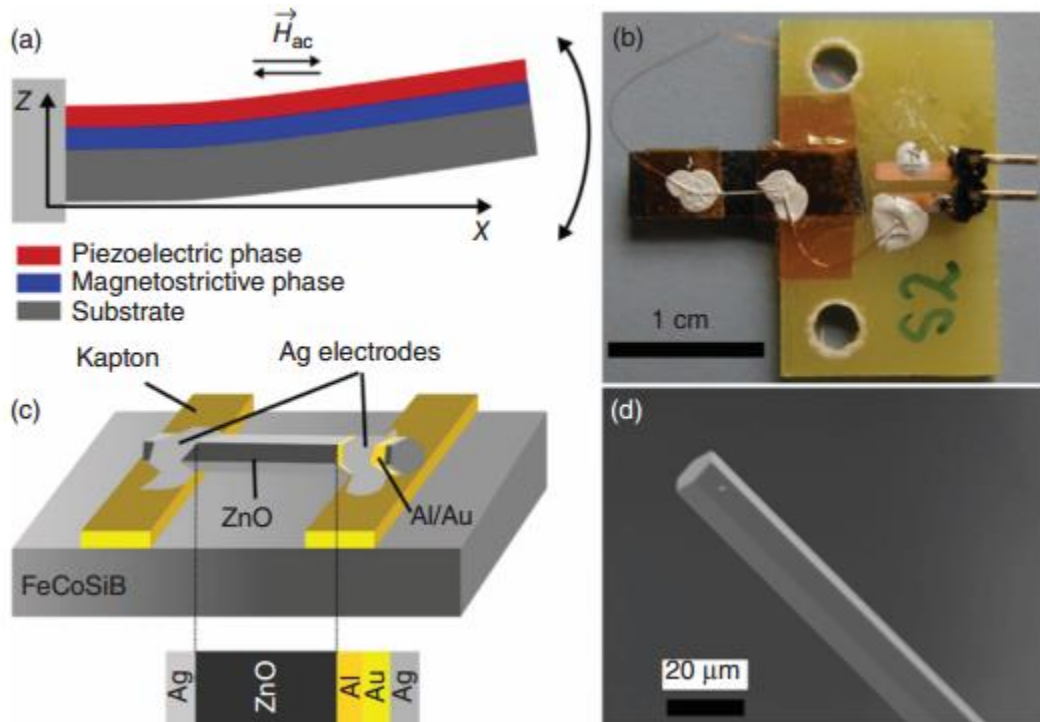
Figure 2.1. (a) Schematic representation of a ME sensor in a 2–2 geometry that is oscillating due to an external applied magnetic field. (b) Digital image of the ME sensor with two Schottky contacts. (c) Schematic representation of the ME sensor design. (d) Scanning electron microscope (SEM) image of a ZnO microneedle with a length of several millimetres. The SEM image (d) of the ZnO microneedle clearly features the hexagonal base plane of the wurtzite structure [7].

The most promising applications of polymer-based magnetoelectric materials are discussed in the following chapters.

2.2 Polymer-based magnetoelectric sensors

The working principle of ME materials, which results in the appearance of a voltage in the presence of magnetic field variation, allows magnetic sensing in a simple and direct way (Figure 2.2) [6].
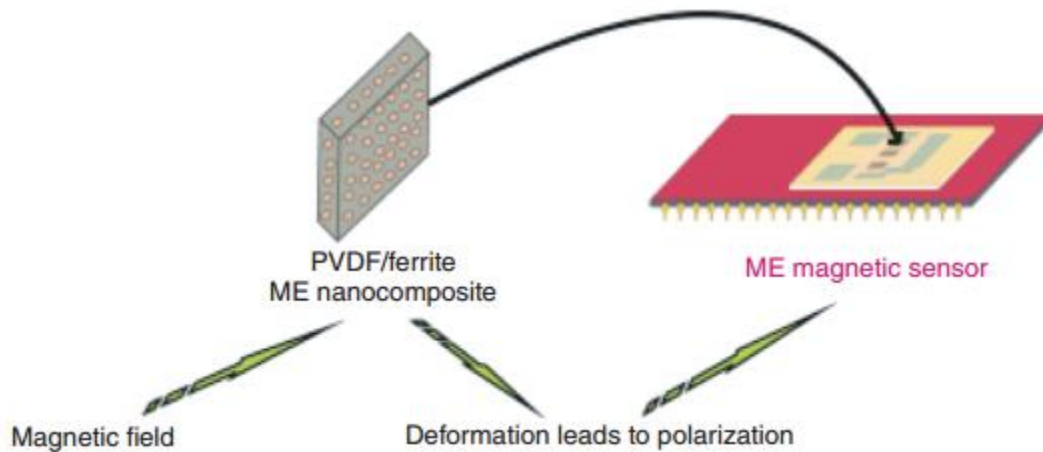
Figure 2.2. Representation of the ME magnetic field sensing mechanism [4].

Magnetic field sensors have been widely used for centuries; the first few applications were based on navigation and localization, using the earth's magnetic field as a tool [8]. However, nowadays measuring the magnetic field is not always the ultimate goal, as changes or disturbances in magnetic fields allow to indirectly measure distinct parameters such as electric current, linear and angular positions, speed, and vehicle detection, among others [8, 9].

After Nan *et al.*'s [10] suggestion to use polymer-based ME materials for technological applications, several studies were carried out combining different piezoelectric polymers [11-13] and magnetostrictive alloys [10, 14]. The applicability of these materials as sensors depends on some fundamental characteristics including full-scale input (FS), sensitivity, linearity, hysteresis, accuracy, repeatability, and resolution [15]. ME sensors can detect static and dynamic magnetic fields; the FS of a dc magnetic field sensor is directly related to the configuration and the type of magnetostrictive material that composes the ME composite, being in the order of 10 Oe in laminate ME composites based on Metglas [13], 1000 Oe in laminate ME composites with Terfenol-D, 2500 Oe in particulate ME composites with $CoFe_2O_4$ [11] and 5000 Oe in particulate ME materials with $Ni_{0.5}Zn_{0.5}Fe_2O_4$ [16].

With respect to the full set of parameters defining a magnetic field sensor, both ac and dc magnetic field sensors are slightly investigated. An ac magnetic field sensor fabricated from Metglas/PVDF/Metglas laminates was found to have a resolution of 10 pT at resonance frequency (50 kHz) [13] and 30 nT at non-resonance frequency (1 kHz) [17]. The dc magnetic field sensor fabricated with the same materials and structure can sense small variations of up to 8 nT for an ac magnetic field (H_{ac}) of 1 Oe [13]. Sensitivity

was also analysed in a Metglas/PVDF/Metglas laminate ME composite ranging between 0.03 and 0.17 V·Oe^{-1} for a sample with a single piezoelectric layer. On increasing the number of PVDF layers to four, connected in parallel, an enhanced sensitivity ranging between 0.13 and 0.67 V·Oe^{-1} was observed [18]. Another ME laminate composed of $Fe_{64}Co_{17}Si_7B_{12}$ and PVDF bonded in a magnetostrictive–piezoelectric–magnetostrictive (MPM) configuration was used to study the sensitivity, linearity, hysteresis, accuracy, and resolution of dc and ac ME sensors at resonance and non-resonance frequencies. For the dc magnetic field sensor, a correlation coefficient (r^2) of 0.995 and a linearity of 95.9% FSO (full-scale output) in the 0–3 Oe magnetic field range were achieved. The accuracy, hysteresis, sensitivity, and resolution were 99.4% FSO, 1.2% FSO, 30 mV·Oe^{-1}, and 8 μOe. For the ac magnetic field sensor at resonance frequency (48 kHz), a r^2 of 0.9998 and a linearity of 99.4% FSO were obtained. Additionally, the accuracy, sensitivity, and resolution of the sensor were 97.9% FSO, 992 mV·Oe^{-1}, and 300 nOe, respectively. At a non-resonance frequency of 95 kHz, r^2, linearity, accuracy, sensitivity, and resolution were 0.998, 98.6% FSO, 2.3% FSO, 40 mV·Oe^{-1}, and 1 μOe, respectively [19].

In some applications, it is important to measure not only the magnitude but also the direction of the magnetic field vector. This characteristic is particularly important in geomagnetic field sensors for military, industrial, and medical applications [20, 21]. This concept is only possible thanks to the anisotropy of the magnetostrictive/ME response such as the one represented in Figure 2.3.
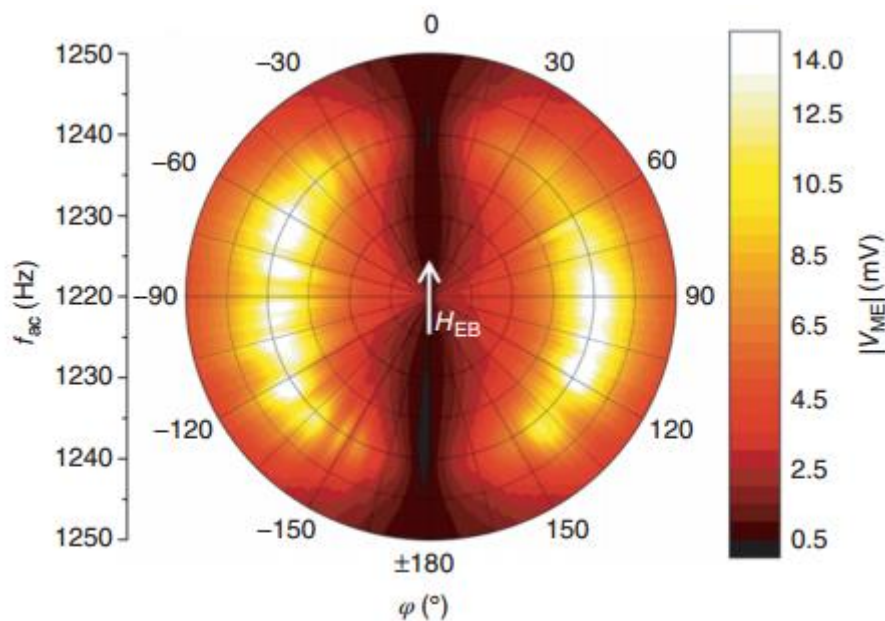
Figure 2.3. Representation of the ME magnetic field sensing mechanism [22].

Such anisotropic response has been reported for a ME laminate composed of Metglas/PVDF, with the maximum α obtained for 0º, 180º, and 360º, when H_{ac} and dc magnetic field (H_{dc}) have the same direction of the Metglas magnetization, and minimum for 90º and 270º, when the magnetic fields and the Metglas magnetization are perpendicular [23].

Anisotropic response has been obtained not only in laminated materials but also in particulate ME nanocomposites of δ-FeO(OH)/P(VDF-TrFE). In this case, the ME effect will not arise from the coupling between the magnetostriction and piezoelectricity but from the alignment of feroxyhyte nanosheets. The maximum α was observed when the H_{dc} was applied perpendicularly to the δ-FeO(OH) length direction (90º and 270º), and no ME response was observed when the magnetic field was applied parallel to the alignment (0º, 180º, and 360º) [21]. In practical applications and to distinguish, for example, the 45º angle from the 135º one, both with the same ME response, two ME materials, should be integrated within the same magnetic sensor with a well-known angle between them [21].

Although the ME detection techniques in most of the reports are based on direct measurements, with the sensor directly connected to a lock-in amplifier or an oscilloscope [17, 24], the development of sensors should take into account the readout electronics for data acquisition. The high output impedance with high capacitive component of ME sensors, due to the piezoelectric layer, leads to the need of specific interface circuits, such as charge amplifiers or voltage amplifiers with high input resistance [15, 25, 26]. Designed for bioimaging applications, a voltage-mode complementary metal-oxide-semiconductor (CMOS) amplifier with an active biasing circuit and a package integration method system was compared with direct measurement and charge amplifier. With this circuit configuration and implementation, high input impedance was achieved with reduced parasitic capacitance. The results show an excellent low-frequency response between 0.5 Hz and 1 kHz at an equivalent signal-to-noise ratio (SNR) value [17, 18].

In turn, the measurement of an electric current can follow different principles; some sensors are based on Ohm's law of resistance, others on Faraday's law of inductance, on Faraday effect, or on magnetic field sensors [27]. Magnetic field sensors show several advantages, as they do not need to be placed in the current path, unlike the ones based on Ohm's law of resistance, and can sense static and dynamic magnetic fields, unlike Faraday's law of inductance sensors [27, 28]. ME current sensors are based on Ampère's law [29].

The study of ME current sensors began in 2004 with Dong *et al.* [30] who presented a ring-type current sensor composed of a circumferentially magnetized and circumferentially poled (C–C) Terfenol-D/PZT sample adapted to detect the vortex magnetic field produced by a straight wire carrying an ac current (I_{ac}). It was concluded that the ME voltage is a linear function of vortex H_{ac}, has a resolution of 10 nT at a non-resonance frequency and a flat frequency response between 10^{-1} and 10^3 Hz [30, 31]. From 2004, more work have been done in electric current sensors with ME ceramic laminate composites, and different configurations have been proposed. A SmFe$_2$/PZT/SmFe$_2$ self-biased ME laminate and a Fe$_{73.5}$Cu$_1$Nb$_3$Si$_{13.5}$B$_9$ nanocrystalline flux concentrator exhibit an approximately linear relationship in the range of 10 mA to 150 A, a sensitivity of 152 mV·A^{-1} at 50 Hz, and a nonlinearity error of 0.01% FS [29, 32]. A ME composite of Metglas/PZT designed as a cantilever structure and with a tungsten proof mass at the end of the cantilever to adjust the ME resonance frequency shows a sensitivity of 114.2 mV·A^{-1} and a resolution of 10 mA at a resonance frequency of 50 Hz [33]. To avoid the necessity of interruption of the power supply that allows the installation or maintenance of the sensor, required in every ring-type and close-magnetic-circuit-type current sensors topologies, a slice-type ME composite of Terfenol-D/PZT was designed. The wire current conductor is coiled with N turns along the slice, generating a H_{ac} along the longitudinal direction of ME material. A current sensitivity of 1.03 mV·mA^{-1} was obtained for 20 turns of the coil [34].

Although a reasonable amount of work on ME ceramic laminate composites have been conducted and there are promising results from them, increasing efforts are being made to develop polymer-based ME current sensors. Their ME coefficient allied to versatility and flexibility can be a key issue in the development of novel ME current sensors applications.

Although ME sensors are not yet commercialized, it is expected that they would be able to compete with both conventional magnetic field and current sensors.

2.3   Polymer-based magnetoelectric actuators

Actuators are materials or devices responsible to produce motion or the signal responsible for moving or controlling a mechanism or system. They are able to change their shape in response to changes in environmental conditions and thus perform mechanical work at nano-, micro-, or macroscale [35].

ME actuators can take advantage of the converse ME effect, producing a magnetic field by applying a voltage, or the direct ME effect, where a magnetic field causes a deformation in the magnetostrictive materials, which will deform the piezoelectric material resulting in a voltage variation.

Several potential applications of ME actuators taking advantage of the magnetic, mechanical, or electrical properties have been explored. Ueno *et al.* were the first to explore ME materials as actuators, proving their capability for magnetic force control, important in applications such as motors or magnetic suspension systems. A device composed of a stack PZT actuator, a rod of Terfenol-D, a ring permanent magnet, and two ferromagnetic plates was developed. In this device, the magnetic force was varied by applying voltage to the PZT, and it was observed that the voltage and the variation of the compressive strain and force are strongly dependent on the sample dimensions. For a voltage of 200 V, the magnetic forces (compressive stress generated by the PZT) reach 40 N with a variation of 10 N [36]. Furthermore, a zero-power magnetic levitation system was developed using Terfenol-D and two PZTs glued to an iron yoke stiff enough to prevent deformation by bending in conjunction with permanent magnets, with a back yoke attached [37] or a linear step motor, in which the stator was composed of four composites of Terfenol-D and PZT with the same configuration explained earlier, achieving step motion with the advantages of low power consumption and low heat generation [38]. A torque-based rotating structure, exploiting the easy-axis orientation in magnetically soft materials, was designed with a Fe–Si–B disk glued between two piezoelectric layers of PZT fibers with an angle of 45º between the two piezoelectric materials and a cylindrical magnet, magnetized diametrically, placed above the ME material. A voltage applied on the piezoelectric element produces a stress, which is transmitted to the magnetostrictive layer, causing a variation in its permeability and consequently in the circuit resistance, which in turn can adjust the magnetic force on a mobile element [39].

ME actuators can also play an important role in biological applications such as adding the magnetic stimulation to the options of the "cell clinic" for single-cell studies (Figure 2.4).
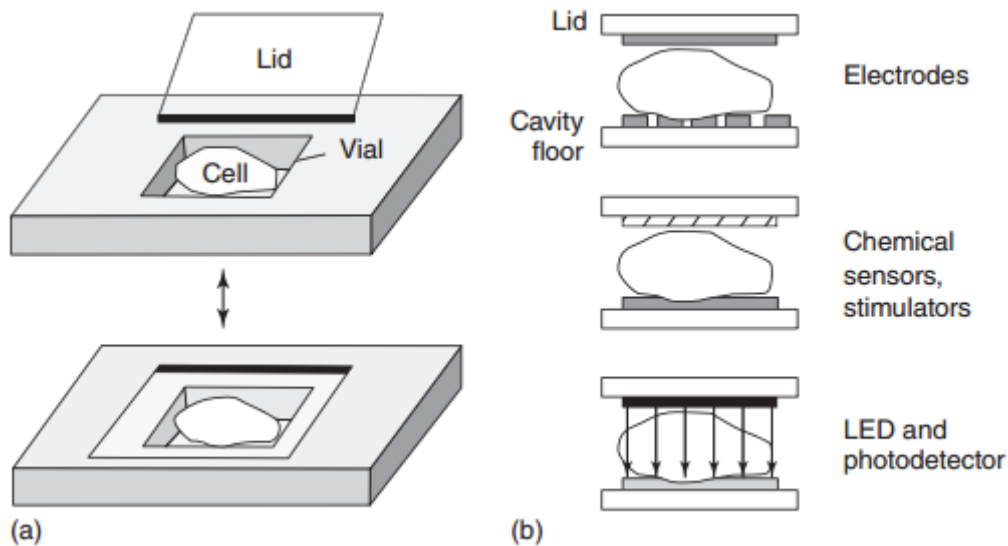
Figure 2.4. (a) "Cell clinic" for single-cell studies. (b) Functionalizing the lid and cavity floor with electrical, chemical, and optical stimulation [40].

Three ME cantilevers composed of a laminate composite of Galfenol and PZT-5H were used to develop a surgical manipulation tool [41]. The position cantilever is capable of producing an up–down movement by applying a magnetic field, and two gripping cantilevers are attached at one of the ends of the positioning cantilever that can produce deflection in a sideway direction, making them suitable for gripping action. The electrical signal generated by the piezoelectric layer is used to sense the bending amplitude of the structure, which is of core importance in a closed-loop control system [41]. A polymer-based ME laminate composite has also been used in the development of a similar microscale surgical tool. Such a polymer-based ME constituted by PVDF and Metglas is more suitable in surgery once it can be easily formed in thin layers, which is preponderant in the fabrication of a millimeter-scale device [42]. Polymer-based ME materials can also be useful in tissue engineering when a patient is immobilized due to serious health condition. In this context, ME biomaterial scaffolds allow to remotely mechanically and/or electrically stimulate tissues from outside of the human body, without the need for patient movement, by the application of an external magnetic field. A particulate ME composite of Terfenol-D and P(VDF-TrFE) was chosen to prove these benefits, enhancing up to ≈25% the cell proliferation, when they are cultured under mechanical and electrical stimulation [43].

2.4   Polymer-based magnetoelectric energy harvesting

The decreasing of the power consumption of electronic sensors and devices allowed the increase of wireless systems, which have several advantages over wired methodologies [44, 45]. These devices are battery powered, but their limit life time increase the interest for alternative solutions such as energy harvesting systems, which can harvest energy such as mechanical vibrations, thermal gradients, light, electromagnetic fields, or radio frequency (RF) radiation from the environment [44, 46, 47]. According to Vullers *et al*. the best solution is the combination of such an energy harvesting device with a small-sized rechargeable battery (or any other energy storage system), since it enables energy autonomy of devices over their entire lifetime [44]. This approach is especially important in wireless sensors network systems, capable of monitoring industrial machines, civil structures, environmental and military devices, as well as implantable devices, placed inside the human body [48, 49]. These applications are usually requested to work for a long time on places with difficult access for replacing or recharging batteries [48].

ME composite materials, combining a piezoelectric phase with a magnetostrictive phase, allow them to harvester either vibration energy or electromagnetic energy. The piezoelectric layer can convert the stress into a voltage through the direct piezoelectric effect and the ME effect can also be used to take advantage of vibration and electromagnetic energies [50, 51]. Vibration energy is one of the most prevalent energies, it is part of human activity, such as walking, and can be found in numerous environments including household goods, automobiles, aeroplanes, industrial equipment, buildings, and bridges [45, 48]. Energy harvesting from electromagnetic energy (Figure 2.5) also offers advantages such as being a renewable and ubiquitous and, therefore, present in difficult to access locations [48, 52]. Electromagnetic energy sources result from radiation emitting devices such as mobile base stations, Wi-Fi routers, satellite communications, radio and TV transmitters, as well as from magnetic and electric fields generated in power distribution lines [46].
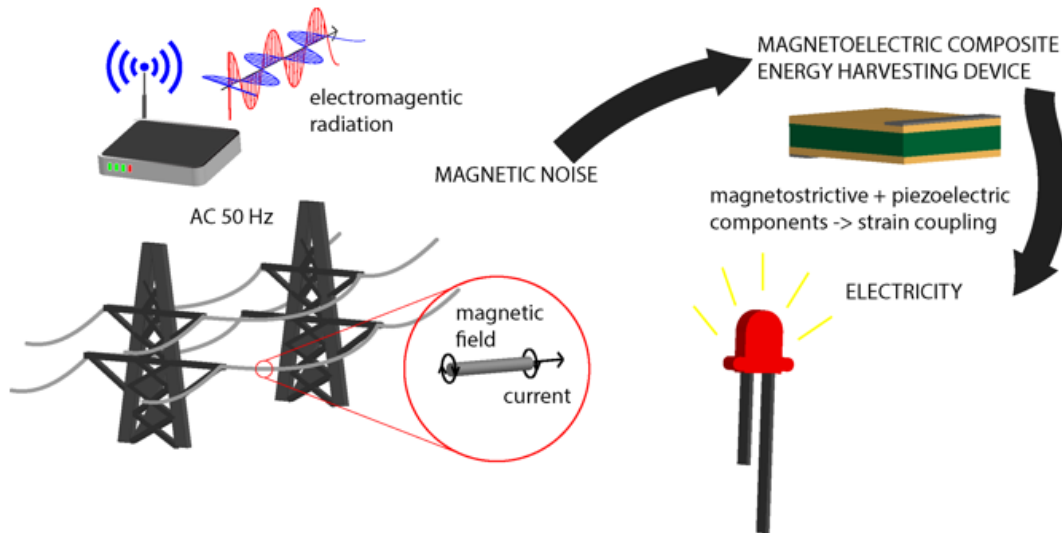
Figure 2.5. Interactions involved in magnetoelectric energy harvesting [53].

The interest of energy harvesting with ME materials began in 2003, when Huang *et al.* presented a vibration energy harvesting device formed by a ME laminate ceramic composite of Terfenol-D/PZT/Terfenol-D able to generate 1.2 mW for 0.5 g acceleration at 30 Hz [54]. After this first study about energy harvesting with ME ceramic composites, many others emerged, either taking advantage of vibration energy or electromagnetic energy, or even both. A vibration energy harvester composed by a cantilever beam, a magnetic circuit, formed by four NdFeB magnets and two magnetic yokes, and four ME laminate ceramic composite of Terfenol-D/Pb($Mg_{1/3}Nb_{2/3}$)O_3–PbTiO$_3$ (PMN-PT)/Terfenol-D were proposed by Dai *et al*. When the harvester is excited by an external vibration, the magnetic circuit moves relatively to the transducer causing magnetic field variations at the magnetostrictive layers, generating stress, which is transmitted to the piezoelectric layer, generating electrical power. The authors first used just one ME composite, achieving 1.44 mW at 26.2 Hz with 1 g acceleration across a 3585 kΩ resistor. Then, they compared these results with the ones obtained with the system with four ME composites samples verifying that it can produce 7.13 mW, across 803 kΩ resistor, from an acceleration of 2.5 g at a resonant frequency of 31 Hz. The output power density of the prototype was 1.1 mW·cm^{-3} [55]. A non-resonant vibration energy harvesting, adapted to harvest energy from low frequency vibrations such as human-body-induced motion, was developed with a NdFeB spherical permanent magnet as a springless proof mass and a ME laminate structure of magnetic shape memory alloy (MSMA)/macro fibre composite (MFC)/MSMA. The devices were tested for d_{31} and d_{33} mode MFC at a 3 g acceleration. For device with d_{31} mode MFC the maximum peak-to-peak open circuit

voltages was 4.92 V at 20 Hz and maximum output power reached 11.2 µW across a 800 Ω resistor. For the device with d_{33} mode MFC the maximum peak-to-peak open circuit voltages was 16.4 V at 15 Hz and maximum output power of 0.98 µW has been obtained across a 80 kΩ resistor. The intentional manual vibration was also tested by authors reaching a maximum peak-to-peak open circuit voltage of 15.12 V and a maximum output power of 82.5 µW across a 800 Ω resistor. The output power density of the fabricated device was 37.3 µW·cm^{-3}. The authors also analysed the contributions of various power generation mechanisms involved in the proposed device. A maximum power output of 245.6 µW and a power density of 118.3 µW·cm^{-3} were obtained for the device with MSMA attached to a MFC cantilever and tungsten carbide ball as a springless proof mass [56].

A ME laminate composite of FeBSiC alloy and PZT fibres mounted on a cantilever beam structure with a tip mass was used to demonstrate that ME composites can harvest both mechanical and magnetic energies. At a frequency of 20 Hz the ME was subjected just to a H_{ac} of 2 Oe, without any mechanical vibrations, generating ≈4 V$_{pp}$ and 0.5 µW·Oe^{-1}·cm^{-3} across a 5 MΩ resistor. The voltage induced at the first bending mode by a mechanical vibration with an acceleration of 0.5 g at 20 Hz without any applied magnetic field was ≈4 V$_{pp}$ and the electric power generated was 0.5 µW·Oe^{-1}·cm^{-3} across a 5 MΩ resistor. When a H_{ac} of 2 Oe and a mechanical vibration of 0.5 g were applied simultaneously the output voltage was ≈8 Vpp [57]. Another structure formed by a cantilever with a Ni beam bonded to a MFC piezoelectric material by an epoxy resin and a series of Ni disks added as tip mass at the free end of cantilever was used to harnessing energy from both vibrations and ac magnetic field at the same time without the need of a dc bias. To quantify the contribution of each type of energy, the open circuit voltage of the energy harvesting at the first three resonance frequency (22.5 Hz, 157.4 Hz and 507.4 Hz) was measured separately under only magnetic field active condition (H_{ac} = 1 Oe), only vibration active condition (a = 0.05 g) and the dual-phase mode (1 Oe and 0.05 g). For the first resonance frequency of 22.5 Hz the voltage harvested by vibration (8.3 V) was much higher than the harvested by magnetic field (0.28 V). However at 507.4 Hz the voltage harvester by magnetic field (2.07 V) was higher than the harvester by vibration (0.56 V). This behaviour results from the strain variation along the ME cantilever structure due to transversal excitation, where the contribution of vibration energy was higher, and longitudinal excitation, which depends of the magnetostriction. The authors

conclude further that the dual-phase mode can harvest approximately the sum of the two energies [58].

A ME formed by Terfenol-D/PZT/Terfenol-D laminate was developed to scavenge energy from the power lines. This noncontact energy harvester uses a magnetic circuit (with four NdFeB magnets and two magnetic yokes) and a Halbach array (with three specially arranged NdFeB magnets) mounted on the free end of a cantilever beam. For a current of 5 A the maximum output power generated by the system was 523 µW under the optimal load resistance of 896 kΩ [59]. A ME transducer formed by Terfenol-D and PZT plates on an ultrasonic horn substrate of Be-bronze were designed to generate electricity from electromagnetic energy and drive a wireless sensor network. The high-Q ultrasonic horn allow decrease the energy loss and gather up the energy at resonance frequency. Using a H_{dc} of 800 Oe and a H_{ac} with a peak-to-peak magnitude of 1 Oe at the resonance frequency of 27 kHz, the structure exhibits a ME voltage coefficient of 2 V·Oe^{-1} and a ME power coefficient of 20 µW·Oe^{-1} [52].

Although the high number of works in ME transducers and structures for energy harvesting systems in ME ceramic laminate composites, there are just few studies focusing on polymer-based ME composites. A ME composite of $Fe_{64}Co_{17}Si_7B_{12}$ amorphous alloy and PVDF in a MPM configuration was used to evaluate a polymer-based ME composite as energy harvester system of electromagnetic energy in the range of low frequency (LF), as well as the effect of the length of the ME laminate on power output. Samples with 3, 1 and 0.5 cm can produce 6.4 µW for a H_{ac} of 0.45 Oe, 0.30 µW for a H_{ac} of 0.11 Oe, and 0.04 µW for a H_{ac} of 0.06 Oe, respectively. The resonance frequency and the H_{dc} increase with decreasing sample length, being 46.8 kHz and 4.7 Oe for 3 cm long ME, 172 kHz and 17.6 Oe for 1 cm long ME, and 337 kHz and 34.5 Oe for 0.5 cm long ME [60].

An energy harvesting system that suffers variations of power and voltage over the time cannot power directly circuits. An adequate power management circuit is in this way required, and in the case of vibration and electromagnetic energy harvesters, where the voltage produced is ac, it should use an ac–dc converter [44]. A simple full-wave bridge voltage rectifier with a filter capacitor [61] or a voltage multitier circuit can be used to convert the ME ac voltage induced on the laminated composite into a dc voltage suitable for low-power electronic devices. The voltage multiplier circuit apart from rectifying the voltage induced into the ME composite, amplifies it in order to obtain sufficient voltage to charge a battery [60]. The performance of five interface circuits, a full-wave bridge

rectifier, two Cockcroft–Walton voltage multipliers (with 1 and 2 stages) and two Dickson voltage multipliers (with 2 and 3 stages), was evaluated to optimize the output power of a polymer-based ME composite formed by $Fe_{61.6}Co_{16.4}Si_{10.8}B_{11.2}$/PVDF/$Fe_{61.6}Co_{16.4}Si_{10.8}B_{11.2}$. The maximum output power was 12.3 µW for a load resistance of 180 kΩ, obtained with 2 stages Dickon voltage multiplier. The full-wave bridge rectifier obtained the lowest output power of 7.8 µW under a 12 kΩ resistor [62].

Li *et al*. presented different circuits designed for wireless sensor network, either using vibration or electromagnetic energy [52, 63-65]. In an electromagnetic energy harvester a strong magnetic generator and a magnetic antenna were used to provide the enough magnetic energy for the ME transducer, due to the small magnetic energy-flux density (<10 µW·cm^{-2}) and intensity of magnetic field (<1 µT) in the natural environment. As a consequence, it is difficult to realize an energy harvesting system by using a small ME energy harvesting device. In addition to the ac–dc converter, a matching and stepping-up circuit, formed by a transformer and a tuning capacitor, have been used to improve the maximum output power and voltage of ME transducer. Moreover, after the rectifier circuit, and due to the weak output of the transducer that makes impossible to power directly a wireless sensor network node by just use a matching and stepping-up circuit, a switching capacitor network [52] or an instantaneous-discharge circuit [63] were proposed. The switching capacitor network allows to charge the storage capacitors in parallel, and when the voltage across the capacitors achieves a threshold, the capacitors are switched and the capacitor is discharged. The discharging time was controlled according to the power consumption and operation cycle of the load. With a charging period of 26 min and a discharge time of 620 ms, the authors obtained an output voltage with the sensor node load of 3 V that can drive a wireless sensor node having a power consumption of 75 mW at transmitting and 1 mW at receiving [52]. The use of a power instantaneous-discharge circuit, composed of a separated excited flyback step-up circuit and a burst-signal generator, allows to power a wireless sensor node with an operation time of 620 ms and a power of 18 mW during the data reception and a transmission time of 5 ms and power of 75 mW during the data transmission. The charging voltage across the storage supercapacitor at a charging time of 26 min was 0.45 V [63]. A management circuit for vibration energy harvester with an upconversion matching circuit, two rectifiers, a storing capacitor, a control circuit, a burst generator and an instantaneous pulse discharge circuit were proposed to improve the results of conventional management circuits that due to the lower operating frequency have a very large matching inductance

($\approx$9000 H) and a very large size. The harvester with a vibrating acceleration of 1 g can drive a wireless sensor node with an output power of 110 mW [64]. A management circuit using a multiwinding upconversion current transformer for power-line energy harvesting has been also proposed. It allows to power a wireless sensor node with an operation time of 200 ms and a power of 18 mW during the data reception and a transmission time of 4 ms and power of 60 mW during the data transmission. The charging voltage across the storage supercapacitor at a charging time of 19 min was 3.51 V [65].

2.5   Polymer-based magnetoelectric antennas

ME materials are extremely attractive for applications as antennas, similar to the one designed by Wang *et* al. (Figure 2.6) [66].
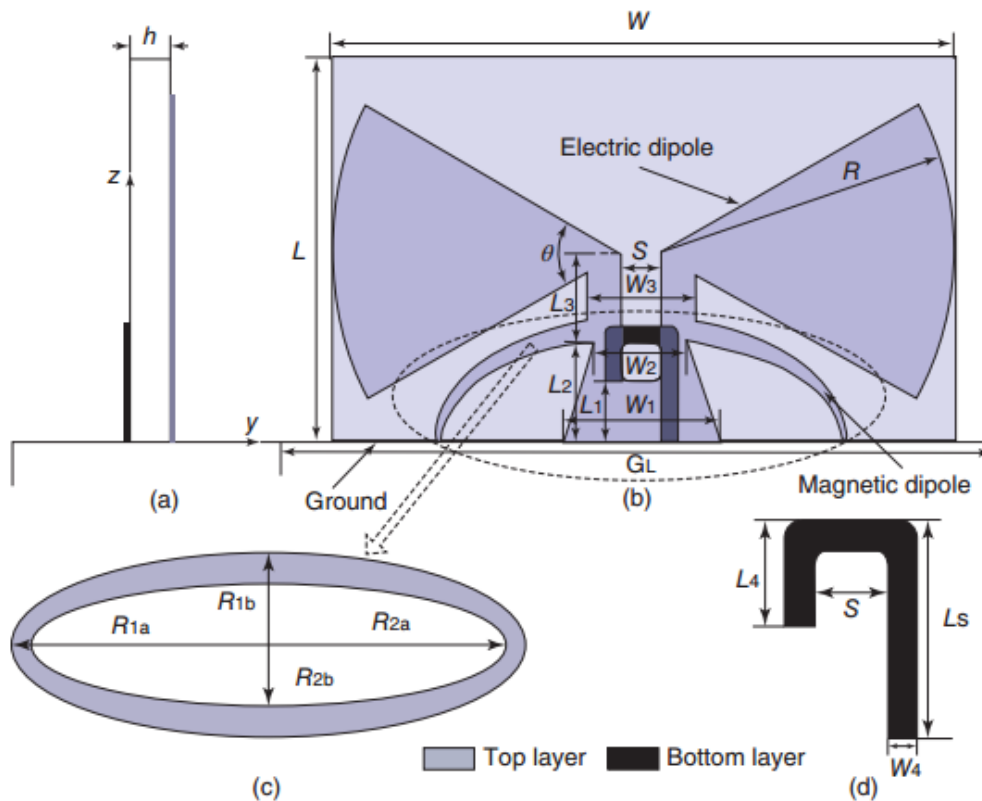
Figure 2.6. Geometry of the proposed antenna. (a) x-axis side view; (b) y-axis side view; (c) structure of elliptical ring; and (d) part of transition balloon at the bottom layer [66].

The design and characterization of a miniaturized 100 MHz antenna based on ME composites was first reported by Petrov *et al.* [67]. Nickel zinc ferrite/bismuth strontium titanate composites with high and equal permeability (μ_r) and permittivity (ε_r) have been synthesized and used as the substrate for a microstrip antenna. The composite produced

by ceramic processing also facilitates impedance matching to free space. The dipole antenna consisted of a composite substrate with a diameter of 22 cm and thickness of 0.85 cm. Scattering parameter data have shown an antenna miniaturization factor of 7 –10 at 100 MHz, in agreement with the proposed theory.

Knowing that achieving relative permeability larger than 1 in antenna substrates can lead to antenna miniaturization, enhanced bandwidth, and tunable resonant frequencies, metallic magnetic films and self-biased ferrite films were introduced as a practical means to tune a patch antenna by loading a commercially available substrate [68]. Novel antenna designs with metallic magnetic films and self-biased NiCo-ferrite films were also discussed. Magnetic patch antennas were demonstrated at 2.1 GHz with a tuning resonant frequency range of 5–10 MHz (with the metallic magnetic films) and 7–23 MHz (with self-biased ferrite films). Three different cases of annular ring antennas with NiCo-ferrite films loading have also been designed, fabricated, and evaluated. The optimized ME antennas with self-biased magnetic films can realize a tuning range of 3–20 MHz, which shifts from 1.72 to 1.717 GHz and 1.70 GHz, indicating that self-biased magnetic films do lead to minimized antenna by shifting down the resonant frequency.

Challenged by the stringent requirements imposed on the performance of base station antennas for mobile communications, the magnetoelectric dipole was invented. The antenna composed of a planar electric dipole and a triangular-shaped loop antenna has a small thickness of 0.16 λ_0, a wide bandwidth of about 40% (standing-wave ratio (SWR) ≤ 1.5) and a stable gain of around 8.4 dBi [69]. The radiation pattern of the antenna is stable across all the working frequencies, with low back radiation. The developed antenna was dc grounded, which fulfilled the requirement for applications in outdoor base stations of mobile communication stations. Such innovative designs can easily be modified to operate with other polarizations. More significantly, the results presented in this paper confirmed the strength of the complementary antenna concept for developing high-performance ME antennas for modern wireless communications.

The same ME dipole approach was used in the development of a novel dual-wideband double layer. Unidirectional antenna with a modified horned reflector for second-generation (2G)/third-generation (3G)/long-term evolution (LTE) applications is proposed. The design has been verified through measurements on a prototype of the antenna. The results show good performance in terms of wider bandwidth and stable gain, which are 24.4% (790–1010 MHz) and 7.2 ± 0.6 dBi for the lower band, 67.3% (1.38–2.78 GHz) and 7.5 ± 0.8 dBi for the upper band. Furthermore, both simulated and

measured results show low cross-polarization, low back radiation, and symmetrical *E*- and *H*-plane patterns. Moreover, compared with the existing ME dipole antennas, the proposed antenna, which is completely made of copper, can be easily fabricated at low cost and hence is suitable for 2G/3G/LTE systems [70].

One consequence of the previous work was the design of a novel broadband ±45° dual-polarized antenna composed of four square metallic plates, four rectangular metallic posts, two orthogonal Γ-shaped probes, and a box-shaped reflector [71]. The estimated overlapped impedance bandwidth is 48% with a SWR ≤ 1.5 in the 1.69–2.76 GHz range. The obtained gains vary from 7.6 to 9.3 dBi and from 7.6 to 9.4 dBi for port 1 and port 2, respectively. The isolation between the two ports is higher than 30 dB. The suggested antenna accomplishes a low cross-polarization level of less than ≈-20 dB and a low back radiation level of less than ≈-30 dB over the operating frequency range. With a broadband 90° phase shifter and a power divider, the optimized antenna can radiate circularly polarized (CP) wave and exhibits a wide impedance bandwidth (SWR ≤ 2) of 90% in the 1.23–3.23 GHz range, which covers the whole 3-dB axial-ratio (AR) bandwidth of 82% from 1.28 to 3.05 GHz. In such a working frequency band, the projected CP antenna has a broadside gain higher than 5 dBi for frequencies ≥ 1.45 GHz. By analysing the common overlapped bandwidth limited by the impedance, AR, and gain, it is concluded that the produced ME antenna exhibits an effective bandwidth of ≈70%. Such features validate the use of dual-polarized and CP antennas on mobile and wireless communications applications.

After the successful work on ceramic-based ME antennas, similar concepts were embedded in investigations on polymer-based ME composites.

In this way, cobalt/polymer magnetic nanocomposites have been synthesized and characterized for their microstructure and properties (permeability, permittivity, dielectric, and magnetic losses) from 100 MHz to 2 GHz to study their suitability as polymer-based ME antenna [72]. Oxide-passivated cobalt nanoparticles were dispersed in epoxies to form nanocomposite toroids and thin-film resonator structures on organic substrates. Permeabilities of 2.10 and 2.65 were measured up to 500 MHz, respectively, with 25–50 and 5 nm nanoparticles in the nanocomposites. The loss tangent ranged from 0.02 to 0.04 at these frequencies. A combination of stable permeability of ∼2 at 1–2 GHz and permittivity of ∼7 was achieved with nanocomposites having 5 nm cobalt nanoparticles. The magnetic nanomaterials described in this work can overcome the

limitations from domain-wall and eddy-current losses in microscale metal–polymer composites, leading to enhanced frequency stability.

Keeping in mind the development of polymer-based ME antennas, ME response at the radio frequency range has been studied as a function of temperature [73]. For that purpose, fabricated laminate composites comprising $Fe_{61.6}Co_{16.4}Si_{10.8}B_{11.2}$ alloy as the magnetostrictive element and PVDF as the piezoelectric one were utilized. The $Fe_{61.6}Co_{16.4}Si_{10.8}B_{11.2}$ amorphous ribbons exhibited good magnetic properties, with a magnetostriction close to 30 ppm and a piezomagnetic coefficient in as-quenched state, for a long ribbon of 21.4×10^{-3} ppm·A·m^{-1}. Such values, already within the radio frequency range, render such short laminated composites very interesting in applications related to near-field communications.

The high temperature features of such antennas can be optimized by using high-temperature polyamides and copolyamides that exhibit high temperature stability.

2.6 Polymer-based magnetoelectric memories

To fulfill the intense demand of multimedia storage, many efforts are being made to develop storage technologies with higher storage speed and density [74]. In two-state (0–1) memories, the memory material is a magnetic tunnel junction that involves an insulating tunnel barrier sandwiched by two magnetic electrodes [75]. The resistance of those junctions highly depends on the relative orientation of the magnetic moments, which is used to regulate the memory state (0 or 1) [76]. Such coded magnetic bits can then be read out nondestructively by detecting the resistance changes; nevertheless, in the writing procedure, the magnetic bits are typically encoded by the use of high magnetic fields, which is a process relatively slow and energetically expensive [77]. Such setbacks can be overcome with the manipulation of the magnetization direction by the use of an electric field, taking advantage of the ME effect (Figure 2.7) [78].
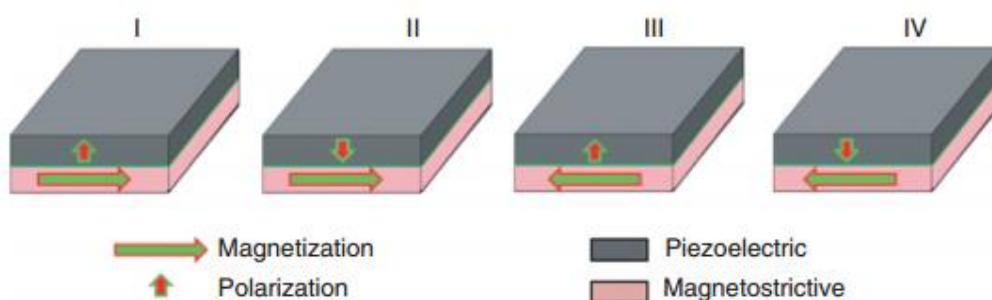
Figure 2.7. Representation of a four states memory based on ME materials [4].

For this new kind of multistate memory, the multiferroicity is the essential element for the information storage, while the ME or the magnetodielectric effect is the mechanism for the reading and writing methods [79].

Such four-state memory was introduced with the development of the ME PZT/Co bilayer composite [79]. Co was used for its proven capability in magnetic recording and PZT for its appropriate ferroelectric properties. The composite was obtained by direct bonding of one layer of PZT to other layer of Co with an epoxy binder. The polarization and magnetization states of the PZT/Co bilayer composite can be controlled by the application of magnetic/electric fields and the combination between the remnant ferroelectric polarization and magnetization. Results have shown four-state memory signals of 15.8, -4.4, 5.5, and -11.3 µV, which demonstrate the huge potential of the ME PZT/Co bilayer.

Tiercelin *et al.* proposed a different concept aiming to obtain a room temperature ME memory [80]. By depositing a magnetoelastic nanostructured multilayer (TbCo$_2$(5 nm)/FeCo(5 nm)) with the required uniaxial characteristic onto a commercial piezoelectric actuator (from Piezomechanik Gmbh.), the effective anisotropy of the magnetic element was controlled by the applied voltage and used to switch magnetization from one state to another, as a result of the inverse magnetostrictive effect. Preliminary simulations have shown that the properties of the existing materials are compatible with the development of the nanoscale devices [81]. By size reduction, densities up to 40 Gbits·cm^{-2} (for each layer), low energy, and nonvolatile memories are expected. Given the very low expected power, such a device is a strong candidate for vertical integration of several layers, quickly increasing the memory density.

Knowing that the in-progress electronic market demands are closely related to the use of flexible and elastic materials [82], not only the magnetic and ferroelectric properties of materials but also their mechanical properties will play a crucial role in the future [83]. Thus the replacement of the piezoelectric PZT by a piezoelectric polymer in four-state ME memories will meet such challenges [84]. Electroactive polymers can be deposited by inkjet printing, spin coating, or vacuum evaporation on a multiplicity of substrates for the fabrication of memories [85]. In this way, polymers, may also acquire in the near future a more central status in the memory market due to development in polymer-based four-state ME memory devices [4]. Once magnetic and electric fields are used for writing information in four-state ME memories and the ME coefficient is used for reading with the help of a very small bias magnetic field, the ME voltage coefficient

is decisive in the applicability of these new kinds of memories. It is shown in the literature that materials with ME coefficients in the order of 30 mV·cm^{-1}·Oe^{-1} can be used as components for room-temperature four-state ME memory prototypes [86].

In this scope and changing the PZT used by Shi *et al.* [79] by P(VDF-TrFE), Zhao *et al.* reported the ferroelectric control of magnetism in P(VDF-TrFE)/Co heterostructures [87] by observing large magnetization changes of the Co films in response to the ferroelectric switching of P(VDF-TrFE) controlled by an applied electric field (30 V).

Consequently, and after an analysis of the ME coefficients obtained from the different methodologies for the development of polymer-based ME composites, it is possible to verify that almost all of them can be used in the optimization of this kind of multistate memories [4].

2.7 References

[1]   N. Ortega, A. Kumar, J. F. Scott, and R. S. Katiyar, "Multifunctional magnetoelectric materials for device applications," *Journal of Physics Condensed Matter,* vol. 27, 2015.

[2]   J. F. Scott, "Applications of magnetoelectrics," *Journal of Materials Chemistry,* vol. 22, pp. 4567-4574, 2012.

[3]   P. Martins, C. M. Costa, G. Botelho, S. Lanceros-Mendez, J. M. Barandiaran, and J. Gutierrez, "Dielectric and magnetic properties of ferrite/poly(vinylidene fluoride) nanocomposites," *Materials Chemistry and Physics,* vol. 131, pp. 698-705, 2012.

[4]   P. Martins and S. Lanceros-Méndez, "Polymer-based magnetoelectric materials," *Advanced Functional Materials,* vol. 23, pp. 3371-3385, 2013.

[5]   G. Srinivasan, "Magnetoelectric composites," in *Annual Review of Materials Research* vol. 40, ed, 2010, pp. 153-178.

[6]   C. W. Nan, M. I. Bichurin, S. Dong, D. Viehland, and G. Srinivasan, "Multiferroic magnetoelectric composites: Historical perspective, status, and future directions," *Journal of Applied Physics,* vol. 103, 2008.

[7]   J. Gröttrup, S. Kaps, J. Carstensen, D. Smazna, Y. K. Mishra, A. Piorra, *et al.*, "Piezotronic-based magnetoelectric sensor: Fabrication and response," *Physica Status Solidi (A) Applications and Materials Science,* vol. 213, pp. 2208-2215, 2016.

[8]   M. J. Caruso, T. Bratland, C. H. Smith, and R. Schneider, "A new perspective on magnetic field sensing," *Sensors (Peterborough, NH),* vol. 15, pp. 34-46, 1998.

[9]   P. Ripka, "Sensors based on bulk soft magnetic materials: Advances and challenges," *Journal of Magnetism and Magnetic Materials,* vol. 320, pp. 2466-2473, 2008.

[10]   C. W. Nan, M. Li, X. Feng, and S. Yu, "Possible giant magnetoelectric effect of ferromagnetic rare-earth-iron-alloys-filled ferroelectric polymers," *Applied Physics Letters,* vol. 78, pp. 2527-2529, 2001.

[11] P. Martins, A. Lasheras, J. Gutierrez, J. M. Barandiaran, I. Orue, and S. Lanceros-Mendez, "Optimizing piezoelectric and magnetoelectric responses on CoFe2O4/P(VDF-TrFE) nanocomposites," *Journal of Physics D: Applied Physics,* vol. 44, 2011.

[12] D. Guyomar, D. F. Matei, B. Guiffard, Q. Le, and R. Belouadah, "Magnetoelectricity in polyurethane films loaded with different magnetic particles," *Materials Letters,* vol. 63, pp. 611-613, 2009.

[13] J. Zhai, S. Dong, Z. Xing, J. Li, and D. Viehland, "Giant magnetoelectric effect in Metglas/polyvinylidene-fluoride laminates," *Applied Physics Letters,* vol. 89, 2006.

[14] M. P. Silva, P. Martins, A. Lasheras, J. Gutiérrez, J. M. Barandiarán, and S. Lanceros-Mendez, "Size effects on the magnetoelectric response on PVDF/Vitrovac 4040 laminate composites," *Journal of Magnetism and Magnetic Materials,* vol. 377, pp. 29-33, 2015.

[15] J. Fraden, *Handbook of modern sensors: Physics, designs, and applications*: Springer, 2016.

[16] P. Martins, X. Moya, L. C. Phillips, S. Kar-Narayan, N. D. Mathur, and S. Lanceros-Mendez, "Linear anhysteretic direct magnetoelectric effect in Ni 0.5Zn0.5Fe2O4/poly(vinylidene fluoride-trifluoroethylene) 0-3 nanocomposites," *Journal of Physics D: Applied Physics,* vol. 44, 2011.

[17] F. Li, F. Zhao, Q. M. Zhang, and S. Datta, "Low-frequency voltage mode sensing of magnetoelectric sensor in package," *Electronics Letters,* vol. 46, pp. 1132-1134, 2010.

[18] Z. Fang, N. Mokhariwale, F. Li, S. Datta, and Q. M. Zhang, "Magnetoelectric sensors with directly integrated charge sensitive readout circuit-improved field sensitivity and signal-to-noise ratio," *IEEE Sensors Journal,* vol. 11, pp. 2260-2265, 2011.

[19] S. Reis, M. P. Silva, N. Castro, V. Correia, P. Martins, A. Lasheras*, et al.*, "Characterization of Metglas/poly(vinylidene fluoride)/Metglas magnetoelectric laminates for AC/DC magnetic sensor applications," *Materials and Design,* vol. 92, pp. 906-910, 2016.

[20] S. Chen, X. Yang, J. Ouyang, G. Lin, F. Jin, and B. Tong, "Fabrication and characterization of shape anisotropy AlN/FeCoSiB magnetoelectric composite films," *Ceramics International,* vol. 40, pp. 3419-3423, 2014.

[21] P. Martins, A. Larrea, R. Gonçalves, G. Botelho, E. V. Ramana, S. K. Mendiratta*, et al.*, "Novel anisotropic magnetoelectric effect on δ-FeO(OH)/P(VDF-TrFE) multiferroic composites," *ACS Applied Materials and Interfaces,* vol. 7, pp. 11224-11229, 2015.

[22] R. Jahns, A. Piorra, E. Lage, C. Kirchhof, D. Meyners, J. L. Gugat*, et al.*, "Giant magnetoelectric effect in thin-film composites," *Journal of the American Ceramic Society,* vol. 96, pp. 1673-1681, 2013.

[23] X. W. Dong, B. Wang, K. F. Wang, J. G. Wan, and J. M. Liu, "Ultra-sensitive detection of magnetic field and its direction using bilayer PVDF/Metglas laminate," *Sensors and Actuators, A: Physical,* vol. 153, pp. 64-68, 2009.

[24] Z. Xing, J. Li, and D. Viehland, "Modeling and the signal-to-noise ratio research of magnetoelectric sensors at low frequency," *Applied Physics Letters,* vol. 91, 2007.

[25] R. Jahns, H. Greve, E. Woltermann, E. Quandt, and R. H. Knöchel, "Noise performance of magnetometers with resonant thin-film magnetoelectric sensors,"

IEEE Transactions on Instrumentation and Measurement, vol. 60, pp. 2995-3001, 2011.

[26]   Z. P. Xing, J. Y. Zhai, S. X. Dong, J. F. Li, D. Viehland, and W. G. Odendaal, "Modeling and detection of quasi-static nanotesla magnetic field variations using magnetoelectric laminate sensors," *Measurement Science and Technology,* vol. 19, 2008.

[27]   S. Ziegler, R. C. Woodward, H. H. C. Iu, and L. J. Borle, "Current sensing techniques: A review," *IEEE Sensors Journal,* vol. 9, pp. 354-376, 2009.

[28]   P. Ripka, "Electric current sensors: A review," *Measurement Science and Technology,* vol. 21, 2010.

[29]   J. T. Zhang, Y. M. Wen, and P. Li, "A passive current sensor employing self-biased magnetoelectric transducer and high-permeability nanocrystalline flux concentrator," *Rare Metals,* 2015.

[30]   S. Dong, J. F. Li, and D. Viehland, "Circumferentially magnetized and circumferentially polarized magnetostrictive/piezoelectric laminated rings," *Journal of Applied Physics,* vol. 96, pp. 3382-3387, 2004.

[31]   S. Dong, J. F. Li, and D. Viehland, "Vortex magnetic field sensor based on ring-type magnetoelectric laminate," *Applied Physics Letters,* vol. 85, pp. 2307-2309, 2004.

[32]   J. Zhang, P. Li, Y. Wen, W. He, A. Yang, and C. Lu, "Packaged current-sensing device with self-biased magnetoelectric laminate for low-frequency weak-current detection," *Smart Materials and Structures,* vol. 23, 2014.

[33]   C. Lu, P. Li, Y. Wen, A. Yang, C. Yang, D. Wang, *et al.*, "Magnetoelectric composite metglas/PZT-based current sensor," *IEEE Transactions on Magnetics,* vol. 50, 2014.

[34]   X. Yu, G. Lou, H. Chen, C. Wen, and S. Lu, "A Slice-Type Magnetoelectric Laminated Current Sensor," *IEEE Sensors Journal,* vol. 15, pp. 5839-5850, 2015.

[35]   L. Ionov, "Polymeric actuators," *Langmuir,* vol. 31, pp. 5015-5024, 2015.

[36]   T. Ueno, J. Qiu, and J. Tani, "Magnetic Force Control with Composite of Giant Magnetostrictive and Piezoelectric Materials," *IEEE Transactions on Magnetics,* vol. 39, pp. 3534-3540, 2003.

[37]   T. Ueno and T. Higuchi, "Zero-power magnetic levitation using composite of magnetostrictive/ piezoelectric materials," *IEEE Transactions on Magnetics,* vol. 43, pp. 3477-3482, 2007.

[38]   T. Ueno, C. S. Keat, and T. Higuchi, "Linear step motor based on magnetic force control using composite of magnetostrictive and piezoelectric materials," *IEEE Transactions on Magnetics,* vol. 43, pp. 11-14, 2007.

[39]   O. Geoffroy, D. O'Brien, O. Cugat, and J. Delamare, "Practical and theoretical investigations of a rotating coilless actuator using the inverse magnetostrictive effect," *IEEE Transactions on Magnetics,* vol. 46, pp. 606-609, 2010.

[40]   E. Smela, "Conjugated polymer actuators for biomedical applications," *Advanced Materials,* vol. 15, pp. 481-494, 2003.

[41]   Y. Wang and J. Atulasimha, "A dexterous surgical manipulation tool using self-sensing magnetoelectric actuators," in *ASME 2010 Conference on Smart Materials, Adaptive Structures and Intelligent Systems, SMASIS 2010*, 2010, pp. 767-771.

[42]   J. Clarke and V. B. Sundaresan, "Design and fabrication of a microscale magnetoelectric surgical tool," in *Proceedings of SPIE - The International Society for Optical Engineering*, 2011.

[43]   C. Ribeiro, V. Correia, P. Martins, F. M. Gama, and S. Lanceros-Mendez, "Proving the suitability of magnetoelectric stimuli for tissue engineering applications," *Colloids and Surfaces B: Biointerfaces,* vol. 140, pp. 430-436, 2016.

[44]   R. J. M. Vullers, R. van Schaijk, I. Doms, C. Van Hoof, and R. Mertens, "Micropower energy harvesting," *Solid-State Electronics,* vol. 53, pp. 684-693, 2009.

[45]   S. P. Beeby, M. J. Tudor, and N. M. White, "Energy harvesting vibration sources for microsystems applications," *Measurement Science and Technology,* vol. 17, 2006.

[46]   J. W. Matiko, N. J. Grabham, S. P. Beeby, and M. J. Tudor, "Review of the application of energy harvesting in buildings," *Measurement Science and Technology,* vol. 25, 2014.

[47]   S. Roundy, P. K. Wright, and J. Rabaey, "A study of low level vibrations as a power source for wireless sensor nodes," *Computer Communications,* vol. 26, pp. 1131-1144, 2003.

[48]   G. Zhou, L. Huang, W. Li, and Z. Zhu, "Harvesting ambient environmental energy for wireless sensor networks: A survey," *Journal of Sensors,* vol. 2014, 2014.

[49]   M. A. Hannan, S. Mutashar, S. A. Samad, and A. Hussain, "Energy harvesting for the implantable biomedical devices: Issues and challenges," *BioMedical Engineering Online,* vol. 13, 2014.

[50]   J. Ma, J. Hu, Z. Li, and C. W. Nan, "Recent progress in multiferroic magnetoelectric composites: From bulk to thin films," *Advanced Materials,* vol. 23, pp. 1062-1087, 2011.

[51]   S. Priya, J. Ryu, C. S. Park, J. Oliver, J. J. Choi, and D. S. Park, "Piezoelectric and magnetoelectric thick films for fabricating power sources in wireless sensor nodes," *Sensors,* vol. 9, pp. 6362-6384, 2009.

[52]   P. Li, Y. Wen, P. Liu, X. Li, and C. Jia, "A magnetoelectric energy harvester and management circuit for wireless sensor network," *Sensors and Actuators, A: Physical,* vol. 157, pp. 100-106, 2010.

[53]   F. L. Boughey and S. Kar-Narayan, "Applications of polymer based magnetoelectric materials: Energy harvesting," in *Magnetoelectric Polymer-Based Composites: Fundamentals and Applications*, S. Lanceros-Mendez and P. Martins, Eds., ed: John Wiley & Sons, Ltd., 2017.

[54]   J. Huang, R. C. O'Handley, and D. Bono, "New, high-sensitivity, hybrid magnetostrictive/electroactive magnetic field sensors," in *Proceedings of SPIE - The International Society for Optical Engineering*, 2003, pp. 229-237.

[55]   X. Dai, Y. Wen, P. Li, J. Yang, and M. Li, "Energy harvesting from mechanical vibrations using multiple magnetostrictive/piezoelectric composite transducers," *Sensors and Actuators, A: Physical,* vol. 166, pp. 94-101, 2011.

[56]   S. Ju, S. H. Chae, Y. Choi, and C. H. Ji, "Macro fiber composite-based low frequency vibration energy harvester," *Sensors and Actuators, A: Physical,* vol. 226, pp. 126-136, 2015.

[57]   S. Dong, J. Zhai, J. F. Li, D. Viehland, and S. Priya, "Multimodal system for harvesting magnetic and mechanical energy," *Applied Physics Letters,* vol. 93, 2008.

[58]   Y. Zhou, D. J. Apo, and S. Priya, "Dual-phase self-biased magnetoelectric energy harvester," *Applied Physics Letters,* vol. 103, 2013.

[59] W. He, P. Li, Y. Wen, J. Zhang, A. Yang, and C. Lu, "A noncontact magnetoelectric generator for energy harvesting from power lines," *IEEE Transactions on Magnetics,* vol. 50, 2014.

[60] A. Lasheras, J. Gutiérrez, S. Reis, D. Sousa, M. Silva, P. Martins*, et al.*, "Energy harvesting device based on a metallic glass/PVDF magnetoelectric laminated composite," *Smart Materials and Structures,* vol. 24, 2015.

[61] A. Bayrashev, W. P. Robbins, and B. Ziaie, "Low frequency wireless powering of microsystems using piezoelectric- magnetostrictive laminate composites," *Sensors and Actuators, A: Physical,* vol. 114, pp. 244-249, 2004.

[62] S. Reis, M. P. Silva, N. Castro, V. Correia, J. G. Rocha, P. Martins*, et al.*, "Electronic optimization for an energy harvesting system based on magnetoelectric Metglas/poly(vinylidene fluoride)/Metglas composites," *Smart Materials and Structures,* vol. 25, 2016.

[63] P. Li, Y. Wen, C. Jia, and X. Li, "A magnetoelectric composite energy harvester and power management circuit," *IEEE Transactions on Industrial Electronics,* vol. 58, pp. 2944-2951, 2011.

[64] P. Li, Y. Wen, W. Yin, and H. Wu, "An upconversion management circuit for low-frequency vibrating energy harvesting," *IEEE Transactions on Industrial Electronics,* vol. 61, pp. 3349-3358, 2014.

[65] P. Li, Y. Wen, Z. Zhang, and S. Pan, "A High-Efficiency Management Circuit Using Multiwinding Upconversion Current Transformer for Power-Line Energy Harvesting," *IEEE Transactions on Industrial Electronics,* vol. 62, pp. 6327-6335, 2015.

[66] H. Wang, Z. R. Gou, L. Zhang, S. F. Liu, and X. Wei Shi, "A novel broadband magnetoelectric antenna," *International Journal of RF and Microwave Computer-Aided Engineering,* vol. 25, pp. 213-218, 2015.

[67] R. V. Petrov, A. S. Tatarenko, S. Pandey, G. Srinivasan, J. V. Mantese, and R. Azadegan, "Miniature antenna based on magnetoelectric composites," *Electronics Letters,* vol. 44, pp. 506-508, 2008.

[68] G. M. Yang, X. Xing, A. Daigle, M. Liu, O. Obi, J. W. Wang*, et al.*, "Electronically tunable miniaturized antennas on magnetoelectric substrates with enhanced performance," *IEEE Transactions on Magnetics,* vol. 44, pp. 3091-3094, 2008.

[69] K. M. Luk and B. Wu, "The magnetoelectric dipolea wideband antenna for base stations in mobile communications," *Proceedings of the IEEE,* vol. 100, pp. 2297-2307, 2012.

[70] B. Feng, W. Hong, S. Li, W. An, and S. Yin, "A dual-wideband double-layer magnetoelectric dipole antenna with a modified horned reflector for 2G/3G/LTE applications," *International Journal of Antennas and Propagation,* vol. 2013, 2013.

[71] M. Li and K. M. Luk, "Wideband magnetoelectric dipole antennas with dual polarization and circular polarization," *IEEE Antennas and Propagation Magazine,* vol. 57, pp. 110-119, 2015.

[72] P. M. Raj, H. Sharma, G. P. Reddy, N. Altunyurt, M. Swaminathan, R. Tummala*, et al.*, "Cobalt-polymer nanocomposite dielectrics for miniaturized antennas," *Journal of Electronic Materials,* vol. 43, pp. 1097-1106, 2014.

[73] A. Lasheras, J. G. Etxebarria, A. Maceiras, M. S. Sebastián, J. M. Barandiarán, J. L. Vilas*, et al.*, "Radio Frequency Magnetoelectric Effect Measured at High Temperature," *IEEE Transactions on Magnetics,* vol. 51, 2015.

[74]   K. H. Burrell, D. H. Kaplan, P. Gohil, D. G. Nilson, R. J. Groebner, and D. M. Thomas, "Improved charge coupled device detectors for the edge charge exchange spectroscopy system on the DIII-D tokamak," *Review of Scientific Instruments,* vol. 72, pp. 1028-1033, 2001.

[75]   Z. H. U. Jian-Gang, "Magnetoresistive random access memory: The path to competitiveness and scalability," *Proceedings of the IEEE,* vol. 96, pp. 1786-1798, 2008.

[76]   M. Julliere, "Tunneling between ferromagnetic films," *Physics Letters A,* vol. 54, pp. 225-226, 1975.

[77]   Y. Yan and S. Priya, "Multiferroic magnetoelectric composites/hybrids," in *Hybrid and Hierarchical Composite Materials*, C. S. Kim, C. Randow, and T. Sano, Eds., ed: Springer, 2015, pp. 95-160.

[78]   M. Bibes and A. Barthélémy, "Multiferroics: Towards a magnetoelectric memory," *Nature Materials,* vol. 7, pp. 425-426, 2008.

[79]   Z. Shi, C. Wang, X. Liu, and C. Nan, "A four-state memory cell based on magnetoelectric composite," *Chinese Science Bulletin,* vol. 53, pp. 2135-2138, 2008.

[80]   N. Tiercelin, Y. Dusch, A. Klimov, S. Giordano, V. Preobrazhensky, and P. Pernod, "Room temperature magnetoelectric memory cell using stress-mediated magnetoelastic switching in nanostructured multilayers," *Applied Physics Letters,* vol. 99, 2011.

[81]   N. Tiercelin, Y. Dusch, V. Preobrazhensky, and P. Pernod, "Magnetoelectric memory using orthogonal magnetization states and magnetoelastic switching," *Journal of Applied Physics,* vol. 109, 2011.

[82]   H. Coufal, L. Dhar, and C. D. Mee, "Materials for magnetic data storage: The ongoing quest for superior magnetic materials," *MRS Bulletin,* vol. 31, pp. 374-375, 2006.

[83]   R. H. Dee, "Magnetic tape: The challenge of reaching hard-disk-drive data densities on flexible media," *MRS Bulletin,* vol. 31, pp. 404-408, 2006.

[84]   L. Li, Q. D. Ling, S. L. Lim, Y. P. Tan, C. Zhu, D. S. H. Chan*, et al.*, "A flexible polymer memory device," *Organic Electronics: physics, materials, applications,* vol. 8, pp. 401-406, 2007.

[85]   J. Ouyang, C. W. Chu, C. R. Szmanda, L. Ma, and Y. Yang, "Programmable polymer thin film and non-volatile memory device," *Nature Materials,* vol. 3, pp. 918-922, 2004.

[86]   J. Wu, Z. Shi, J. Xu, N. Li, Z. Zheng, H. Geng*, et al.*, "Synthesis and room temperature four-state memory prototype of Sr3Co2Fe24O41 multiferroics," *Applied Physics Letters,* vol. 101, 2012.

[87]   X. Zhao, Y. Zhang, J. Wang, Q. Zhan, X. Wang, H. Huang*, et al.*, "Ferroelectric control of magnetism in P(VDF–TrFE)/Co heterostructure," *Journal of Materials Science: Materials in Electronics,* vol. 26, pp. 7502-7506, 2015.
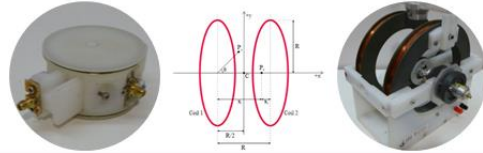
3 Magnetoelectric response measuring system development

The development of a system for magnetoelectric materials characterization is reported in this chapter. The designs and implementation, as well as the validation of the system are presented.
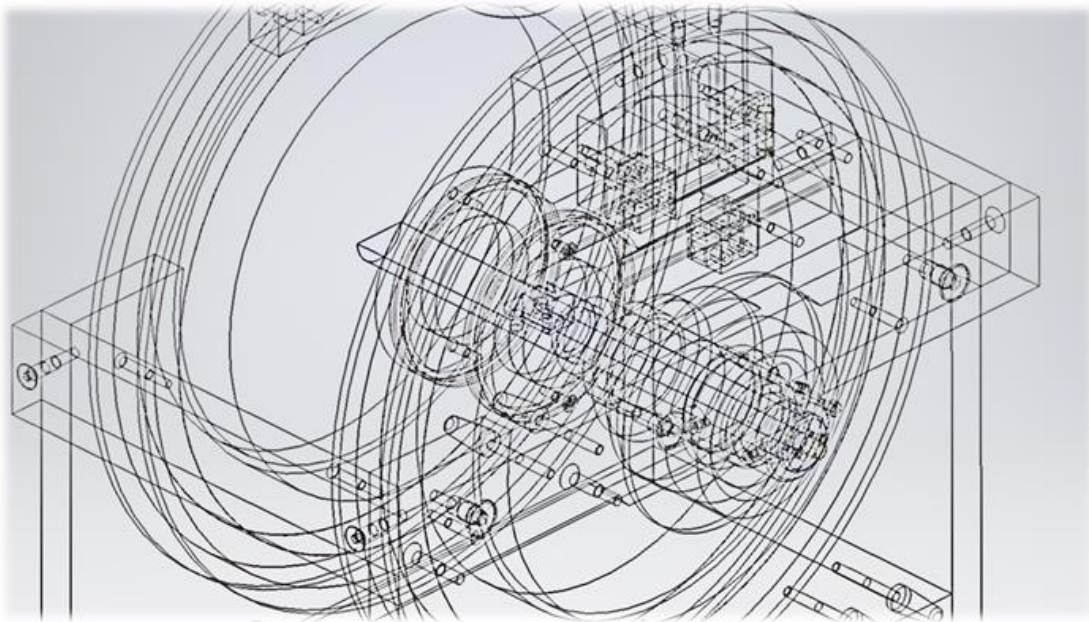
3.1 System design

The magnetoelectric (ME) coefficient (α), through the direct ME effect, allows relating the variation of the polarization generated by a ME composite, when subject to magnetic field variations (equation 3.1) and is the way to classify ME composites [1, 2].

$$\alpha = \frac{\partial \vec{P}}{\partial \vec{H}} \qquad (3.1)$$

A ME measurement system should be able to produce a controlled magnetic field, which will induce the magnetostrictive element to change its dimensions, and when these variations occur, the coupled piezoelectric element also change its dimensions, generating an output voltage, which will be analysed.

The ME effect can be measured directly by four different methods: static, quasi-static, dynamic and magnetic pulse [3, 4]. In the static method, a dc magnetic field (H_{dc}) is applied to the ME sample, being the ME output voltage measured, with a high input impedance electrometer, as a function of increasing magnetic field [5]. In the quasi-static method, a H_{dc}, varying slowly over the time, is applied to the ME sample and the ME signal is measured also with a high input impedance electrometer. The measurement begins and ends with a null magnetic field, thus, it is possible to have a base line to correct the measured plot [5, 6]. However, both methods can lead to erroneous conclusions, once during poling some charges can be accumulated at the grain boundaries, moving later towards the electrodes during the measurement [3]. The dynamic method, the most used in composites [4], consists in the application of two magnetic fields, a H_{dc} and a small ac magnetic field (H_{ac}), simultaneously. The voltage generated in the ME sample is measured with a lock-in amplifier tuned to the H_{ac} frequency. In this way, it is possible to explore the ME effect of a sample at different field magnitudes and under different time scales, by changing the H_{dc} or the H_{ac} frequency, respectively. Moreover, it is possible to reduce the noise, measure the signal phase shift and avoid the problem of charge accumulation. On the other hand, this method can report lower ME coefficients than other methods, due to periodic discharge, which occurs through sample resistance, at low frequencies, or through the capacitance effects, at high frequencies [3]. Lastly, the magnetic pulse method is usually used to study the frequency dependence of the ME voltage coefficients for frequencies up to 1 MHz, avoiding the sharp drop in H_{ac} due to the coils inductance. Pulses of rectangular shape parallel to a bias magnetic field are

applied to the ME sample, being the measured ME voltage analysed by Fourier analysis [7]. Recently, another magnetic pulse method, using an adapted configuration, was used to combine advantages of both quasi-static and dynamic methods. By using a pulse field magnetometer, it is possible to quantify the ME response of the materials [4].

Materials characterization implies reliable and reproducible data. In this way, it is necessary to design and develop a system able to do that for ME samples. The developed system will be based in the dynamic method, which allows to recreate the same conditions as the ones found in device application. It implies the generation of dc and ac magnetic fields to stimulate the sample and also to measure the voltage generated by the ME sample. This involves the development of a system constituted by three independent but correlated parts, represented with different colours in Figure 3.1. Besides that, the optimum H_{dc} depends on the magnetostrictive material that compose the ME composite, being, for example, in the order of 10 Oe in laminated composites based on Metglas and 2500 Oe in particulate ME nanocomposites with $CoFe_2O_4$ [2]. So, there was a need to develop two systems, one to produce low dc magnetic fields and another for high dc magnetic fields.
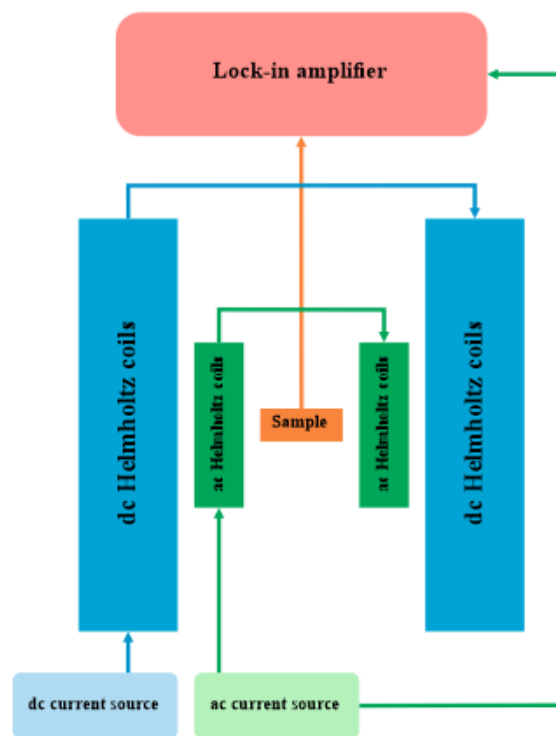
Figure 3.1. Schematic representation of the developed ME measurement system.

The H_{dc}, in the low dc magnetic field ME measurement system, will be produced by a Helmholtz coil sourced via a dc current provided by a Keithley 2400, which can

generate currents from 50 pA to 1 A. Regarding the high dc magnetic field ME measurement system, the H_{dc} is provided by a home-made electromagnet powered by a Kepco BOP 20-20M bipolar operational power supply, which can generate currents up to 20A. For both systems, a superimposed H_{ac} will be created by a Helmhotz coil sourced with an ac current provided either by an ac current source, such as the Keithley 6221, which can generate currents from 100 fA to 100 mA, with frequencies ranging from 1 mHz to 100 kHz, or by a signal generator, such as the Agilent 33220A, which can generate currents with frequencies ranging from 1 µHz to 20 MHz. The voltage induced in the ME sample will be measured by a lock-in amplifier, such as the Standford Research SR530, which has an input impedance of 100 MΩ and can measure voltages in a frequency ranging from 0.5 Hz to 100 kHz. The choice of the Helmholtz coils is related with need to have a highly uniform magnetic field along the space between the coils [8]. A lock-in amplifier is chosen due to its ability to measure very small ac signals in the presence of much larger noise levels.

3.2   Helmholtz coils design

Helmholtz coils, developed for the first time over a century ago and named in honour of the German physicist Hermann von Helmholtz [9], have been used for calibrating magnetic field sensors, to perform compatibility and susceptibility tests in electronic devices, for magnetic field measurements, bioelectromagnetic applications, and cancellation of the Earth's magnetic field, among others [10-12].

To develop a pair of Helmholtz coils two identical coils are required, parallel to each other and separated by a distance equal to their radius, as shown in Figure 3.2. The coils should be connected in series, so that the electric signal can flow in the same direction in both coils, thus ensuring that the magnetic fields add up. The magnetic field produced by the coils can be static or dynamic, it is perpendicular to the plane of the coils, with the direction determined by the right hand rule and is highly uniform in the space between the coils [10, 13].
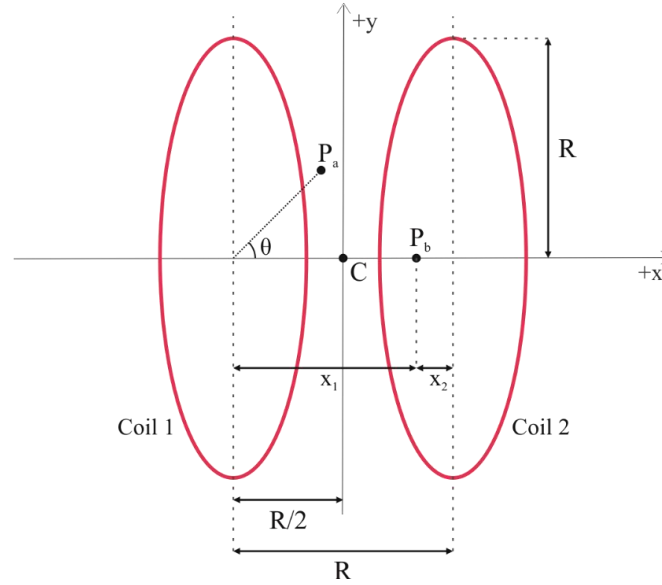
Figure 3.2. Representation and dimensions for construction of the Helmholtz coils.

The magnetic field, along the x-axis, at any point P of Figure 3.2, due to both coils is described by equation 3.2 [10, 11].

$$H_x = H_1 + H_2 = \frac{N_1 I R_1^2}{2(x_1^2 + R_1^2)^{3/2}} + \frac{N_2 I R_2^2}{(x_2^2 + R_2^2)^{3/2}} \tag{3.2}$$

where, N is the number of turns on each coil, I is the electric current through the coils (in Amperes) and R is the radius of each coil (in meters). Moreover, according to Helmholtz coils theory $N_1 = N_2 = N$ and $R_1 = R_2 = R$, resulting in the equation 3.3.

$$H_x = \frac{N I R^2}{2} \left(\frac{1}{(x^2 + R^2)^{3/2}} + \frac{1}{((R - x)^2 + R^2)^{3/2}} \right) \tag{3.3}$$

At the centre of the coil pair $x = R/2$, and the magnetic field is given by equation 3.4.

$$H_C = \left(\frac{4}{5} \right)^{\frac{3}{2}} \frac{N}{R} I \tag{3.4}$$

Thus, the magnetic field is proportional to N and I, and inversely proportional to R. So, to produce an uniform magnetic field between the coils it is necessary to take into account the accuracy with which the Helmholtz coils are constructed, their dimensions, distance between them and the number of turns, as well as the value of the current [10, 14].

From equation 3.4 it can be calculated the dimensions and the number of turns of the coils, in order to achieve the targeted values of magnetic field, taking into account the current supplied by the current sources. Regarding the low dc magnetic field ME measurement system, it is defined a maximum H_{dc} of 20 Oe, considering that the used

magnetostrictive alloys, Vitrovac and Metglas, do not require higher magnetic fields. In this way, the dc Helmholtz coils were constructed with a radius of 10 cm and 240 turns, allowing also a minimum H_{dc} of approximately 10 µOe. The ac Helmholtz coils were constructed with a radius of 3 cm and 50 turns, for the generation of magnetic fields up to 1 Oe. Regarding the high dc magnetic field ME measurement system, the H_{dc} was generated by an electromagnet, allowing H_{dc} up to 6 kOe. The ac Helmholtz coils were constructed with a radius of 3.5 cm and 60 turns, in order to generate magnetic fields up to 1 Oe.

3.3 Implementation

The different components of the system were designed in the Autodesk Inventor, a computer-aided design (CAD) software, which allows design, visualization and simulation of the system.

As mentioned before, the ME measurements imply the generation of two magnetic fields, one dc and one ac, which are superimposed and applied to the sample. Therefore, the developed structure is composed by two Helmholtz coils, one for the generation of the H_{dc} and another for the H_{ac}. In order to ensure that the ME sample is positioned in the centre of the coils, a sample holder was developed, which also connect the output signal to the lock-in amplifier.

3.3.1 Low dc magnetic field ME measurement system

Figure 3.3 shows the dc and ac Helmholtz coils of the ME measurement system.
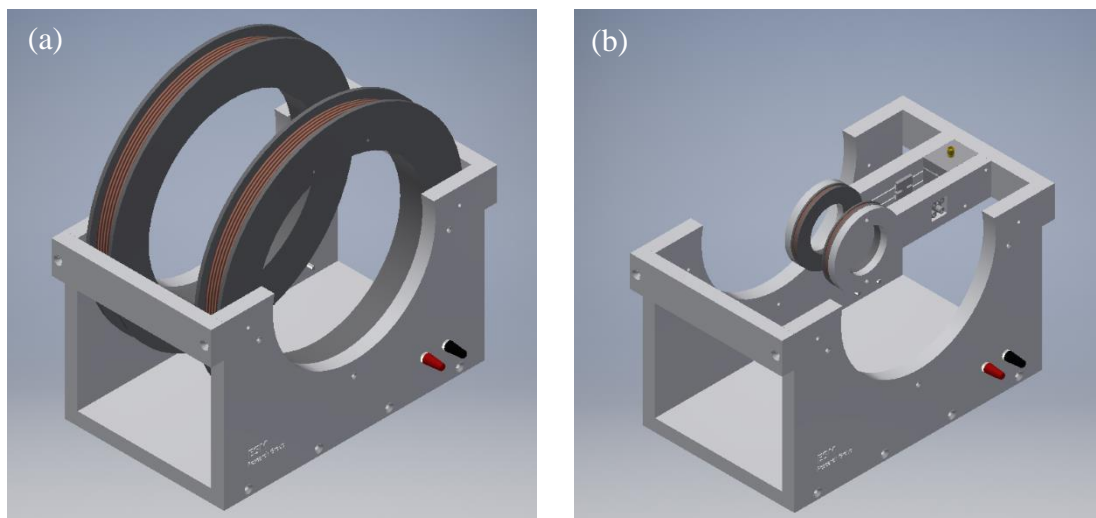
Figure 3.3. Helmholtz coils and their support of low dc magnetic field ME measurement system: (a) dc Helmholtz coils and (b) ac Helmholtz coils.

The system support was constructed in nylon, which is an easy machining polymer, able to absorb vibrations, with good chemical and mechanical resistance, excellent electrical insulation, and lightweight. The coils support were built in polyvinyl chloride (PVC), with characteristics similar to nylon, standing out for its rigidity, which is good for the winding process. For coil winding was used a copper wire with enamel coating. Regarding dc Helmholtz coils, with a radius of 10 cm and 240 turns, it was used a 1.0 mm diameter wire, able to support 1.1 A. For ac Helmholtz coils, with a radius of 3 cm and 50 turns, it was used a 0.32 mm diameter wire, able to support 0.11 A.

Figure 3.4 shows the two sample holders used, one for conventional essays (Figure 3.4a and Figure 3.4c) and another for anisotropic essays (Figure 3.4b and Figure 3.4d).
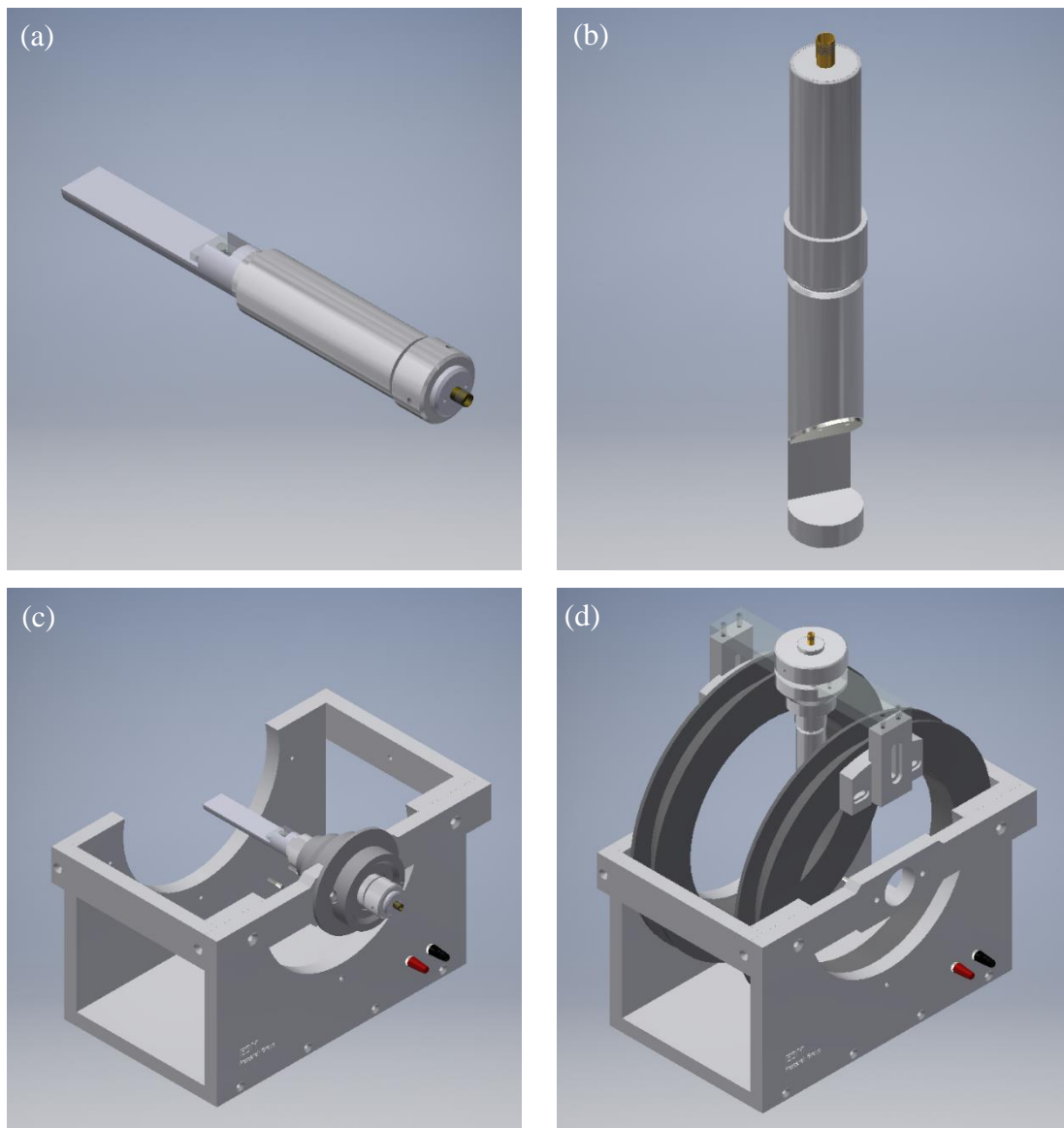
Figure 3.4. Sample holders developed: (a) for conventional ME essays, and (b) for anisotropic ME essays. Sample holders positioned in the system: (c) for conventional essays, and (d) for anisotropic essays.

Both sample holders were built in nylon, mainly for its capacity to absorb vibrations. Aluminium has also been used, since it can form an electrical shield, moreover, is a lightweight, soft, and non-magnetic metal. It is also suitable for machining, having excellent corrosion resistance. Acrylic was used at the top of the structure to allow a better visualization. Furthermore, it is possible to easily remove both sample holders from the structure, allowing to connect the ME samples in a safe and simple way for testing. The connection between the sample holder and the lock-in amplifier was performed by a coaxial cable, being the sample hold connector from gold for noise reduction.

Figure 3.5 shows the CAD and a photography of the ME measurement system, with both Helmholtz coils, for the generation of ac and low dc magnetic fields, and the sample holder for conventional essays.
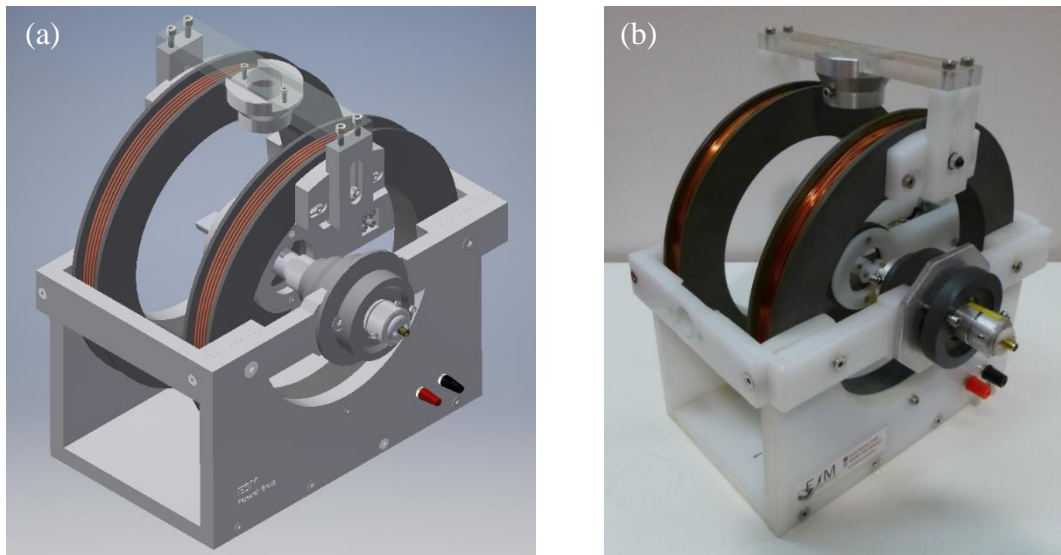
Figure 3.5. ME measurement system: (a) CAD and (b) photography.

3.3.2 High dc magnetic field ME measurement system

Figure 3.6 shows the ac Helmholtz coils and sample holder for the high dc magnetic field ME measurement system.
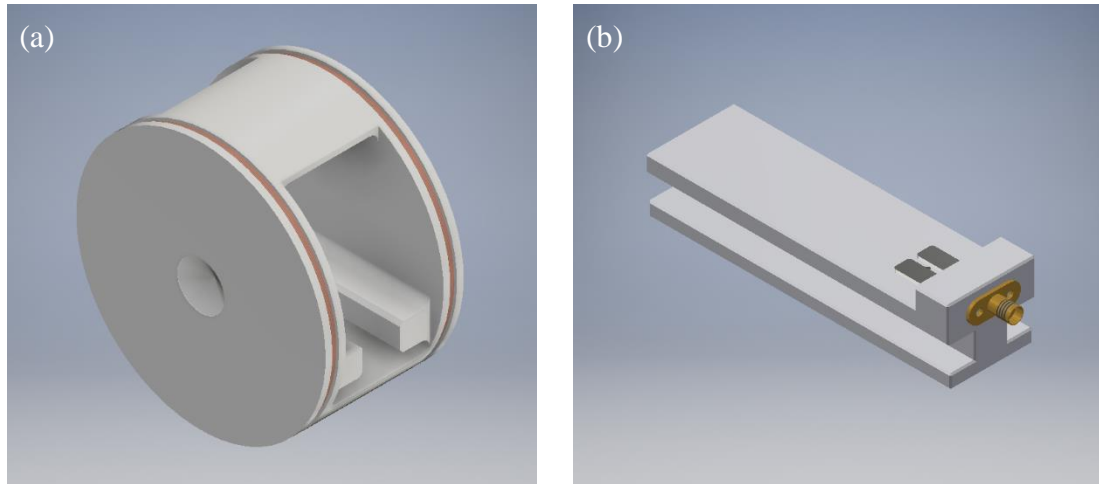
Figure 3.6. (a) Helmholtz coils and (b) sample holder for the high dc magnetic field ME measurement system.

The ac Helmholtz coils were built in a single piece to facilitate their placement in the middle of the electromagnet. The sample holder was developed in order to be placed into the ac coils before their placement in the electromagnet. All the structure was built in nylon. The coil winding was from copper wire with enamel coating. It was used a wire with 0.32 mm diameter, able to support 0.11 A.

Figure 3.7 shows the CAD and a photography of the ac Helmholtz coils with the sample holder used in the ME measurement system with high dc magnetic fields.
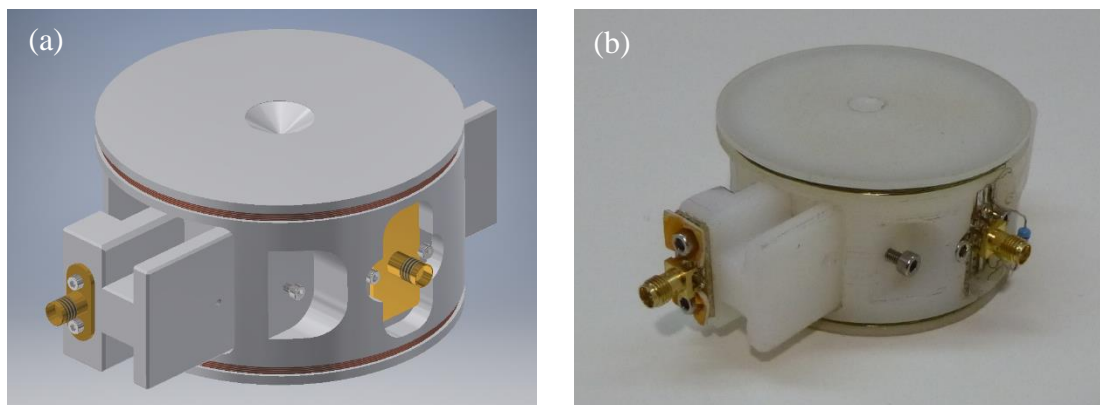
Figure 3.7. Representation of the ac Helmholtz coils for high dc magnetic field ME measurement system: (a) CAD and (b) photography.

3.4   Validation

The validation of both ME measurement systems was carried out in two steps. First a gaussmeter (Hirst GM08) was used to compare the measured magnetic field with the calculated field through the equation 3.4. After that, a ME characterization test was

carried out for a polymer-based ME laminate composite in the low dc magnetic field ME measurement system and for a polymer-based ME nanocomposite in the high dc magnetic field ME measurement system.

To perform a ME characterization, and to obtain α as a function of the H_{dc}, H_{ac} and frequency values should be maintained constant. The induced ME voltage (ΔV) in the piezoelectric layer was measured with the lock-in amplifier and α was determined by equation 3.5:

$$\alpha = \frac{\Delta V}{t \cdot H_{ac}} \tag{3.5}$$

where t and H_{ac} are the piezoelectric polymer thickness and the ac magnetic field, respectively.

3.4.1 Low dc magnetic field ME measurement system

Figure 3.8 shows the tests carried out for the calibration of the low dc magnetic field ME measurement system. The relation between the calculated and measured magnetic fields for dc Helmholtz coils (Figure 3.8a) and ac Helmholtz coils (Figure 3.8b) was evaluated. Figure 3.8c presents a ME characterization test for a ME laminate composite of poly(vinylidene fluoride) (PVDF)/Metglas. ME characterization was performed by applying simultaneously a H_{dc} ranging from 0 to 20 Oe and a superimposed H_{ac} of 0.1 Oe at 48 kHz.
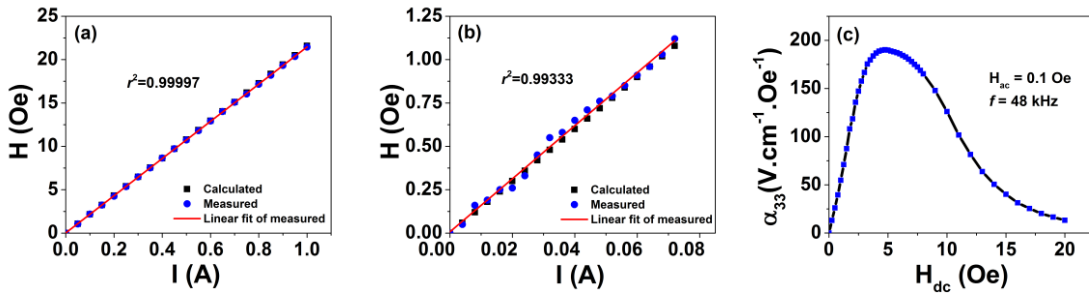
Figure 3.8. Comparison of magnetic field calculated and measured for (a) dc Helmholtz coils and (b) ac Helmoltz coils; (c) ME characterization test of PVDF/Metglas.

Figure 3.8a and Figure 3.8b show that the measured values are in agreement with the calculated ones. Figure 3.8c reveals an increase of the ME response with increasing H_{dc} up to 4.75 Oe, at which the maximum ME output voltage is reached (α_{33}=190 V·cm^{-1}·Oe^{-1}). This behaviour is related with the increase of the piezomagnetic coefficient up to the optimum 4.75 Oe. With a further increase of H_{dc}, a decrease of the induced voltage is observed, resulting from the saturation of the magnetostrictive response [15].

3.4.2   High dc magnetic field ME measurement system

Figure 3.9a and Figure 3.9b show the tests carried out for the calibration of the high dc magnetic field ME measurement system. The ME characterization test for a ME nanocomposite of poly(vinylidene fluoride-trifluoroethylene) (P(VDF-TrFE))/CoFe$_2$O$_4$ (Figure 3.9b) was performed by applying simultaneously a H_{dc} ranging from 0 to 5 kOe and a superimposed H_{ac} of 1 Oe at 5 kHz.
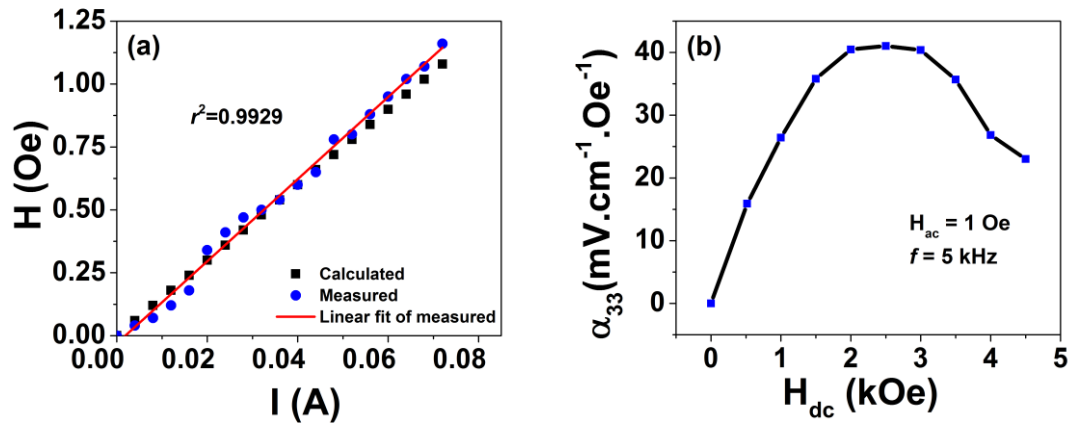
Figure 3.9. (a) Comparison of the calculated and measured magnetic field on ac Helmholtz coils; (b) ME characterization test of the P(VDF-TrFE)/CoFe$_2$O$_4$ composite.

Figure 3.9a shows the relation between the calculated and measured magnetic field for the ac Helmholtz coils. It is verified that the measured values are in agreement with the calculated ones. Figure 3.9b reveals an increase of the ME response with increasing H_{dc} up to 2.25 kOe, at which the maximum ME output voltage is reached (α_{33}=41.3 mV·cm^{-1}·Oe^{-1}).

3.5   References

[1]   W. Eerenstein, N. D. Mathur, and J. F. Scott, "Multiferroic and magnetoelectric materials," *Nature,* vol. 442, pp. 759-765, 2006.

[2]   P. Martins and S. Lanceros-Méndez, "Polymer-based magnetoelectric materials," *Advanced Functional Materials,* vol. 23, pp. 3371-3385, 2013.

[3]   G. V. Duong, R. Groessinger, M. Schoenhart, and D. Bueno-Basques, "The lock-in technique for studying magnetoelectric effect," *Journal of Magnetism and Magnetic Materials,* vol. 316, pp. 390-393, 2007.

[4]   G. V. Duong, R. S. Turtelli, and R. Groessinger, "Magnetoelectric properties of CoFe2O4-BaTiO3 core-shell structure composite studied by a magnetic pulse method," *Journal of Magnetism and Magnetic Materials,* vol. 322, pp. 1581-1584, 2010.

[5]   M. Mahesh Kumar, A. Srinivas, S. V. Suryanarayana, G. S. Kumar, and T. Bhimasankaram, "An experimental setup for dynamic measurement of magnetoelectric effect," *Bulletin of Materials Science,* vol. 21, pp. 251-255, 1998.

[6]   J. P. Rivera, "A short review of the magnetoelectric effect and related experimental techniques on single phase (multi-) ferroics," *European Physical Journal B,* vol. 71, pp. 299-313, 2009.

[7]   Y. K. Fetisov, K. E. Kamentsev, A. Y. Ostashchenko, and G. Srinivasan, "Wide-band magnetoelectric characterization of a ferrite-piezoelectric multilayer using a pulsed magnetic field," *Solid State Communications,* vol. 132, pp. 13-17, 2004.

[8]   K. Kaminishi and S. Nawata, "Practical method of improving the uniformity of magnetic fields generated by single and double Helmholtz coils," *Review of Scientific Instruments,* vol. 52, pp. 447-453, 1981.

[9]   M. S. Crosser, S. Scott, A. Clark, and P. M. Wilt, "On the magnetic field near the center of Helmholtz coils," *Review of Scientific Instruments,* vol. 81, 2010.

[10]   E. L. Bronaugh, "Helmholtz coils for calibration of probes and sensors: limits of magnetic field accuracy and uniformity," in *IEEE International Symposium on Electromagnetic Compatibility*, 1995, pp. 72-76.

[11]   E. R. Javor and T. Anderson, "Design of a Helmholtz coil for low frequency magnetic field susceptibility testing," in *IEEE International Symposium on Electromagnetic Compatibility*, 1998, pp. 912-917.

[12]   R. A. Schill Jr and K. Hoff, "Characterizing and calibrating a large helmholtz coil at low ac magnetic field levels with peak magnitudes below the earth's magnetic field," *Review of Scientific Instruments,* vol. 72, pp. 2769-2776, 2001.

[13]   S. R. Trout, "Use of Helmholtz Coils for Magnetic Measurements," *IEEE Transactions on Magnetics,* vol. 24, pp. 2108-2111, 1988.

[14]   C. F. de Melo, R. L. Araújo, L. M. Ardjomand, N. S. Ramos Quoirin, M. Ikeda, and A. A. Costa, "Calibration of low frequency magnetic field meters using a Helmholtz coil," *Measurement: Journal of the International Measurement Confederation,* vol. 42, pp. 1330-1334, 2009.

[15]   S. Reis, M. P. Silva, N. Castro, V. Correia, P. Martins, A. Lasheras*, et al.*, "Characterization of Metglas/poly(vinylidene fluoride)/Metglas magnetoelectric laminates for AC/DC magnetic sensor applications," *Materials and Design,* vol. 92, pp. 906-910, 2016.
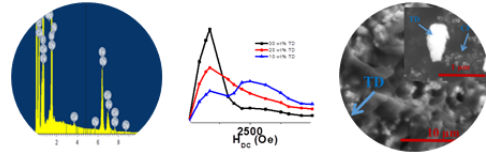
4 Wide-range magnetoelectric response of hybrid polymer composites based on filler type and content

Flexible films of Terfenol-D/CoFe$_2$O$_4$/P(VDF-TrFE) magnetoelectric nanocomposite were produced and their morphologic, piezoelectric, magnetic and magnetoelectric properties investigated. The films showed a wide-range dual-peak ME response at room temperature with the ME coefficient increasing with the weight content of Terfenol-D.

4.1 Introduction

Magnetic sensors and energy harvesters have attracted much interest in recent years due to their wide range of applications, which include navigation systems, medical sensors, non-destructive material testing, building monitoring, agriculture management and biomedical areas [1-4], among others.

Traditional magnetic sensors show important disadvantages, which include the need for a power supply, low spatial resolution, a complex fabrication process, miniaturization problems (for device dimensions on the order of micrometers), high-cost assembly, the need for temperature compensation circuits, large initial offset and reduced accuracy. Furthermore, those devices do not meet increasing industry demands in terms of flexibility, versatility, light weight, cost, complicated shape allowance or low-temperature fabrication processing, hindering their use in novel and rapidly growing application areas such as flexible or wearable devices [3, 5].

Polymer-based magnetoelectric (ME) materials are attracting increasing attention as they can solve the above-mentioned problems due to their cheap, facile, scalable and low-temperature fabrication methods, the absence of large leakage currents, the ability to be fabricated in a variety of forms – such as thin sheets or moulded shapes – and, in some cases, their biocompatibility [2, 5-8].

ME coefficients on polymer-based ME materials are of the same order of magnitude as the best ones obtained in materials that are already being used/investigated as magnetic sensors and/or energy harvesters. This fact encourages the emergence of a new generation of polymer-based ME devices [9, 10]. The ME voltage coefficient, as the figure of merit of a magnetic field sensor, describes the variation of the electric field as a function of the applied magnetic field [3]. However, magnetoelectric composites present strong ME effects only near an optimum dc magnetic field, where the effective piezomagnetic coefficient of the magnetostrictive layer is at its maximum, this fact being the main disadvantage of magnetoelectric devices, as it compromises their use in high-sensitivity miniaturized magnetic devices [3].

Trying to solve such limitations, some efforts have been devoted to obtaining a multi-peak ME phenomenon on ME devices such as the one proposed by *Chen et al.* [3]. In their study, the interaction between Terfenol-D and FeSiB resulted in dual-peak occurrence, the first peak being caused by the strong exchange coupling effect between

Terfenol-D and FeSiB layers and the second peak being caused by the maximum of the dynamic piezomagnetic coefficient q_{33} of the Terfenol-D layer. This pioneer report proved that it was possible to tailor and optimize the ME response by combining different magnetostrictive components in the same ME composite. On the other hand, the developed composite was a laminated structure with several drawbacks, such as the effective ME coupling of the (2-2) film connectivity being limited by the clamping of the films to the substrate and detrimental dielectric leakage currents [11]. A possible solution would be the use of nanocomposites, which offer advantages such as higher flexibility, simpler fabrication, easy shaping, miniaturization possibilities, and the absence of degradation at the piezoelectric/magnetostrictive interface [12, 13].

Thus, it is scientifically and technologically relevant to obtain a multi-peak ME response on ME nanocomposites to match material's properties and responses with the ones suitable for practical applications [3].

In this work, two types of highly magnetostrictive particles, Terfenol-D and $CoFe_2O_4$, were added to a poly(vinylidene fluoride-trifluoroethylene) (P(VDF-TrFE)) piezoelectric matrix, aiming to tailor the ME response of polymer-based composites through the variation of the magnetostrictive filler type and content.

Terfenol-D microparticles were selected once they exhibited the highest room temperature magnetostrictive coefficient (600 ppm) among the microparticles. $CoFe_2O_4$ nanoparticles were selected due to having the highest magnetostriction ($\approx$200 ppm) among ferrite nanoparticles [14, 15]. Additionally, the optimum dc magnetic field, where the effective piezomagnetic coefficient of the magnetostrictive particles is maximized, is different for the two particle types, allowing a double-peak phenomenon of the ME response of the Terfenol-D/$CoFe_2O_4$/P(VDF-TrFE) hybrid composite. P(VDF-TrFE) was selected as the piezoelectric matrix due to its highest piezoelectric responses among polymer materials over a wide range of temperatures [9, 16].

4.2   Materials and Methods

4.2.1   Materials

N,N-Dimethylformamide (DMF, pure grade) was supplied by Fluka (Milwaukee, WI, USA) and P(VDF-TrFE) was supplied by Solvay Solexis (West Deptford, NJ, USA). $CoFe_2O_4$ nanoparticles were purchased from Nanoamor (Houston, TX, USA) with dimensions between 35–55 nm. Terfenol-D powder with a mean particle size of $\approx$1 μm

was obtained from ETREMA Products, Inc. (Ames, IA, USA). All chemicals were used as received without further purification.

4.2.2   Terfenol-D/CoFe$_2$O$_4$/P(VDF-TrFE) Composite Preparation

The multiferroic composites were prepared following procedures reported on [2, 9, 12]. Briefly, the selected filler content of the magnetostrictive phase (Terfenol-D and CoFe$_2$O$_4$) was added into DMF solvent and placed in an ultrasound bath for 8 h aiming to ensure a good dispersion of the magnetostrictive phase. P(VDF-TrFE) polymer was then added and mixed for 2 h with a Teflon mechanical stirrer in an ultrasound bath to prevent magnetic agglomeration during the mixing process. The resulting mixture was spread on a clean glass substrate and solvent evaporation and polymer melting were performed inside an oven for 10 min at 210 ºC. P(VDF-TrFE) crystallization was achieved by cooling down the composite films to room temperature ($\approx$25 ºC). At the end of the process, the $\approx$50 µm-thick films were peeled from the glass substrate. Flexible ME composite films were prepared with 40% weight content (wt %) of magnetostrictive filler. It has been shown that for such filler content, the films can be poled without electric breakdown and good ME coupling and flexibility are obtained [12]. To study the influence of each magnetostrictive particle type on the ME response of the developed Terfenol-D/CoFe$_2$O$_4$/P(VDF-TrFE) nanocomposites, three distinct samples were produced (further refereed in the chapter by the name provided in parenthesis): hybrid composites with 10 wt % (0.02 in volume fraction) of Terfenol-D and 30 wt % (0.13 in volume fraction) of CoFe$_2$O$_4$ (10TD/30CFO); 20 wt % (0.05 in volume fraction) of Terfenol-D and 20 wt % (0.08 in volume fraction) of CoFe$_2$O$_4$ (20TD/20CFO); and 30 wt % (0.08 in volume fraction) of Terfenol-D and 10 wt % (0.04 in volume fraction) of CoFe$_2$O$_4$ (30TD/10CFO).

4.2.3   Terfenol-D/CoFe$_2$O$_4$/P(VDF-TrFE) Composite Characterization

The morphology of the Terfenol-D/CoFe$_2$O$_4$/P(VDF-TrFE) composites was evaluated via scanning electron microscopy (SEM) with a Quanta 650 FEI scanning electron microscope (Hillsboro, OR, USA) at 10 kV. Before SEM, samples were coated with gold by magnetron sputtering. Further, composition analysis was carried out by energy-dispersive X-ray microanalysis (EDS) from 0 to 13 keV.

In order to optimize the piezoelectric response, poling of the Terfenol-D/CoFe$_2$O$_4$/P(VDF-TrFE) nanocomposites was performed in a home-made chamber, after an optimization procedure, by corona poling at 10 kV during 120 min at 120 ºC and

cooling down to room temperature under the applied electric field. The piezoelectric response (d_{33}) of the composites was evaluated with a wide range d_{33}-meter (model 8000, APC Int Ltd., Mackeyville, PA, USA). Room temperature magnetic hysteresis loops were measured with a Microsense 2.2 Tesla Vibrating Sample Magnetometer (VSM) (Lowell, MA, USA).

The ME coefficient α_{33} was measured with the application of both dc and ac magnetic fields along the direction of the electrical polarization of the composites, i.e., perpendicular to the surface.

The ac driving magnetic field of 1 Oe amplitude at ≈ 8 kHz (resonance of the Terfenol-D/CoFe$_2$O$_4$/P(VDF-TrFE) composites) was delivered by a pair of Helmholtz coils and the dc field with a maximum value of 0.5 T was applied by an electromagnet.

The resonance frequency (f_r) of the composites was calculated by using equation 4.1:

$$f_r = \frac{n}{2t}\sqrt{\frac{E_y}{\rho}} \tag{4.1}$$

where n, t, E_Y and ρ are the harmonic mode order, thickness, in-plane Young's modulus and density of the composites, respectively. The produced ME voltage (ΔV) was measured with a Standford Research Lock-in amplifier (SR530, Sunnyvale, CA, USA). Circular 1.4 mm-diameter gold electrodes were sputtered on the opposite sides of the samples prior to the ME characterization.

The ME coefficient α_{33} was determined through equation 4.2:

$$\alpha_{33} = \frac{\Delta V}{t \cdot H_{ac}} \tag{4.2}$$

where ΔV is the ME voltage generated in the composite, H_{ac} the ac magnetic field and t the thickness of the ME composite.

4.3 Results and Discussion

After the flexible samples, such as the one represented in the inset of Figure 4.1a, were obtained, SEM images were taken in order to verify the dispersion and distribution of the magnetostrictive particles inside the P(VDF-TrFE) matrix.
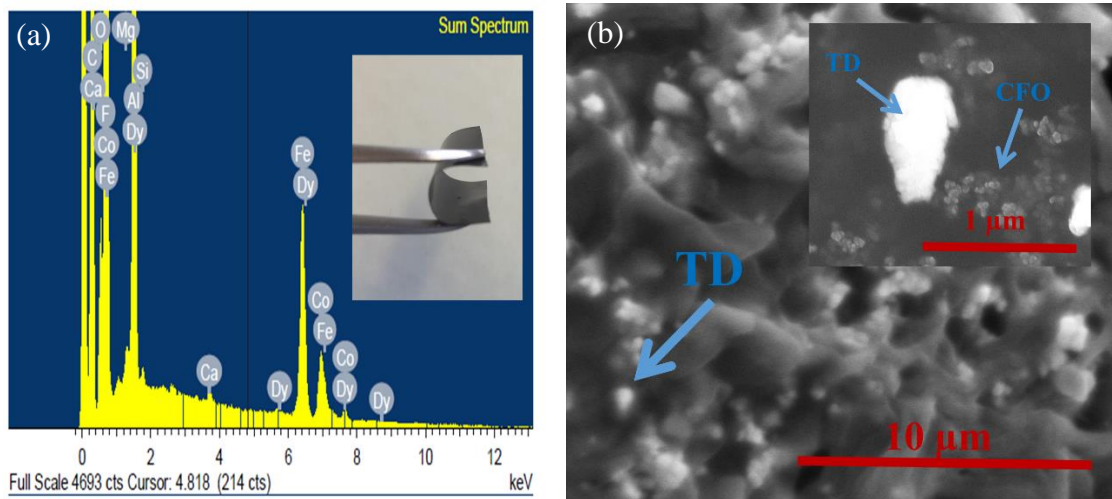
Figure 4.1. (a) EDS analysis of the 20TD/20CFO composite (inset reveals a photograph of such a flexible composite); and (b) SEM image showing the TD dispersion on the 20TD/20CFO composite as a magnification showing both magnetostrictive particles (inset).

Additionally, the data in Figure 4.1a prove the joint presence on the composites of elements of both magnetostrictive particles, Tb, Dy and Fe from TD and Co, Fe and O from CFO.

Figure 4.1b reveals a good distribution of both particle types inside the polymer. Such a good distribution was also observed in the other composite compositions (10TD/30CFO and 30TD/10CFO – images not shown). Additionally, the different size range of TD and CFO fillers was evidenced.

Once the ME response of the TD/CFO/P(VDF-TrFE) composite emerged from the strain-mediated coupling between the piezoelectric and magnetic responses, the effect of the filler content and type on these responses was evaluated, as shown in Figure 4.2.
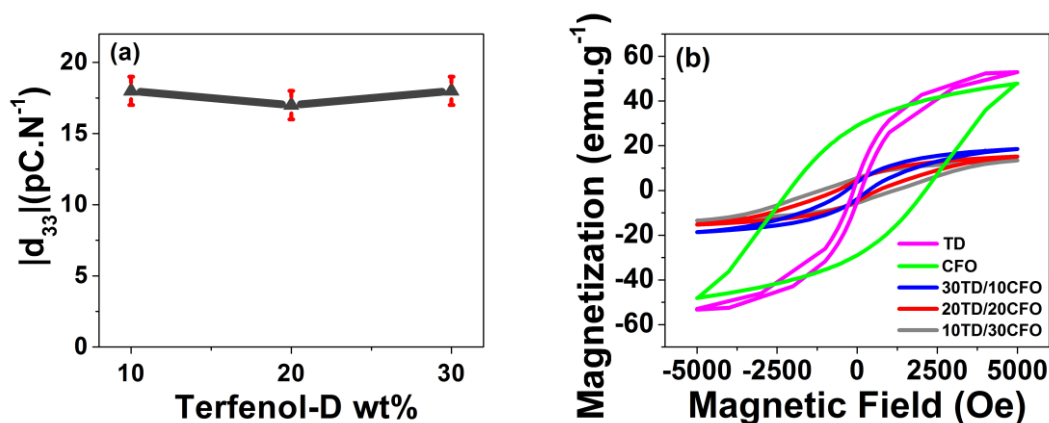
Figure 4.2. (a) Variation of the modulus of the piezoelectric response, $|d_{33}|$ value, as a function of TD/CFO/P(VDF-TrFE) composite composition; (b) magnetic response of the TD/CFO/P(VDF-TrFE) composites.

Figure 4.2a shows that the introduction of magnetic fillers on the polymer matrix led to a small decrease in the piezoelectric response ($\leq 20\%$; 18 pC·N^{-1}) when compared to the piezoelectric response of neat P(VDF-TrFE) (-22 pC·N^{-1}). This fact is attributed to the disruption of the polymer matrix, in particular at the interfaces with the fillers. Nevertheless, such a piezoelectric response is still suitable for obtaining high ME coefficients in polymer nanocomposites.

Magnetic measurements at room temperature (Figure 4.2b) allowed us to obtain the magnetic behaviour of such composites and compare them with the pure powders (TD and CFO) (Table 4.1).

Table 4.1. Magnetic properties (magnetization saturation at 5000 Oe: M_S; remanent magnetization: M_R and coercive field: H_C).

Sample	M_S (emu·g^{-1})	M_R (emu·g^{-1})	H_C(Oe)
TD powder	52.9	4.9	117.5
CFO powder	47.8	28.8	2100.3
30TD/10CFO	18.5	3.7	355.7
20TD/20CFO	15.1	4.6	648.1
10TD/30CFO	13.3	5.5	1225.2

It is noted that the M_S value decreased with the increasing CFO content (from 18.5 to 13.3 emu·g^{-1}) once the CFO powder had a lower M_S (47.8 emu·g^{-1}) when compared to the TD powder (52.9 emu·g^{-1}). On the contrary, the M_R and H_C values increased (from 3.7 to 5.5 emu·g^{-1} and from 355.7 to 1225.2 Oe, respectively) with the increasing CFO content, once CFO had higher M_R and H_C values (28.8 emu·g^{-1} and 2100.3 Oe) when compared to the TD powder (4.9 emu·g^{-1} and 117.5 Oe). Results from Table 4.1 also reveal that the coexistence of both magnetostrictive particles on the same polymeric composite did not hinder the overall magnetic response.

The appropriate piezoelectric and magnetic responses of the composites being proved, the dependence of the resonant ME voltage coefficient for the TD/CFO/P(VDF-TrFE) composites with the dc bias magnetic field and Terfenol-D content is presented in Figure 4.3.
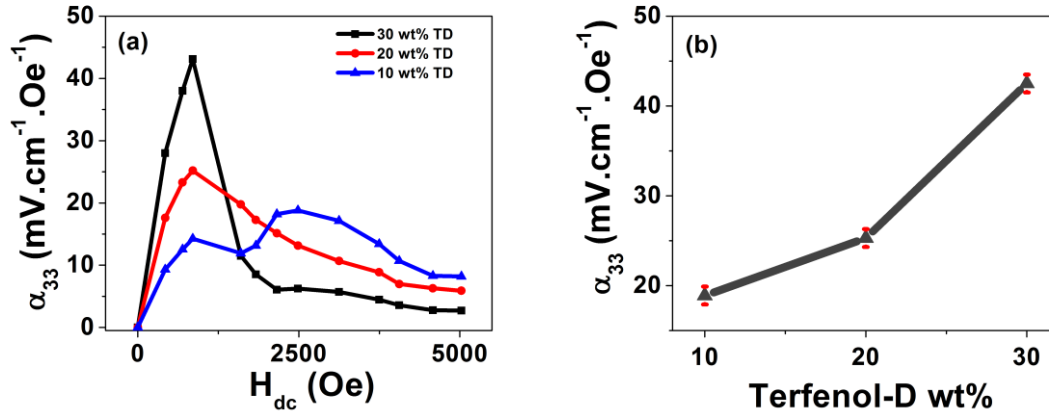
Figure 4.3. (a) ME voltage coefficient (α_{33}) as a function of H_{dc} for the Terfenol-D/CoFe$_2$O$_4$/P(VDF-TrFE) composites; (b) variation of the Terfenol-D/CoFe$_2$O$_4$/P(VDF-TrFE) highest α_{33} value as a function of composite composition.

Due to the magnetostrictive properties of the fillers, the maximum ME response of the TD/P(VDF-TrFE) and CFO/P(VDF-TrFE) hybrid composites usually takes place at 800–1200 Oe and 2000–3000 Oe magnetic field ranges, respectively [17].

In the composite with a lower CFO content, 30TD/10CFO, the ME voltage peak was almost entirely derived from the TD magnetostrictive phase, although another hump is observable in the 2200–3600 Oe field range.

In the 20TD/20CFO composite, a ME response with a broad peak as a result of the magnetostrictive properties of both TD and CFO fillers was verified. The 10TD/30CFO composite revealed a double-peak with maximum output voltages at the H_{dc} at which the magnetostrictive coefficient of each nanoparticle type was saturated, with 850 and 2500 Oe for TD and CFO, respectively [12].

Due to the higher magnetostrictive coefficient of TD as compared to CFO (600 and 200 ppm, respectively), the composite with the higher content of TD particles reached a higher ME response (Figure 4.3b) than the one with the higher CFO content (30 and 18 mV·cm^{-1}·Oe^{-1}, respectively).

Such results demonstrate that it is possible to tailor the ME response of the nanocomposites by combining different magnetostrictive fillers in the same composite, allowing the fabrication of high-sensitivity miniaturized magnetic devices [3]. Additionally, such a non-single-peak ME response is also useful for energy-harvesting devices once it allows a larger energy-harvesting performance in a broader magnetic field range.

4.4 Conclusions

Nanocomposite films based on highly magnetostrictive CFO nanoparticles and TD microparticles dispersed in a piezoelectric P(VDF-TrFE) matrix were prepared by solvent casting with an overall filler content ≈40 wt %. The obtained multiferroic nanocomposites revealed a stable piezoelectric response ($\approx$-18 pC·N^{-1}) that is independent of the weight ratio between the fillers. The magnetization saturation values decrease (from 18.5 to 13.3 emu·g^{-1}), whereas the remanent magnetization and coercive field values increase (from 3.7 to 5.5 emu·g^{-1} and from 355.7 to 1225.2 Oe, respectively) with the increasing CFO content.

Additionally, these films showed a strong ME coupling at room temperature with the ME coefficient increasing with the TD content up to 42.3 mV·cm^{-1}·Oe^{-1}, for the sample with 30 wt %. As compared to films with just one magnetostrictive filler, the developed polymer-based composite films showed a double-peak wide-range ME response, together with the highest ME response found on polymer-based particulate composites.

4.5 References

[1]   S. Reis, M. P. Silva, N. Castro, V. Correia, J. G. Rocha, P. Martins*, et al.*, "Electronic optimization for an energy harvesting system based on magnetoelectric Metglas/poly(vinylidene fluoride)/Metglas composites," *Smart Materials and Structures,* vol. 25, 2016.

[2]   P. Martins, A. Larrea, R. Gonçalves, G. Botelho, E. V. Ramana, S. K. Mendiratta*, et al.*, "Novel anisotropic magnetoelectric effect on δ-FeO(OH)/P(VDF-TrFE) multiferroic composites," *ACS Applied Materials and Interfaces,* vol. 7, pp. 11224-11229, 2015.

[3]   L. Chen and X. Dai, "Magnetic sensors based on magnetoelectric laminate multiferroic heterostructures with dual-peak phenomenon," *Journal of Computational and Theoretical Nanoscience,* vol. 12, pp. 2842-2845, 2015.

[4]   J. S. Noh, "Conductive elastomers for stretchable electronics, sensors and energy harvesters," *Polymers,* vol. 8, 2016.

[5]   S. Reis, M. P. Silva, N. Castro, V. Correia, J. Gutierrez, A. Lasheras*, et al.*, "Optimized anisotropic magnetoelectric response of Fe61.6Co16.4Si10.8B11.2/PVDF/Fe61.6Co16.4Si10.8B11.2 laminates for AC/DC magnetic field sensing," *Smart Materials and Structures,* vol. 25, 2016.

[6]   C. Ribeiro, V. Correia, P. Martins, F. M. Gama, and S. Lanceros-Mendez, "Proving the suitability of magnetoelectric stimuli for tissue engineering applications," *Colloids and Surfaces B: Biointerfaces,* vol. 140, pp. 430-436, 2016.

[7]   H. Palneedi, V. Annapureddy, S. Priya, and J. Ryu, "Status and perspectives of multiferroic magnetoelectric composite materials and applications," *Actuators,* vol. 5, 2016.

[8]   T. Prabhakaran and J. Hemalatha, "Flexible films of β-phase poly(vinylidene fluoride)/ZnFe2O4 polymer nanocomposite for magnetoelectric device applications," *Science of Advanced Materials,* vol. 6, pp. 1313-1321, 2014.

[9]   P. Martins, M. Silva, and S. Lanceros-Mendez, "Determination of the magnetostrictive response of nanoparticles via magnetoelectric measurements," *Nanoscale,* vol. 7, pp. 9457-9461, 2015.

[10]   X. Zhao, Y. Zhang, J. Wang, Q. Zhan, X. Wang, H. Huang, *et al.*, "Ferroelectric control of magnetism in P(VDF–TrFE)/Co heterostructure," *Journal of Materials Science: Materials in Electronics,* vol. 26, pp. 7502-7506, 2015.

[11]   Y. Li, Z. Wang, J. Yao, T. Yang, Z. Wang, J. M. Hu, *et al.*, "Magnetoelectric quasi-(0-3) nanocomposite heterostructures," *Nature Communications,* vol. 6, 2015.

[12]   P. Martins, Y. V. Kolen'Ko, J. Rivas, and S. Lanceros-Mendez, "Tailored Magnetic and Magnetoelectric Responses of Polymer-Based Composites," *ACS Applied Materials and Interfaces,* vol. 7, pp. 15017-15022, 2015.

[13]   F. Belhora, A. Hajjaji, S. Touhtouh, A. E. Ballouti, D. Guyomar, and Y. Boughaleb, "Magnetoelectricity in polyurethanes nanocomposites," *Molecular Crystals and Liquid Crystals,* vol. 628, pp. 124-129, 2016.

[14]   K. Jin and J. Aboudi, "Macroscopic behavior prediction of multiferroic composites," *International Journal of Engineering Science,* vol. 94, pp. 226-241, 2015.

[15]   J. Kaleta, D. Lewandowski, and R. Mech, "Magnetostriction of field-structural composite with Terfenol-D particles," *Archives of Civil and Mechanical Engineering,* vol. 15, pp. 897-902, 2015.

[16]   R. I. Mahdi, W. C. Gan, and W. H. Abd Majid, "Hot plate annealing at a low temperature of a thin ferroelectric P(VDF-TrFE) film with an improved crystalline structure for sensors and actuators," *Sensors (Switzerland),* vol. 14, pp. 19115-19127, 2014.

[17]   Y. Zeng, G. Bao, J. Yi, G. Zhang, and S. Jiang, "The influence of inducing magnetic field on the magnetoelectric effect of particulate magnetoelectric composites," *Journal of Alloys and Compounds,* vol. 630, pp. 183-188, 2015.
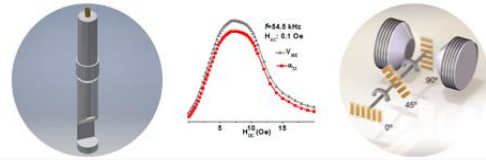
5 Optimized anisotropic magnetoelectric response of $Fe_{61.6}Co_{16.4}Si_{10.8}B_{11.2}$/PVDF/$Fe_{61.6}Co_{16.4}Si_{10.8}B_{11.2}$ laminates for ac/dc magnetic field sensing

The anisotropic magnetoelectric effect of a $Fe_{61.6}Co_{16.4}Si_{10.8}B_{11.2}$/PVDF/ $Fe_{61.6}Co_{16.4}Si_{10.8}B_{11.2}$ laminate composites has been used for the development of a magnetic field sensor able to detect both the magnitude and direction of ac and dc magnetic fields.
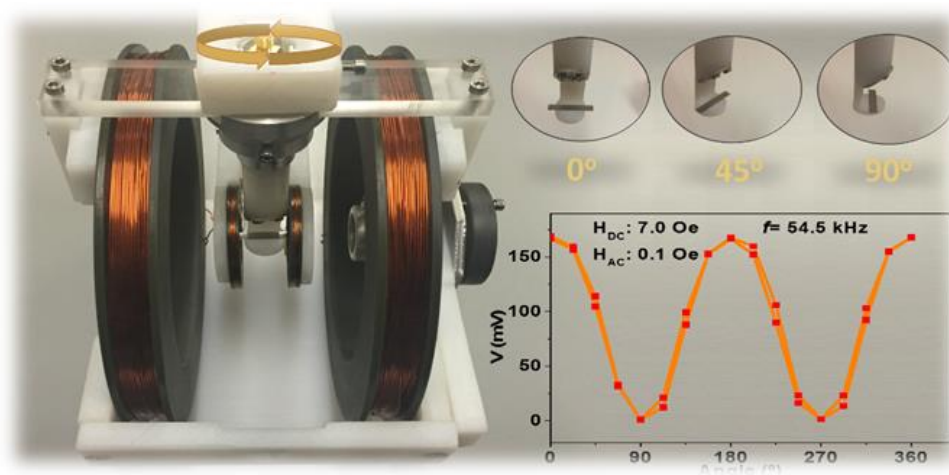
5.1 Introduction

Magnetic field sensors have been widely used for centuries, being the first applications related to navigation and localization, using the Earth's magnetic field as a tool [1]. Nowadays, measuring the magnetic field is not always the final and desired objective. Thus, variations or disturbances in magnetic fields allow us to indirectly measure distinct parameters such as electric current, linear and angular position, speed, object detection and identification, among others [1, 2].

Some magnetic field sensors, such as optically pumped magnetometers, nuclear-precession magnetometers and Overhauser magnetometers are only able to measure the magnetic field magnitude, commonly known as total field magnetometers [3]. Nevertheless, nowadays, applications of magnetic sensing in areas, such as the automotive industry, navigation and electronics impose increasing demand for vector magnetometers [4].

The most advanced vector instruments, which simultaneously measure magnitude and direction, are those using the Hall effect, with their basic principle involving a well-defined and well-understood physical phenomenon [5, 6]. However, such instruments have important drawbacks, such as their complicated fabrication process, low spatial resolution, miniaturization problems (for device dimensions on the order of micrometers), the need for temperature compensation circuits and operational amplifiers, high-cost assembly, the numerous electrical connections between individual elements and subsystems, reduced accuracy, and large initial offset [5-8]. Additionally, traditional magnetic sensors such as fluxgates, superconducting quantum interference devices (SQUIDs), search-coils, anisotropic magnetoresistance (AMR), giant magnetoresistance (GMR) and giant magnetoimpedance (GMI) do not meet increasing industry demands in terms of flexibility, versatility, weight, cost, complicated shape allowance or low-temperature fabrication processing, hindering their use in novel and rapidly growing application areas such as flexible or wearable devices [9-11].

On the other hand, magnetic sensors built with polymer-based magnetoelectric (ME) materials have attracted increasing attention due to their facile, cheap, low-temperature and scalable production methods, the absence of large leakage currents, the ability to fabricate them in a variety of forms – such as thin sheets or moulded shapes – tailored mechanical properties, and in some cases biocompatibility [10, 12, 13].

Three main types of polymer-based ME composites can be found in the literature: nanocomposites, *polymer as a binder* and laminated composites. Among them, polymer-based ME laminates show the largest ME coefficients and respond to a broad range of magnetic fields, being therefore the most suitable ME materials for the development of magnetic sensors [10, 14].

Despite the advantages previously mentioned and the increasing scientific/technological interest in anisotropic magnetic sensors [9, 10, 12, 15], only one report can be found in the literature regarding the development of magnetic field sensors from ME-polymer-based laminates, since the determination of both the magnitude and direction of the magnetic field was revealed to be a challenging task [16]. Even after the work of Dong *et al*, focusing on the anisotropic ME coupling on bilayer PVDF/FCSB laminates, the magnetic sensor still needs to be optimized and the main characteristics that will determine its applicability range (including sensitivity, linearity and accuracy) [17-19] have not been reported [20-22].

Thus, in this work, such characteristics are reported for $Fe_{61.6}Co_{16.4}Si_{10.8}B_{11.2}$ (FCSB)/poly(vinylidene fluoride) (PVDF)/FCSB ME laminates.

The choice of the FCSB/PVDF/FCSB composite was related to the highest ME response of this configuration [10]. Furthermore, this configuration and material selection takes advantage of the chemical and thermal stability, flexibility, high electrical resistivity, low loss and low processing temperature of PVDF, together with the high magnetic permeability, high piezomagnetic coefficient and magnetic anisotropy of FCSB [10, 16].

5.2 Experimental

A metallic glass of nominal composition FCSB was fabricated "home-made" by the single-roller quenching method, obtaining a long ribbon (several meters) with 5 mm × 25 µm cross section. The measured main magnetic properties of this alloy are a saturation magnetization of $\mu_0 M_S = 14\ 000$ Oe, a magnetic susceptibility of $\chi \approx 36\ 000$, and a saturation magnetostriction of $\lambda_S = 20$ ppm.

Two equal pieces of this amorphous magnetostrictive ribbon with a length of 30 mm were cut from the ribbon, and glued (Figure 5.1a) with a DEVCON 5 min epoxy (0.7 GPa Young's modulus) to both sides of a 30 mm × 5 mm × 52 µm PVDF (Measurements

Specialties) layer poled along the thickness direction (piezoelectric coefficient d_{33} = -33 pC·N^{-1}).
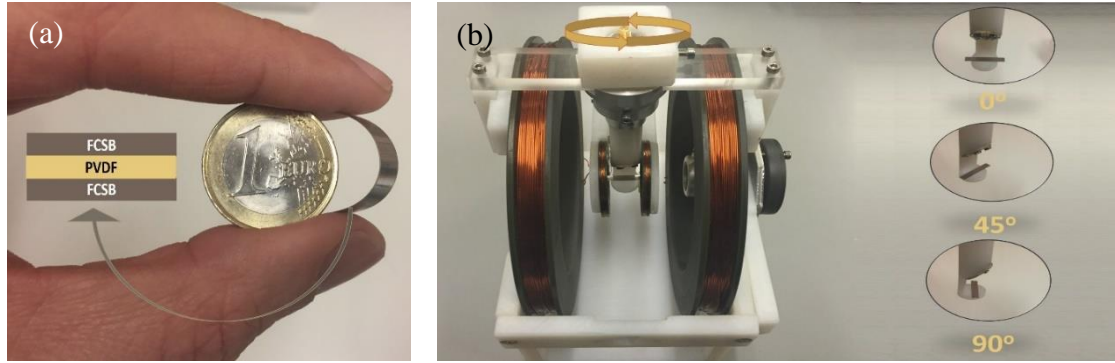
Figure 5.1. (a) Flexible ME laminate sample and schematic representation of the different layers; (b) representation of the ME measureent setup.

The samples were measured in a system composed of two Helmholtz coils, one generating the dc magnetic field (H_{dc}) in the range 0 to 20 Oe, and another generating the ac magnetic field (H_{ac}) in the range 0 to 0.25 Oe. The voltage induced by the PVDF layer was measured with a (Stanford Research SR530) lock-in amplifier.

In order to determine the resonance frequency of the composite, the H_{dc} and H_{ac} values were maintained constant (7 Oe and 0.1 Oe, respectively) and the frequency was changed from 5 kHz to 100 kHz. The dc magnetic field sensor characterization was performed by keeping the H_{ac} and frequency values constant (0.1 Oe and 54.5 kHz, respectively). The ac magnetic field sensor characterization was carried out by keeping the H_{dc} and frequency values constant (7 Oe and 54.5 kHz, respectively).

For the ME anisotropic measurements, the angle between the sample and the magnetic field direction was changed from 0 to 360º (Figure 5.1b), with both magnetic fields H_{dc} and H_{ac} kept constant (7 Oe and 0.1 Oe, respectively).

The ME coefficient (α_{33}) was determined through equation 5.1,

$$\alpha_{33} = \frac{\Delta V}{t \cdot H_{ac}} \tag{5.1}$$

where ΔV, t and H_{ac} are the induced ME voltage, the PVDF thickness and the ac magnetic field, respectively.

The linearity and accuracy of a sensor are typically expressed as a percentage of the full-scale output (FSO), i.e., the ratio of the maximum output deviation (Δ) divided by the FSO (as shown in equation 5.2) [23].

$$\%FSO = \frac{\Delta}{FSO} \times 100\% \tag{5.2}$$

The linearity Δ value was determined by the maximum output deviation from the linear fit and the accuracy Δ value was determined by the maximum output deviation between the data for the same magnetic field value.

5.3 Results and discussion

5.3.1 Magnetoelectric response optimization

Before sensor characterization, the optimum H_{dc} and frequency values of the FCSB/PVDF/FCSB composite were determined by optimizing the magnetoelectric output voltage, V_{ME}, values (Figure 5.2).
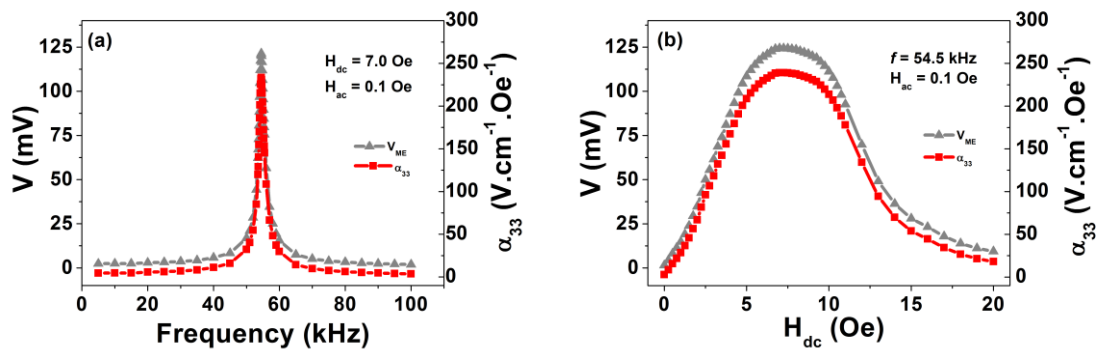
Figure 5.2. Magnetoelectric voltage (V_{ME}) and ME coefficient (α_{33}) as a function of: (a) frequency and (b) H_{dc}.

Figure 5.2 shows that the highest room temperature ($\approx 25°C$) ME voltage response of 121.4 mV is obtained at the 54.5 kHz electromechanical resonance frequency (Figure 5.2a). Such resonance results from the acoustic oscillations in the composite, sample geometry and mechanical coupling parameters between the layers [24-27]. Furthermore, the ME voltage increases with increasing H_{dc} up to 7 Oe, at which the maximum ME voltage is reached (α_{33} =239 V·cm^{-1}·Oe^{-1}, Figure 5.2b). Such behaviour is related to the increase of the piezomagnetic coefficient up to the optimum dc magnetic field. With a further increase of the H_{dc}, a decrease in the induced ME voltage occurs, resulting from the saturation of the magnetostriction response [16, 28, 29].

5.3.2 Magnetoelectric response anisotropy

In order to study the anisotropic ME response of the FCSB/PVDF/FCSB laminate, Figure 5.3 shows the ME voltage as a function of the angle between the sample length and the applied magnetic fields at resonance (54.5 kHz, Figure 5.3a) and non-resonance frequencies (10 kHz, Figure 5.3b) at the optimum H_{dc} magnetic field (7 Oe).
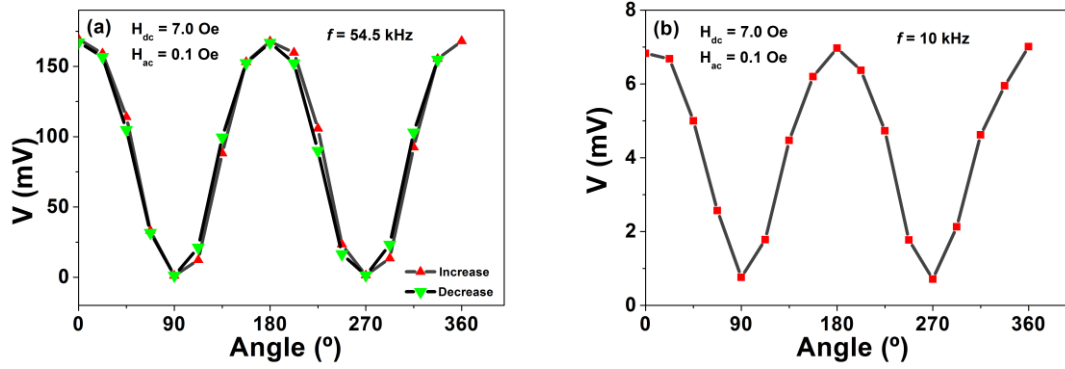
Figure 5.3. V_{ME} value variation with the angle between 0 and 360º at: (a) resonance frequency and (b) non-resonance frequency.

Figure 5.3a shows a V_{ME} maximum of 167.8 mV for 0, 180 and 360 degrees (where the magnetic fields have the same direction of FCSB magnetization) and a minimum of 1.4 mV for 90 and 270 degrees (where the magnetic fields and FCSB magnetization are perpendicular) for the 54.5 kHz resonance frequency. There is a good match between the measurements performed with an increasing H_{dc} (up-measurement) and a decreasing H_{dc} (down-measurement).

In turn, Figure 5.3b shows that V_{ME} has a maximum of 7 mV for 0, 180 and 360 degrees and a minimum of 0.8 mV for 90 and 270 degrees when the measurements are performed at the non-resonance frequency of 10 kHz.

Thus, both for resonance and non-resonance frequencies, the V_{ME} decreases with the variation of the angle between 0 and 90 degrees, increasing again until a new maximum at 180º is reached. The same behaviour occurs between 180 and 360 degrees. Such results are explained by the anisotropic behaviour of the piezomagnetic coefficient (q) and the magnetostrictive coefficient (λ_{33}) in the magnetostrictive layers that depend on the angle of applied H_{dc} [16]. Despite the anisotropic ME response at non-resonance frequencies (10 kHz) being ≈20 times lower than the anisotropic ME response at resonance frequencies (54.5 kHz), Figure 5.3 demonstrates that it is possible to use FCSB/PVDF/FCSB anisotropic-based magnetic sensors over a wide range of frequencies between 5 kHz and 100 kHz.

5.3.3 Accuracy, linearity and sensitivity

The suitability of the FCSB/PVDF/FCSB composite as an innovative magnetic field sensor was determined by obtaining its accuracy, linearity and sensitivity for three distinct ranges 0–1.6 Oe, 0–3.5 Oe and 0–5 Oe for the dc sensor and 0–0.05 Oe, 0–0.1 Oe and 0–0.25 Oe for the ac sensor.

Figure 5.4 shows the voltage/H_{dc} curves for the three ranges.
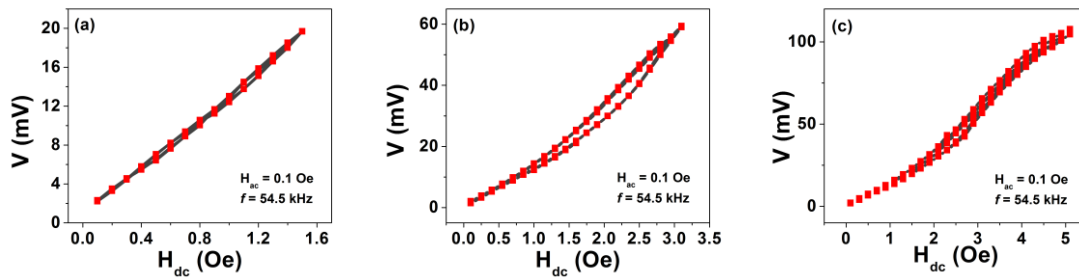
Figure 5.4. Characterization of the dc magnetic field sensor along the H_{dc} range: (a) 0–1.6 Oe, (b) 0–3.5 Oe and (c) 0–5 Oe.

In order to evaluate the dc magnetic field sensor features, H_{ac} was kept constant (0.1 Oe and 54.5 kHz) and H_{dc} was varied between three ranges, 0–1.6 Oe, 0–3.5 Oe and 0–5 Oe.

Figure 5.4 shows that the ME voltage generated in the composite increases with increasing H_{dc} due to: (i) the increase of the piezomagnetic coefficient in those ranges; and (ii) the non-saturated magnetostriction over the three evaluated H_{dc} ranges [16, 28, 29].

Figure 5.4 also shows a small ME hysteresis at a H_{dc} higher than 1 Oe as a result of the magnetic hysteresis of the FCSB alloy [30]. Nevertheless, such hysteresis does not significantly affect the accuracy, linearity or sensitivity values of the FCSB/PVDF/FCSB dc magnetic field sensor (Table 5.1).

Table 5.1. FCSB/PVDF/FCSB dc magnetic field sensor characteristics as obtained in this work, and a comparison with recent related sensors based on different types of technology.

Parameter/range	0–1.6 Oe	0–3.5 Oe	0–5 Oe	Related sensors/technology
Accuracy (FSO)	98	98	99	99 [31] GMI
Linearity (FSO/r^2)	96/0.998	92/0.97	92/0.98	94/0.998 [32] Magnetic fluid
Sensitivity (mV·Oe^{-1})		15		0.06 [33] Magnetic diodes

Table 5.1 shows that the accuracy and linearity values of the FCSB/PVDF/FCSB sensor are in the same order of the latest GMI, magnetic diode and magnetic fluid dc magnetic field sensors; however, the dc sensitivity of the FCSB/PVDF/FCSB sensor developed in this work is two orders of magnitude higher than the highest magnetic sensitivity reported for anisotropic sensors able detect the magnitude and direction of the dc magnetic field. This allows the practical implementation of the proposed sensor in areas such as magnetic compassing, navigation and magnetic anomaly monitoring [3, 34], among others.

Similar to the procedure carried out for the validation of the composite as a dc magnetic field sensor, the behaviour of the FCSB/PVDF/FCSB laminate as an ac magnetic field sensor was studied in three distinct H_{ac} ranges, 0–0.05 Oe, 0–0.01 Oe and 0–0.25 Oe (Figure 5.5) while maintaining the H_{dc} constant at 7.0 Oe.
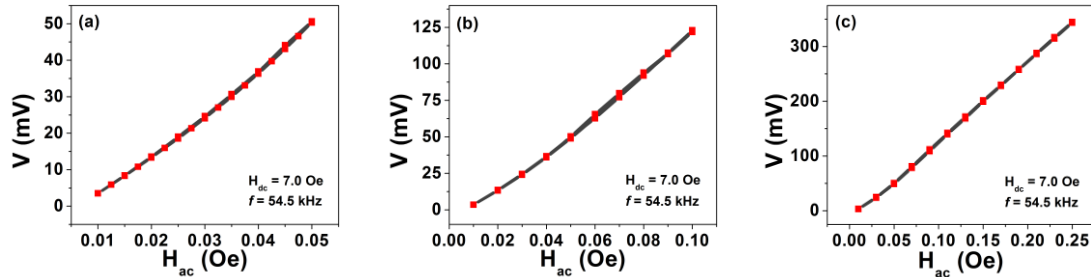
Figure 5.5. Characterization of the ac magnetic field sensor at the H_{ac} range: (a) 0–0.05 Oe, (b) 0–0.1 Oe and (c) 0–0.25 Oe.

Figure 5.5 proves the non-existence of hysteresis in the evaluated H_{ac} ranges, which will lead to a better linearity. Similar to the results shown in Figure 5.4, Figure 5.5 shows an increase of the ME voltages with increasing H_{ac}, which has just been explained by equation 5.1: for a given ME coefficient on the same magnetostrictive–piezoelectric–magnetostrictive (MPM) laminate and under the same H_{dc} conditions, a higher H_{ac} will lead to a higher ΔV_{ME}.

Plots from Figure 5.5 allow us to obtain the accuracy, linearity and sensitivity values of the FCSB/PVDF/FCSB ac magnetic field sensor, as defined in the experimental part (Table 5.2).

Table 5.2. FCSB/PVDF/FCSB ac magnetic field sensor characteristics as obtained in this work, and a comparison with other recent related sensors using different types of technology.

Parameter/range	0–0.05 Oe	0–0.1 Oe	0–0.25 Oe	Related sensors/technology
Accuracy (FSO)	98	98	99	96-98 [35-37] MRI, TV, HE
Linearity (FSO/r^2)	96/0.996	98/0.996	99/0.9993	97-98 [37, 38] HE, GMI
Sensitivity (mV·Oe^{-1})		1400		≤700 [38, 39] GMI, GMR

Similar to the evaluation of the FCSB/PVDF/FCSB laminates as a dc magnetic field sensor, Table 5.2 shows that the FCSB/PVDF/FCSB ac magnetic field sensor competes with state-of-the-art GMI, GMR, the Hall effect (HE), tuned varistors (TV) and magnetic resonance imaging (MRI) sensors in terms of accuracy and linearity, leading to a better performance in terms of sensitivity – up to two times higher than those based on GMI.

By analysing the performance of both dc and ac magnetic field sensors together, it is found that the values reported in the present work are both among the best reported in the

literature with respect to accuracy and linearity, leading to better sensitivity than other sensing technology, such as AMR (8 mV·Oe^{-1}) and GMR (80 mV·Oe^{-1}).

The magnetic sensing ability of these H_{dc} and H_{ac} ranges has previously proved to be quite useful in magnetoencephalography and magnetocardiography, motion detection, engine control, linear and angular acceleration monitoring, as well as in magnetic sensing relating to current sensors, speed sensors, angular sensors, electronic steering, battery management, vehicle transmission and digital compasses [10, 40, 41].

5.3.4   Reproducibility

Since the reproducibility of magnetic field sensors is an issue of main concern [19, 42], it was studied by turning the H_{dc} on and off 20 times (Figure 5.6a), by turning the H_{ac} on and off 20 times (Figure 5.6b), and by monitoring the stability of the ME voltage response over a week.
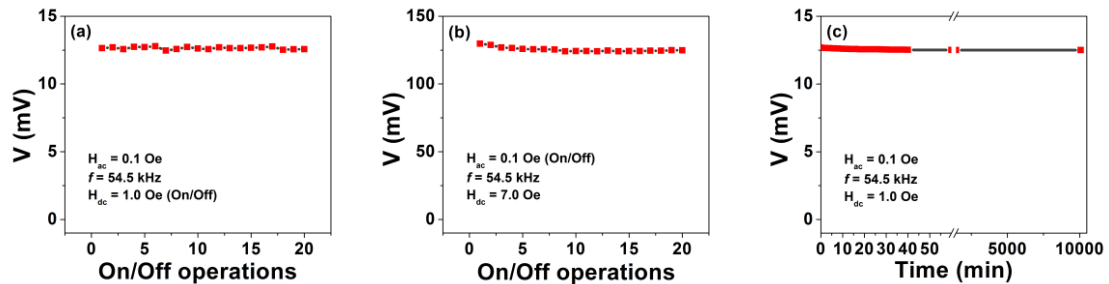
Figure 5.6. Reproducibility of the FCSB/PVDF/FCSB sensor with: (a) dc magnetic field on/off switching, (b) ac magnetic field on/off switching and (c) over time.

Figure 5.6 demonstrated the excellent reproducibility of the FCSB/PVDF/FCSB magnetic field sensor since the accuracy errors resulting from the dc magnetic field on/off switching, from the ac magnetic field on/off switching and from time stability are lower than 1%.

5.4   Conclusions

An innovative magnetic field sensor based on FCSB/PVDF/FCSB laminates is proposed. Such a sensor is able to detect both ac and dc magnetic field magnitude and direction, based on the anisotropic ME effect.

The reported accuracy and linearity values for both dc (99% and 92%) and ac (99% and 99%) magnetic field sensing are among the highest reported in the literature with respect to ME magnetic field sensing, and comparable with the ones reported for other conventional types of sensing technology, such as GMI, GMR or MRI.

Furthermore, the achieved sensitivity levels of the FCSB/PVDF/FCSB laminate – 15 and 1400 mV·Oe^{-1} respectively for dc and ac magnetic field sensing – are higher than those of conventional magnetic field sensors.

Such features, as well as the excellent reproducibility (higher than 99%) and flexibility of the FCSB/PVDF/FCSB sensor make it very attractive for the magnetic field sensing industry.

5.5 References

[1]   M. J. Caruso, T. Bratland, C. H. Smith, and R. Schneider, "A new perspective on magnetic field sensing," *Sensors (Peterborough, NH),* vol. 15, pp. 34-46, 1998.

[2]   P. Ripka, "Sensors based on bulk soft magnetic materials: Advances and challenges," *Journal of Magnetism and Magnetic Materials,* vol. 320, pp. 2466-2473, 2008.

[3]   J. Lenz and A. S. Edelstein, "Magnetic sensors and their applications," *IEEE Sensors Journal,* vol. 6, pp. 631-649, 2006.

[4]   V. Luong, J. Jeng, B. B. Lai, J. Hsu, C. Chang, and C. Lu, "Design of three-dimensional magnetic field sensor with single bridge of spin-valve giant magnetoresistance films," in *2015 IEEE International Magnetics Conference, INTERMAG 2015*, 2015.

[5]   C. Sander, C. Leube, T. Aftab, P. Ruther, and O. Paul, "Isotropic 3D silicon hall sensor," in *Proceedings of the IEEE International Conference on Micro Electro Mechanical Systems (MEMS)*, 2015, pp. 893-896.

[6]   S. Lozanova, S. Noykov, and C. Roumenin, "Three-dimensional magnetometer based on subsequent measurement principle," *Sensors and Actuators, A: Physical,* vol. 222, pp. 329-334, 2015.

[7]   A. L. Khvalin, "A Vector Magnetometer for Measuring Weak Fields," *Measurement Techniques,* vol. 57, pp. 1184-1188, 2015.

[8]   A. L. Herrera-May, L. A. Aguilera-Cortés, P. J. García-Ramírez, and E. Manjarrez, "Resonant magnetic field sensors based on MEMS technology," *Sensors,* vol. 9, pp. 7785-7813, 2009.

[9]   M. Alnassar, A. Alfadhel, Y. P. Ivanov, and J. Kosel, "Magnetoelectric polymer nanocomposite for flexible electronics," *Journal of Applied Physics,* vol. 117, 2015.

[10]   P. Martins and S. Lanceros-Méndez, "Polymer-based magnetoelectric materials," *Advanced Functional Materials,* vol. 23, pp. 3371-3385, 2013.

[11]   M. Q. Le, F. Belhora, A. Cornogolub, P. J. Cottinet, L. Lebrun, and A. Hajjaji, "Enhanced magnetoelectric effect for flexible current sensor applications," *Journal of Applied Physics,* vol. 115, 2014.

[12]   P. Martins, A. Larrea, R. Gonçalves, G. Botelho, E. V. Ramana, S. K. Mendiratta, *et al.*, "Novel anisotropic magnetoelectric effect on δ-FeO(OH)/P(VDF-TrFE) multiferroic composites," *ACS Applied Materials and Interfaces,* vol. 7, pp. 11224-11229, 2015.

[13]   P. Martins, A. C. Lopes, and S. Lanceros-Mendez, "Electroactive phases of poly(vinylidene fluoride): Determination, processing and applications," *Progress in Polymer Science,* vol. 39, pp. 683-706, 2014.

[14]   M. P. Silva, P. Martins, A. Lasheras, J. Gutiérrez, J. M. Barandiarán, and S. Lanceros-Mendez, "Size effects on the magnetoelectric response on PVDF/Vitrovac 4040 laminate composites," *Journal of Magnetism and Magnetic Materials,* vol. 377, pp. 29-33, 2015.

[15]   V. Sudarsanan, C. Lekha, and V. Saravanan, "Multiferroic / magneto-electric composite thin films: A review of recent patents," *Recent Patents on Materials Science,* vol. 7, pp. 99-102, 2014.

[16]   X. W. Dong, B. Wang, K. F. Wang, J. G. Wan, and J. M. Liu, "Ultra-sensitive detection of magnetic field and its direction using bilayer PVDF/Metglas laminate," *Sensors and Actuators, A: Physical,* vol. 153, pp. 64-68, 2009.

[17]   R. Boll and K. J. Overshott, *Sensors: Magnetic Sensors* vol. 5, 2008.

[18]   F. Chen, Y. Jiang, and L. Jiang, "3×3 coupler based interferometric magnetic field sensor using a TbDyFe rod," *Applied Optics,* vol. 54, pp. 2085-2090, 2015.

[19]   T. Liu, Y. Chen, Q. Han, and X. Lu, "Magnetic field sensor based on U-bent single-mode fiber and magnetic fluid," *IEEE Photonics Journal,* vol. 6, 2014.

[20]   C. S. Park, D. Avirovik, S. Bressers, and S. Priya, "Low-frequency nanotesla sensitivity in Metglas/piezoelectric/carbon fiber/piezoelectric composites with active tip mass," *Applied Physics Letters,* vol. 98, 2011.

[21]   Y. K. Fetisov, D. A. Burdin, D. V. Chashin, and N. A. Ekonomov, "High-sensitivity wideband magnetic field sensor using nonlinear resonance magnetoelectric effect," *IEEE Sensors Journal,* vol. 14, pp. 2252-2256, 2014.

[22]   J. G. Tao, Y. Y. Jia, H. Wu, and J. G. Yang, "Low-frequency nanotesla resolution of magnetic field detection in Metglas/magnetostrictive/piezoelectric laminates," in *Advanced Materials Research* vol. 960-961, ed, 2014, pp. 695-699.

[23]   G. Singh, O. Guyon, P. Baudoz, N. Jovanovich, F. Martinache, T. Kudo, *et al.*, "Lyot-based low order wavefront sensor: Implementation on the Subaru Coronagraphic Extreme Adaptive Optics System and its laboratory performance," in *Proceedings of SPIE - The International Society for Optical Engineering*, 2014.

[24]   F. Yang, Y. M. Wen, P. Li, M. Zheng, and L. X. Bian, "Resonant magnetoelectric response of magnetostrictive/piezoelectric laminate composite in consideration of losses," *Sensors and Actuators, A: Physical,* vol. 141, pp. 129-135, 2008.

[25]   M. I. Bichurin, D. A. Filippov, V. M. Petrov, V. M. Laletsin, N. Paddubnaya, and G. Srinivasan, "Resonance magnetoelectric effects in layered magnetostrictive-piezoelectric composites," *Physical Review B - Condensed Matter and Materials Physics,* vol. 68, pp. 1324081-1324084, 2003.

[26]   D. A. Filippov, M. I. Bichurin, V. M. Petrov, V. M. Laletin, N. N. Poddubnaya, and G. Srinivasan, "Giant Magnetoelectric Effect in Composite Materials in the Region of Electromechanical Resonance," *Technical Physics Letters,* vol. 30, pp. 6-8, 2004.

[27]   D. A. Filippov, "Theory of the magnetoelectric effect in ferromagnetic-piezoelectric heterostructures," *Physics of the Solid State,* vol. 47, pp. 1118-1121, 2005.

[28]   Y. S. Koo, K. M. Song, N. Hur, J. H. Jung, T. H. Jang, H. J. Lee, *et al.*, "Strain-induced magnetoelectric coupling in BaTiO3/Fe3O4 core/shell nanoparticles," *Applied Physics Letters,* vol. 94, 2009.

[29]   Y. X. Zheng, Q. Q. Cao, C. L. Zhang, H. C. Xuan, L. Y. Wang, D. H. Wang, *et al.*, "Study of uniaxial magnetism and enhanced magnetostriction in magnetic-annealed polycrystalline CoFe2O4," *Journal of Applied Physics,* vol. 110, 2011.

[30] Z. Turgut, H. Kosai, T. Bixel, J. Scofield, S. L. Semiatin, and J. Horwath, "Hysteresis loss analysis of soft magnetic materials under direct current bias conditions," *Journal of Applied Physics,* vol. 117, 2015.

[31] M. Zidi, A. Asfour, and J. P. Yonnet, "RMS-to-DC converter for GMI magnetic sensor," *IEEE Transactions on Magnetics,* vol. 51, 2015.

[32] J. Yao and D. Li, "Research on the linearity of a magnetic fluid micro-pressure sensor," *Sensors and Actuators, A: Physical,* vol. 229, pp. 36-41, 2015.

[33] X. Zhao, X. Yang, Y. Yu, T. Wu, and D. Wen, "Characteristics of 2D magnetic field sensor based on magnetic sensitivity diodes," *AIP Advances,* vol. 5, 2015.

[34] S. M. Gillette, T. Fitchorov, O. Obi, L. Jiang, H. Hao, S. Wu*, et al.*, "Effects of intrinsic magnetostriction on tube-topology magnetoelectric sensors with high magnetic field sensitivity," *Journal of Applied Physics,* vol. 115, 2014.

[35] L. Huang and S. Lee, "Effect of sensor positioning error on the accuracy of magnetic field mapping result for NMR/MRI," *Progress in Superconductivity and Cryogenics (PSAC),* vol. 17, pp. 28-32, 2015.

[36] R. K. Pandey, W. A. Stapleton, I. Sutanto, and M. Shamsuzzoha, "Voltage-Biased Magnetic Sensors Based on Tuned Varistors," *Journal of Electronic Materials,* vol. 44, pp. 1100-1109, 2015.

[37] X. Cheng, Z. Zhang, F. Li, and S. Liu, "Hall-effect closed-loop current sensor based on an optimized magnetic core structure," *Journal of Computational and Theoretical Nanoscience,* vol. 11, pp. 1121-1128, 2014.

[38] V. M. García-Chocano and H. García-Miquel, "DC and AC linear magnetic field sensor based on glass coated amorphous microwires with Giant Magnetoimpedance," *Journal of Magnetism and Magnetic Materials,* vol. 378, pp. 485-492, 2015.

[39] V. S. Luong, J. T. Jeng, B. L. Lai, J. H. Hsu, C. R. Chang, and C. C. Lu, "Design of 3-D Magnetic Field Sensor with Single Bridge of Spin-Valve Giant Magnetoresistance Films," *IEEE Transactions on Magnetics,* vol. 51, 2015.

[40] Y. J. Wang, J. Q. Gao, M. H. Li, Y. Shen, D. Hasanyan, J. F. Li*, et al.*, "A review on equivalent magnetic noise of magnetoelectric laminate sensors," *Philosophical Transactions of the Royal Society A: Mathematical, Physical and Engineering Sciences,* vol. 372, 2014.

[41] I. N. Soloviev, M. I. Bichurin, and R. V. Petrov, "Magnetoelectric magnetic field sensors," in *Progress in Electromagnetics Research Symposium*, 2012, pp. 1359-1362.

[42] K. Singal, R. Rajamani, M. Ahmadi, A. S. Sezen, and J. E. Bechtold, "Magnetic sensor for configurable measurement of tension or elasticity with validation in animal soft tissues," *IEEE Transactions on Biomedical Engineering,* vol. 62, pp. 426-437, 2014.
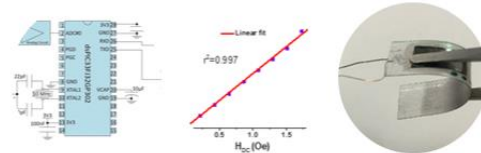
6 Fabrication and characterization of high-performance polymer-based magnetoelectric dc magnetic field sensors devices

A dc magnetic field sensor based on a magnetoelectric PVDF/Metglas composite was developed. By incorporating a charge amplifier, an ac–rms converter and a microcontroller with an on chip analog to digital converter, the magnetoelectric voltage response is not distorted, the linearity is maintained, and the magnetoelectric output voltage increases.
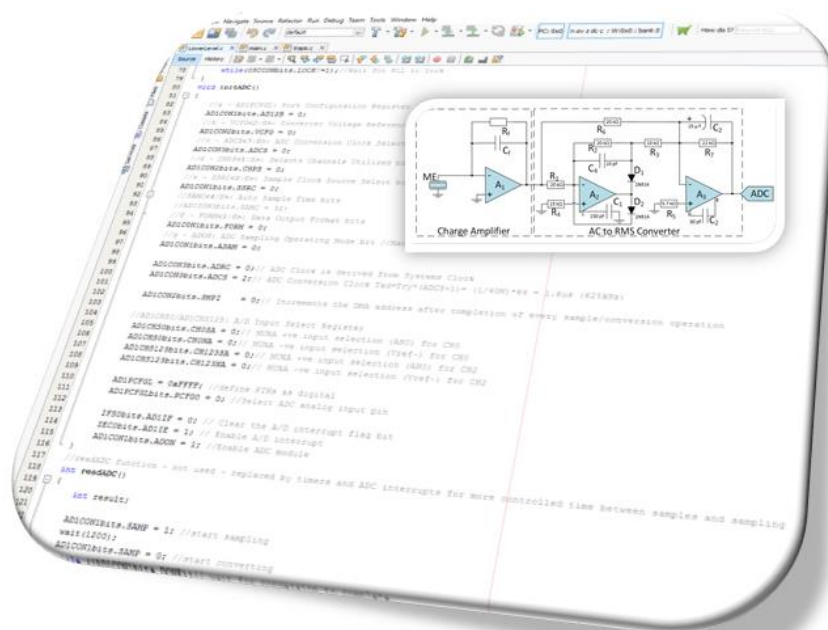
6.1 Introduction

Magnetic field sensors have several characteristics, depending on the application requirements, and can be found in small integrated circuit devices, commonly placed in gadgets, domestic, and industrial electronic utilities, among others [1, 2]. Magnetic sensors have, thus, become an essential measuring tool in a range of application areas including biomedicine, multimedia, automobile, and military, just to mention some of them [3, 4]. There are a large variety of specifications for this kind of sensors, being magnetic field range, sensitivity, sensor noise, sensor size, cross-field error, hysteresis, and offset drift the most important ones [1, 5]. Each specification is particularly relevant if it is essential for the intended application. In this way, there are large market opportunities for the different types of magnetic sensors. From the different magnetic sensing technologies, the ones based on Hall effect are those with the largest market share due to their high linearity and no saturation effects in their operation range, being able to reach a sensitivity up to 5 $V \cdot T^{-1}$ [6]. Nevertheless, as the applications of magnetic sensing devices in areas such as automotive industry, navigation, and electronics impose increasing demand for vector magnetometers with high precision, the inability on the precise measurement of the magnetic field vector with Hall effect materials is a large drawback in its application potential [7]. Hall sensors suffer from high signal noise, cross-sensitivity between measurement axes due to angular errors or the planar Hall effect, and the inability to measure magnetic fields at precise locations [8]. In addition, industry constantly demands for smaller, cheaper, and low-powered magnetic sensors, even when the sensitivity is sacrificed; the decrease of the size and a simple integration being exclusion factors for a large variety of applications [3]. In order to solve these problems, magnetoelectric (ME) sensors based on composites have become an object of increasing interest in the scientific community, mainly motivated by their potential applications as magnetic sensing devices [9, 10], allowing the measurement of ac and dc field vector [11, 12]. The figure of merit on those ME composites is quantified by the α_{33} ME coefficient [13, 14], such effect being a consequence of a stress-mediated interaction between the magnetostrictive phase and the piezoelectric phase. However, the piezoelectric phase material is usually a ceramic that has some drawbacks, such as being costly, rigid, and fragile, leading to an expensive processing and a difficult implementation, especially for microelectromechanical systems (MEMS) fabrication [15]. Such limitations constitute

the main reasons why flexible smart magnetic sensing devices have been barely used in commercial applications. The best way to overcome such limitations and to open novel application routes is the use of flexible and nonbrittle ME composites based on piezoelectric polymers [13]. In contrast with ceramic-based ME composites, polymer-based ME composites can be easily fabricated by conventional low-temperature processing into a variety of forms, such as thin sheets or moulded shapes, and can exhibit improved mechanical properties, meeting the latest market demands [13, 15]. In this way, different magnetic sensors based on polymer-based ME composite have been built and tested in order to find the composites with the best ME coupling among the many available possibilities; different number of layers, materials, layer sizes, and thicknesses, among others [16-20]. Further, studies report on the combination of different piezoelectric polymers [21-23], and magnetostrictive rare-earth-iron alloys [24, 25]. The applicability of these materials as sensors not only depend on the ME coupling, but also on some practical characteristics, such as their full-scale input (FS), sensitivity, linearity, and resolution [26]. ME sensors can detect static and dynamic magnetic fields, the FS of a dc magnetic field sensor being directly related to the configuration and the type of magnetostrictive material that composes the ME composite, in the order of 0 to 10 Oe in laminated ME composites based on Metglas [23], 0 to 1000 Oe in laminated ME composites with Terfenol-D, 0 to 2500 Oe in particulate ME composites with $CoFe_2O_4$ [21], and 0 to 5000 Oe in particulate ME composites with $Ni_{0.5}Zn_{0.5}Fe_2O_4$ [27].

Despite the large interest on polymer-based ME sensing materials, the signal generated by the ME composite through the piezoelectric layer is in the form of a charge variation, in this way, being highly susceptible to electromagnetic interference and grid noise. This means that there is an urgent need for the optimization of the ME signal-processing conditions and for the improvement of the circuit configurations, in order to reduce environmental noise sources [9, 28]. The most used approach to decrease such noise is by using a charge amplifier circuit [9, 29], as it converts the charge signal into a voltage signal, amplifies the initial amplitude, and filters the low-frequency noise [30]. As the amplifier and its peripheral components themselves may disrupt the signal with its internal spectral and Johnson noise in the feedback-loop resistor [31], the choice of the amplifier is critical for a successful application [30] (Figure 6.1).
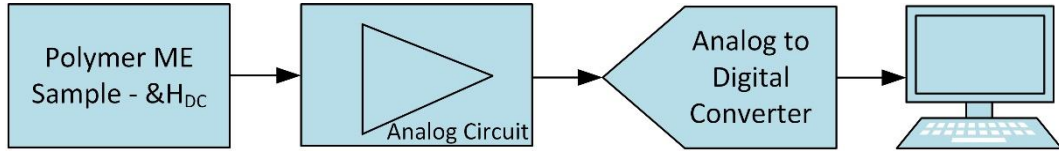
Figure 6.1. Schematic representation of the different components of the polymer-based ME sensing device.

In this way, this work will combine a charge amplifier, an ac–rms converter, and a microcontroller with an on-chip analog-to-digital converter (ADC) with a poly(vinylidene fluoride) (PVDF)/Metglas ME composite as a sensing element, in order to develop a magnetic sensing device which corresponds to the most demanding market requirements, i.e., no signal distortion, low drift, high linearity, accuracy, and sensitivity. The selection of the PVDF/Metglas composite as a sensing element is related to the high sensitivity, low noise, high magnetic permeability, and piezomagnetic coefficient of Metglas [32, 33], and to the highest piezoelectric coefficient among all polymers, stability, flexibility, large electrical resistivity, and low dielectric losses of PVDF [34]. This combination provides PVDF/Metglas composites with the highest ME response and magnetic sensitivity among all polymer-based ME materials [13].

6.2   Methods

6.2.1   ME composite fabrication

The ME laminate sensor was fabricated with a commercial β-PVDF (Measurement Specialties, Hampton, VA, USA) layer with dimensions of 10 mm × 30 mm × 52 µm, poled along the thickness direction and a magnetostrictive layer of Metglas (2605SA1, Hitachi Metals Europe GmbH, Germany) with dimensions of 5 mm × 27 mm × 25 µm, and magnetized along the longitudinal direction. The polymer-based laminate was produced by bonding the PVDF and Metglas layers with M-Bond 600 epoxy (Vishay Precision Group, Malvern, PA, USA) in a vacuum process for three hours at 50 ℃.

The magnetic sensing experiments were performed in a system composed by two Helmholtz coils (aligned with the Earth's magnetic field) in order to generate a dc magnetic field (H_{dc}) ranging from -4 to 4 Oe via a dc input current provided by a Keithley 2400, and a superimposed ac magnetic field (H_{ac}) of 0.68 Oe via an ac current provided by the Agilent 33220A signal generator. ME measurements were performed in three stages: first, the samples were characterized by measuring the voltage induced in the PVDF layer by the magnetic field variation with a lock-in amplifier (Stanford Research

SR530); second, a Rigol DS 1074Z oscilloscope was used to measure the voltage at the electronic circuits; and finally a C# application was used to develop the user interface.

Since the ME sample behaves like an antenna being susceptible to electromagnetic noise, the ME signal was measured using the lock-in amplifier, in order to apply a narrow band-pass filter to the ME signal. The lock-in amplifier was synchronized using the same ac signal from the signal generator Agilent 33220A.

To detect the electromechanical resonance frequency of the composite, H_{dc} and H_{ac} values were maintained constant (4 and 0.68 Oe, respectively), and the frequency was changed from 5 kHz to 100 kHz. The optimum H_{dc} was achieved by keeping the H_{ac} and frequency values constant (0.68 Oe and 25.4 kHz, respectively). The ME coefficient (α_{33}) was determined through

$$\alpha_{33} = \frac{\Delta V}{t \cdot H_{ac}} \tag{6.1}$$

where ΔV, t and H_{ac} are the induced ME voltage, the PVDF thickness, and the ac magnetic field intensity value, respectively.

6.2.2 Analog ME signal conversion

In order to obtain the sensor signal to be read by an ADC, the charge signal generated by the ME sample must be converted to voltage by the use of a charge amplifier. As the signal variations over time are small and the focus of this chapter is a dc magnetic field sensor, the ME ac voltage signal was coupled to an ac–rms converter, establishing a ME dc signal and reducing the sampling speed requirements.

Figure 6.2 displays schematically the two phases of the signal conditioning process, the first stage consisting of a charge amplifier and the second an ac–rms converter.
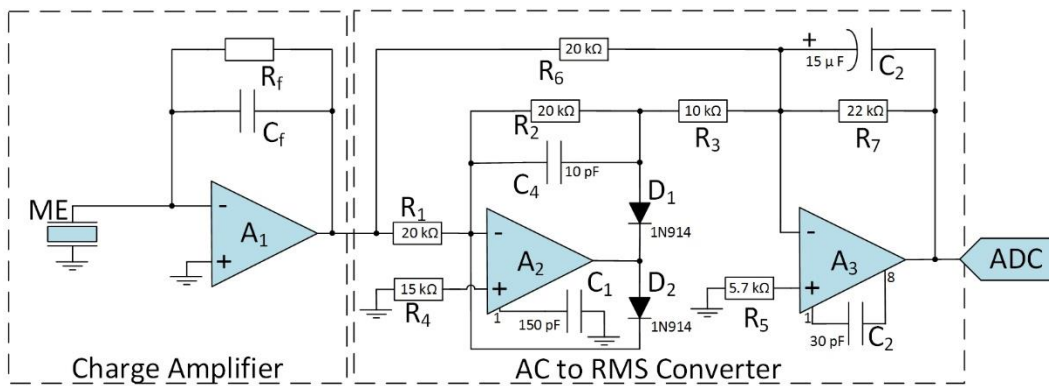
Figure 6.2. ME signal modulation circuit with two different stages. In the first stage there is a charge amplification resulting in an ac voltage output signal, followed by a second stage, working as an ac-to-dc voltage converter, which results in a dc level corresponding to the original ac input rms value.

The first stage of the circuit shown in Figure 6.2 displays a feedback loop and is composed by a capacitor (C_f) and a resistor (R_f) in parallel, together with a MCP6021 amplifier (A1). This amplifier was selected due its high input impedance, low input bias current, and high-frequency gain [29]. In a charge signal, this circuit topology works as a high-pass filter [35]. As the operating frequency of the sensor ranges in the tens of kilohertz, the cutting frequency generated by this filter works as an optimum method to reduce low-frequency electrical grid noise. The charge amplifier gain can be calculated by equation 6.2, and the high-pass filter cutting frequency (f_{HPF}) by equation 6.3 [35, 36].

$$Gain = \frac{1}{C_f}(mV/C) \qquad (6.2)$$

$$f_{HPF} = \frac{1}{2\pi R_f C_f} \qquad (6.3)$$

The main concerns with the selection of the suitable feedback loop components values are related with an optimized commitment between the amplifier gain, a filter cutting frequency below the ME operating signal frequency, and a feedback resistor below 1 GΩ, in order to keep the input bias current as low as possible. Input bias current is an important aspect to take into account in order to get the most of the ME signal transmitted from the amplifier (A1) instead of being consumed by it [29, 36]. The values selected for C_f and R_f were 33 pF and 220 kΩ, respectively. These values were chosen in order to get the necessary amplifier gain and, simultaneously, having a cut-off frequency high-pass filter at 22 kHz, just below the resonant frequency of 25.4 kHz.

The second stage represented in Figure 6.2 accurately converts the ac signals to its rms values up to frequencies above 100 kHz [37]. The ac to rms converter was built using of-the-shelf components together with LM301AN amplifiers (A2 and A3). Further, 1N914 diodes (D$_1$ and D$_2$), and the 150 and 30 pF capacitors (C$_1$ and C$_2$) were selected following the reference datasheet recommendations. The time-constant filter must be higher than the maximum period of the ac input signal and can be calculated from [38].

$$T = R_7 \times C_2 \qquad (6.4)$$

6.2.3 Digital ME signal processing

With the purpose of having a continuous updating program informing on the amplitude of the H_{dc}, the sensor analog data were converted to digital through the aid of a digital signal processor (DSP).

Figure 6.3 displays the scheme used to convert the analog signal into digital through the microcontroller with an on-chip ADC, and transmit it to a computer terminal.
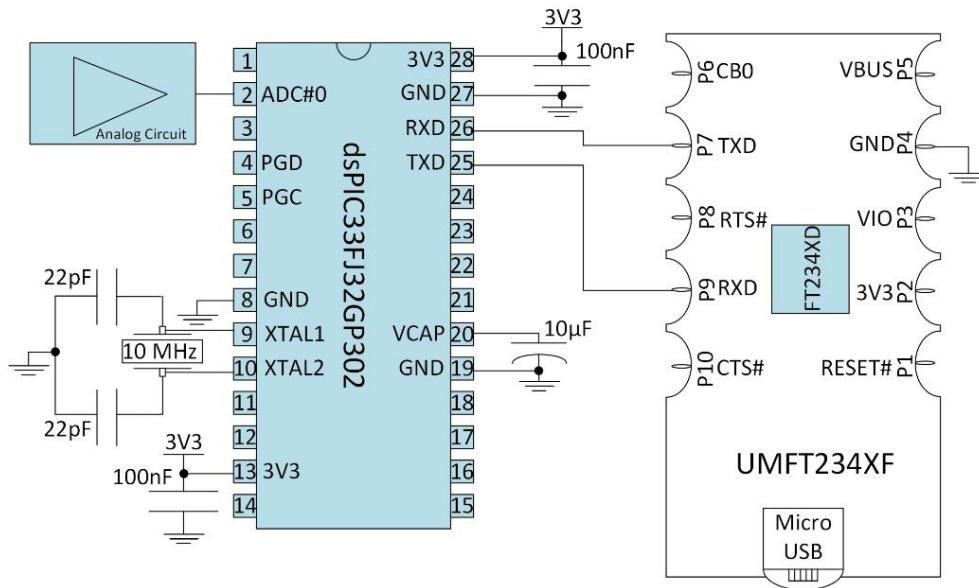
Figure 6.3. Analog-to-digital converter circuit, to which the analog circuit from Figure 6.2 was connected.

The used microcontroller was a dsPIC33FJ32GP302 from Microchip, and a UMFT234XF board from Future Technology Devices International (FTDI) was used for universal serial bus (USB) connection. This microcontroller was selected as it has a 10-bits-resolution ADC and an universal asynchronous receiver/transmitter (UART) communication. The circuit was built with the required decoupling and storage capacitors, following the design guidelines present in the microcontroller datasheet. This module was carefully mounted, taking into account the in-circuit serial programming (ICSP) connections to be easily programmed by Microchip Pickit3® with MPLAB X using XC16 compiler. The microcontroller was programmed to work with an external oscillator with a phase locked loop (PLL), achieving the maximum operating speed available of 40 MIPS (million instructions per second). The ADC was programmed to take 20 samples per second and its interrupt routine was controlled by a timer, which controls the flux of operation between peripherals. When it is not converting, the microcontroller is sending the previous sample via UART to the UMFT234XF board with a 921600 bps baud rate. The algorithm represented in Figure 6.4 illustrates the system process. The system takes each sample from the analog circuit, separates each sample in two bytes, and then communicates it via USB with a FTDI emulated communication port (COM).
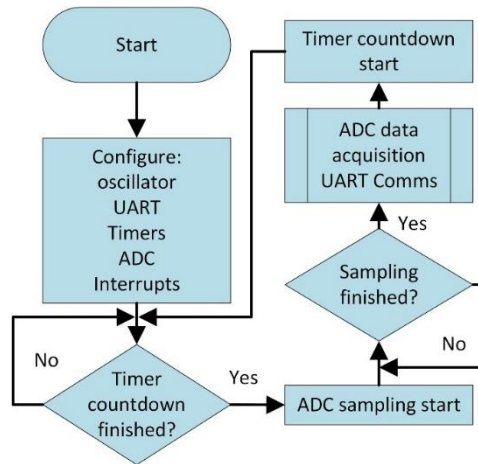
Figure 6.4. Digital circuit operating algorithm: ADC interrupt sampling, data storage, and UART communication control.

Using the data obtained from the system and from the sensor characterization linear equation, the dc magnetic field was calculated and displayed on the screen within a C# application built for that purpose. The application gets the two bytes, MSB (most significant byte) and LSB (less significant byte), joins them to get the sample value, saves in a global variable, and updates the graph as soon as a refresh-rate timer expires. The dc magnetic field value is averaged through the last sent 100 samples saved in a circular buffer.

6.3   Results and Discussion

The ME sample was characterized in terms of resonant frequency, signal amplitude, and magnetic field range; Figure 6.5 illustrates the ME sample response to frequency variation and a representative picture of a sample.
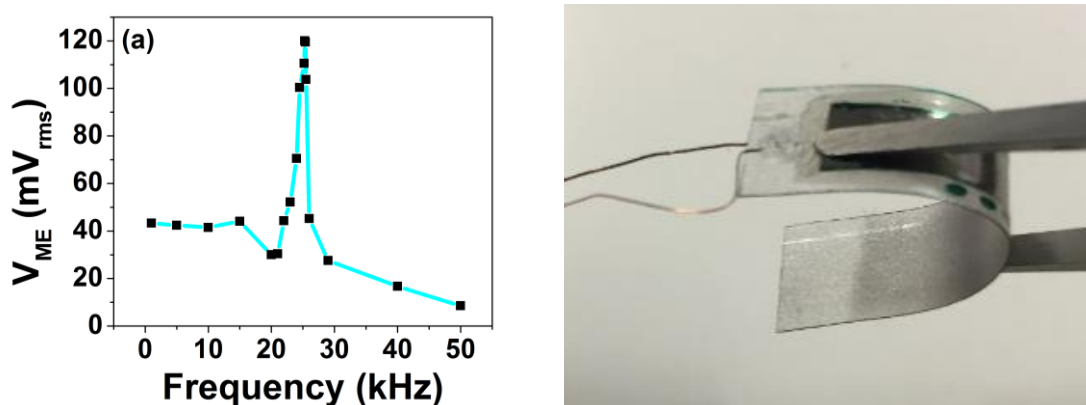
Figure 6.5. (a) ME sample output response as a function of the H_{ac} frequency, setting the H_{dc} at 4 Oe and the H_{ac_rms} amplitude at the maximum output of the Agilent 33220A signal generator (0.68 Oe) and (b) polymer-based PVDF/Metglas sample.

Figure 6.5a shows that the highest ME response was achieved at the electromechanical resonant frequency of 25.4 kHz, this value being influenced by acoustic oscillations in the ME composite, sample size, and by the mechanical coupling parameters between the piezoelectric and magnetostrictive layers [7].

In order to validate the ME sample as a H_{dc} sensor, the response of the ME composite as a function of the H_{dc} was evaluated (Figure 6.6).
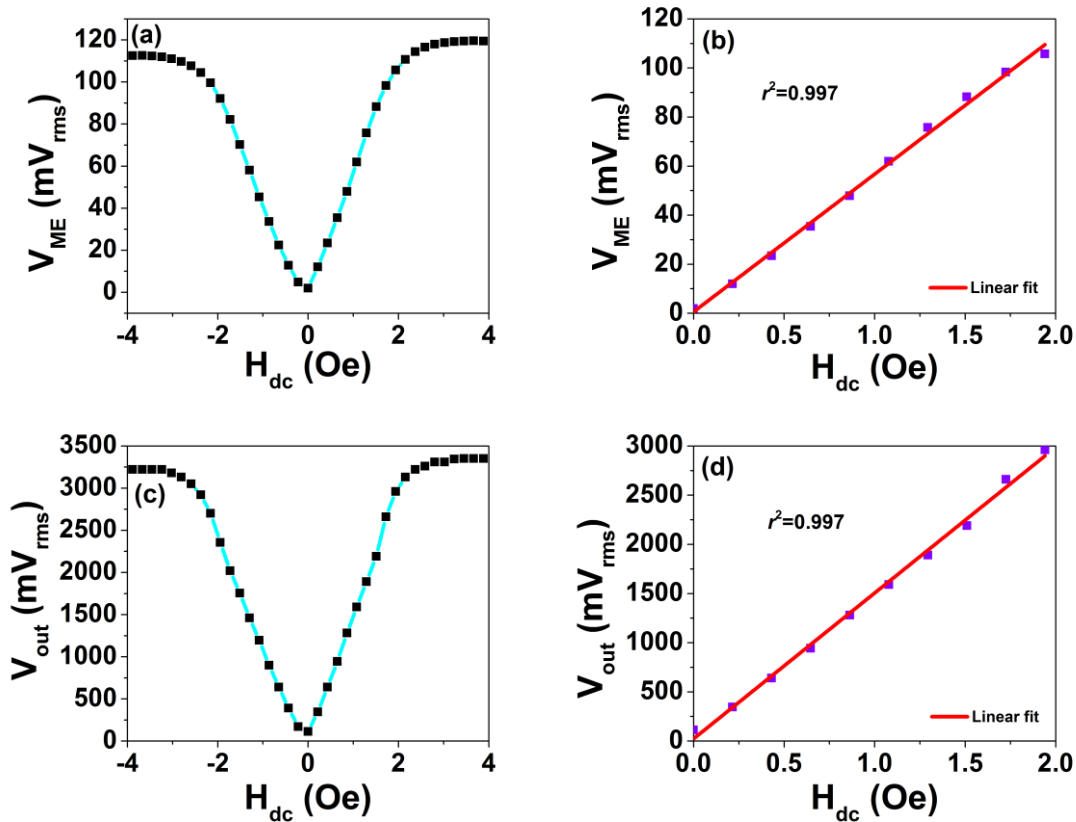
Figure 6.6. (a) ME sample output response to the variation of the H_{dc}, by setting the H_{ac} at 0.68 Oe with a frequency of 25.4 kHz, (b) the ME sample linear response can be found in the range $0 < H_{dc} < 2$ Oe, applying a H_{ac} of 0.68 Oe rms@25.4 kHz, (c) circuit output after the two stages signal conditioning: charge amplification and ac to rms converter, and (d) ME sample plus conditioning circuit amplified, and averaged dc signal linear output at an operating range between $0 < H_{dc} < 2$ Oe.

Figure 6.6a reveals that the ME response increases with increasing H_{dc} up to ≈2 Oe, at which the maximum ME voltage is reached (112 mV; ME coefficient $\alpha_{33}=30$ V·cm⁻¹·Oe⁻¹). Such increase is related with the increase in the piezomagnetic coefficient up to the optimum 2 Oe dc magnetic field. With a further increase of the dc magnetic field, a decrease in the induced ME voltage will occur, resulting from the saturation of the magnetostriction response [7].

Selecting the linear zone of the ME response (0–2 Oe) it is possible to verify $r^2=0.997$. Therefore, it is possible to conclude that, for this range, the fabricated ME

sensor has a large potential for magnetic sensing, once it has low drift at its output. Figure 6.6c reveals an increase in the ME voltage response to a maximum of ≈3.3 V after electronic amplification of the signal conditioning circuit. Figure 6.6c also shows that the nonlinear components of the developed circuit do not distort the original signal produced by the ME composite sample. Such fact together with the choice of an amplifier with an optimized power-supply rejection ratio has, as a consequence, the maintenance of the good linearity of the ME response [39] (r^2=0.997) in the 0–2 Oe range (Figure 6.6d). In order to compare the performance of the ME sensor with a sensor already in the market, a commercial Hall Gaussmeter (Hirst GM08) was used. Both, the ME and the Hall sensors measured the H_{dc} produced by the dc coils; the results being represented in Figure 6.7 and compared with the theoretical value of H_{dc} calculated according to the provided dc current. In both the sensors, a correction related with the earth's magnetic field was performed by taking into consideration the earth's magnetic field equal to 0.45 Oe for the location and date of the experiment.
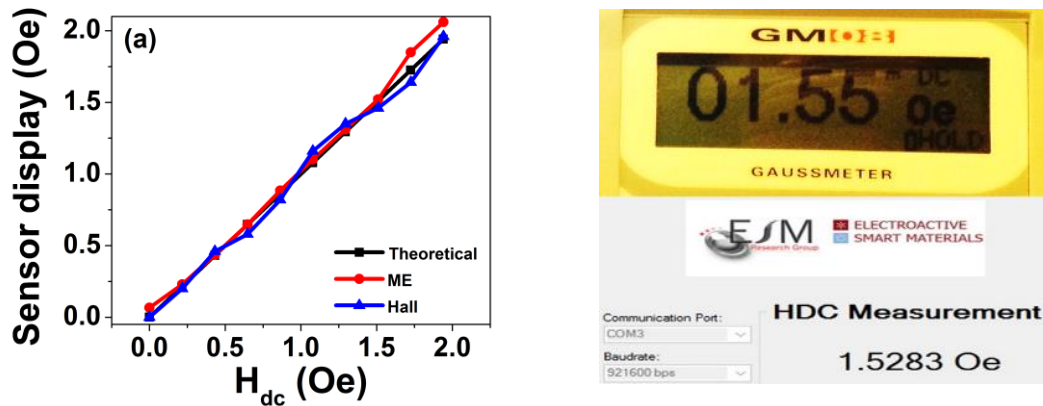
Figure 6.7. (a) Comparison between the theoretical dc magnetic field values and the values provided by the ME sensor and the Hirst GM08 Hall sensor. (b) Display values from the ME sensor (below) and the Hirst GM08 Hall sensor (above) to the theoretical dc magnetic field of 1.5289 Oe.

Figure 6.7 reveals that the ME sensor measurement has maximum drift of 0.12 Oe with an average total drift of 0.04 Oe. In turn, the Hall sensor maximum drift was 0.07 Oe and an average error of 0.16 Oe. Thus, the developed H_{dc} sensor achieved a sensitivity of 1.5 V·Oe^{-1} (15 kV·T^{-1}), 100 times higher than other polymer-based ME dc magnetic sensing devices [7], a 70 nT resolution, comparable to the best reported on ME laminates [12], and shows lower drift when compared to Hall sensors (Table 6.1).

Table 6.1. Comparison between features of ME sensor and the Hall HMIRS GM08 sensor devices

Parameter	ME sensor	Hall sensor	Comparison
Maximum drift (Oe)	0.12	0.07*	☹
Average drift (Oe)	0.04	0.16*	☺
Sensitivity (kV·T^{-1})	15	0.005**	☺
Resolution (nT)	70	2000**	☺

*measured
**on the operating manual of Hirst GM08 Hall sensor

The determined features (Table 6.1), allied to the ability of an accurately measurement of H_{dc} in the range 0–2 Oe, allows this device to be very attractive for earth's magnetic field sensing, digital compasses, navigation and magnetic field anomaly-detector applications, among others [40, 41].

Further, the complete acquisition system power consumption was 350 mW. It is to notice that the use of a printed circuit board (PCB) with surface-mounted devices (SMD) components and bayonet Neill–Concelman (BNC) connections can allow further improvement in the sensor performance, including reduced power consumption.

6.4 Conclusions

This chapter reported on the development and optimization of a magnetic field sensor, composed of ME PVDF/Metglas composite as an active sensing element, a charge amplifier, an ac–rms converter, and a microcontroller with an on chip ADC.

It was found that the resonance frequency of the device was ≈25.4 kHz, leading to a linear response (r^2=0.997) in the 0–2 Oe dc magnetic field range and a maximum output voltage of 3.3 V ($\alpha_{33effective}$=1000 V·cm^{-1}·Oe^{-1}).

The PVDF/Metglas/electronics sensing device has maximum drift of 0.12 Oe with an average total drift of 0.04 Oe. Those values were for the first time favourably compared with the ones obtained in a comparative Hirst GM08 Hall sensor (maximum drift of 0.07 Oe and an average error of 0.16 Oe).

The developed device achieves a sensitivity of 1.5 V·Oe^{-1} (15 kV·T^{-1}), suitable for magnetic sensing devices such as digital compasses or positioning systems, among others.

6.5 References

[1]   J. Včelák, P. Ripka, and A. Zikmund, "Precise Magnetic Sensors for Navigation and Prospection," *Journal of Superconductivity and Novel Magnetism,* vol. 28, pp. 1077-1080, 2015.

[2]   Z. Q. Zhang, "Two-step calibration methods for miniature inertial and magnetic sensor units," *IEEE Transactions on Industrial Electronics,* vol. 62, pp. 3714-3723, 2015.

[3]   P. Ripka, "Sensors based on bulk soft magnetic materials: Advances and challenges," *Journal of Magnetism and Magnetic Materials,* vol. 320, pp. 2466-2473, 2008.

[4]   Z. Zhang, F. Ni, Y. Dong, C. Guo, M. Jin, and H. Liu, "A novel absolute magnetic rotary sensor," *IEEE Transactions on Industrial Electronics,* vol. 62, pp. 4408-4419, 2015.

[5]   D. Robbes, "Highly sensitive magnetometers-a review," *Sensors and Actuators, A: Physical,* vol. 129, pp. 86-93, 2006.

[6]   P. Ripka and M. Janošek, "Advances in magnetic field sensors," *IEEE Sensors Journal,* vol. 10, pp. 1108-1116, 2010.

[7]   S. Reis, M. P. Silva, N. Castro, V. Correia, J. Gutierrez, A. Lasheras*, et al.*, "Optimized anisotropic magnetoelectric response of Fe61.6Co16.4Si10.8B11.2/PVDF/Fe61.6Co16.4Si10.8B11.2 laminates for AC/DC magnetic field sensing," *Smart Materials and Structures,* vol. 25, 2016.

[8]   C. Wouters, V. Vranković, C. Rössler, S. Sidorov, K. Ensslin, W. Wegscheider*, et al.*, "Design and fabrication of an innovative three-axis Hall sensor," *Sensors and Actuators, A: Physical,* vol. 237, pp. 62-71, 2016.

[9]   Y. Wang, J. Li, and D. Viehland, "Magnetoelectrics for magnetic sensor applications: Status, challenges and perspectives," *Materials Today,* vol. 17, pp. 269-275, 2014.

[10]   J. Han, J. Hu, Y. Yang, Z. Wang, S. X. Wang, and J. He, "A Nonintrusive Power Supply Design for Self-Powered Sensor Networks in the Smart Grid by Scavenging Energy from AC Power Line," *IEEE Transactions on Industrial Electronics,* vol. 62, pp. 4398-4407, 2015.

[11]   P. Martins, A. Larrea, R. Gonçalves, G. Botelho, E. V. Ramana, S. K. Mendiratta*, et al.*, "Novel anisotropic magnetoelectric effect on δ-FeO(OH)/P(VDF-TrFE) multiferroic composites," *ACS Applied Materials and Interfaces,* vol. 7, pp. 11224-11229, 2015.

[12]   S. Reis, M. P. Silva, N. Castro, V. Correia, P. Martins, A. Lasheras*, et al.*, "Characterization of Metglas/poly(vinylidene fluoride)/Metglas magnetoelectric laminates for AC/DC magnetic sensor applications," *Materials and Design,* vol. 92, pp. 906-910, 2016.

[13]   P. Martins and S. Lanceros-Méndez, "Polymer-based magnetoelectric materials," *Advanced Functional Materials,* vol. 23, pp. 3371-3385, 2013.

[14]   C. W. Nan, M. I. Bichurin, S. Dong, D. Viehland, and G. Srinivasan, "Multiferroic magnetoelectric composites: Historical perspective, status, and future directions," *Journal of Applied Physics,* vol. 103, 2008.

[15]   M. Q. Le, F. Belhora, A. Cornogolub, P. J. Cottinet, L. Lebrun, and A. Hajjaji, "Enhanced magnetoelectric effect for flexible current sensor applications," *Journal of Applied Physics,* vol. 115, 2014.

[16]   L. Zhang, S. Wing Or, C. Ming Leung, and S. L. Ho, "DC magnetic field sensor based on electric driving and magnetic tuning in piezoelectric/magnetostrictive bilayer," *Journal of Applied Physics,* vol. 115, 2014.

[17]   Y. K. Fetisov, D. A. Burdin, D. V. Chashin, and N. A. Ekonomov, "High-sensitivity wideband magnetic field sensor using nonlinear resonance magnetoelectric effect," *IEEE Sensors Journal,* vol. 14, pp. 2252-2256, 2014.

[18]   J. Zhang, P. Li, Y. Wen, and X. Huang, "A coil-free dc magnetic sensor utilizing magneto-mechanical damping in giant magnetostrictive material," in *Proceedings of IEEE Sensors*, 2011, pp. 526-529.

[19]   I. N. Soloviev, M. I. Bichurin, and R. V. Petrov, "Magnetoelectric magnetic field sensors," in *Progress in Electromagnetics Research Symposium*, 2012, pp. 1359-1362.

[20]   L. Zhang, S. W. Or, and C. M. Leung, "Voltage-mode direct-current magnetoelectric sensor based on piezoelectric-magnetostrictive heterostructure," *Journal of Applied Physics,* vol. 117, 2015.

[21]   P. Martins, A. Lasheras, J. Gutierrez, J. M. Barandiaran, I. Orue, and S. Lanceros-Mendez, "Optimizing piezoelectric and magnetoelectric responses on CoFe2O4/P(VDF-TrFE) nanocomposites," *Journal of Physics D: Applied Physics,* vol. 44, 2011.

[22]   D. Guyomar, D. F. Matei, B. Guiffard, Q. Le, and R. Belouadah, "Magnetoelectricity in polyurethane films loaded with different magnetic particles," *Materials Letters,* vol. 63, pp. 611-613, 2009.

[23]   J. Zhai, S. Dong, Z. Xing, J. Li, and D. Viehland, "Giant magnetoelectric effect in Metglas/polyvinylidene-fluoride laminates," *Applied Physics Letters,* vol. 89, 2006.

[24]   C. W. Nan, M. Li, X. Feng, and S. Yu, "Possible giant magnetoelectric effect of ferromagnetic rare-earth-iron-alloys-filled ferroelectric polymers," *Applied Physics Letters,* vol. 78, pp. 2527-2529, 2001.

[25]   M. P. Silva, P. Martins, A. Lasheras, J. Gutiérrez, J. M. Barandiarán, and S. Lanceros-Mendez, "Size effects on the magnetoelectric response on PVDF/Vitrovac 4040 laminate composites," *Journal of Magnetism and Magnetic Materials,* vol. 377, pp. 29-33, 2015.

[26]   J. Fraden, "Sensor Characteristics," in *Handbook of modern sensors: Physics, designs, and applications*, ed: Springer, 2016, pp. 13-36.

[27]   P. Martins, X. Moya, L. C. Phillips, S. Kar-Narayan, N. D. Mathur, and S. Lanceros-Mendez, "Linear anhysteretic direct magnetoelectric effect in Ni 0.5Zn0.5Fe2O4/poly(vinylidene   fluoride-trifluoroethylene)   0-3 nanocomposites," *Journal of Physics D: Applied Physics,* vol. 44, 2011.

[28]   L. Rovati and S. Cattini, "Zero-field readout electronics for planar fluxgate sensors without compensation coil," *IEEE Transactions on Industrial Electronics,* vol. 59, pp. 571-578, 2012.

[29]   Z. P. Xing, J. Y. Zhai, S. X. Dong, J. F. Li, D. Viehland, and W. G. Odendaal, "Modeling and detection of quasi-static nanotesla magnetic field variations using magnetoelectric laminate sensors," *Measurement Science and Technology,* vol. 19, 2008.

[30]   X. Zhuang, M. T. Yang, M. L. C. Sing, C. Dolabdjian, P. Finkel, J. Li*, et al.*, "Tunable Magnetoelectric Bending Resonance for Sensing Static Magnetic Fields," *IEEE Sensors Journal,* vol. 16, pp. 662-669, 2016.

[31]   Y. J. Wang, J. Q. Gao, M. H. Li, Y. Shen, D. Hasanyan, J. F. Li*, et al.*, "A review on equivalent magnetic noise of magnetoelectric laminate sensors," *Philosophical*

Transactions of the Royal Society A: Mathematical, Physical and Engineering Sciences, vol. 372, 2014.

[32] H. Zhang, C. Lu, C. Xu, Y. Xiao, J. Gui, C. Lin*, et al.*, "Improved magnetoelectric effect in magnetostrictive/piezoelectric composite with flux concentration effect for sensitive magnetic sensor," *AIP Advances,* vol. 5, 2015.

[33] J. Jin, S. G. Lu, C. Chanthad, Q. Zhang, M. A. Haque, and Q. Wang, "Multiferroic polymer composites with greatly enhanced magnetoelectric effect under a low magnetic bias," *Advanced Materials,* vol. 23, pp. 3853-3858, 2011.

[34] P. Martins, A. C. Lopes, and S. Lanceros-Mendez, "Electroactive phases of poly(vinylidene fluoride): Determination, processing and applications," *Progress in Polymer Science,* vol. 39, pp. 683-706, 2014.

[35] J. Karki, "Signal Conditioning Piezoelectric Sensors," Texas Instruments2000.

[36] E. Bartolome, "Signal conditioning for piezoelectric sensors," Texas Instruments2010.

[37] S. Nappini, T. Al Kayal, D. Berti, B. Nord Èn, and P. Baglioni, "Magnetically triggered release from giant unilamellar vesicles: Visualization by means of confocal microscopy," *Journal of Physical Chemistry Letters,* vol. 2, pp. 713-718, 2011.

[38] "Precision AC/DC Converters," National Semiconductor1969.

[39] J. G. Rocha, *Mosfets and Operational Amplifiers - Theory and Applications.* Porto: Netmove, 2005.

[40] R. Bergs, R. A. Islam, M. Vickers, H. Stephanou, and S. Priya, "Magnetic field anomaly detector using magnetoelectric composites," *Journal of Applied Physics,* vol. 101, 2007.

[41] J. Gao, D. Gray, Y. Shen, J. Li, and D. Viehland, "Enhanced dc magnetic field sensitivity by improved flux concentration in magnetoelectric laminates," *Applied Physics Letters,* vol. 99, 2011.
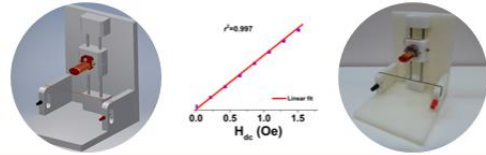
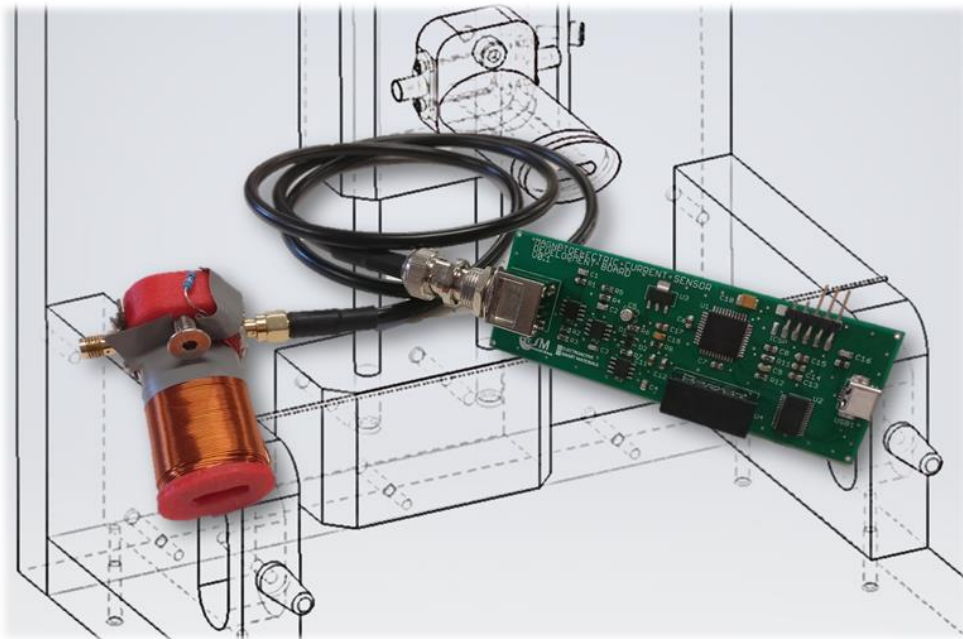# 7 Development of a dc current sensor with high linearity and sensitivity based on the magnetoelectric effect

A dc current sensor based on a magnetoelectric PVDF/Metglas composite, a solenoid and the corresponding electronic instrumentation was developed. With the incorporation of a charge amplifier, a precision ac/dc converter and a microcontroller, the linearity is maintained, the ME output voltage and the sensitivity increase.

7.1   Introduction

Current sensors are widely used in houses, cars and industrial applications. They are essential for protection and control of motors, pumps and overcurrent protectors. Furthermore, they take an important role in production, conversion and energy storage [1, 2]. Such sensors can be classified based upon the underlying fundamental physical principle: Ohm's law of resistance sensors, Faraday's law of induction sensors, magnetic field sensors or Faraday effect sensors [3]. The most commonly used current sensor is the shunt resistor, which is based on Ohm's law. Its simplicity and ability to measure both AC and DC currents are the main advantages of this kind of sensor, however it must be introduced into the current conducting wire, which may generate substantial power loss. Other widely used current sensor is the current transformer, based on Faraday's law of induction. This sensor provides electrical isolation between the measured current and the output signal, but it is unable of measuring DC currents [3]. Moreover in the traditional approaches for current sensing such as ring-type [4] or close magnetic circuit type [5] sensors, the conducting wire should pass through the centre of the ring or the sensor needs to be inserted in series, forcing the wire to be disconnected. These facts lead to complicated measurement procedures.

Magnetic field sensors represent an increasingly attractive alternative for current sensing, being able to sense static and dynamic magnetic fields and ensure the isolation from the current being measured [1, 3]. Hall effect sensors are the most popular and widely used magnetic current sensor mainly due to their compatibility with microelectronic devices [6]. Nonetheless, it has relevant drawbacks such as an offset voltage, which may vary with supply voltage, temperature and stress. In this way, additional circuitry for offset reduction, temperature compensation and signal amplification are required, being the power consumption of these sensors between 100 and 200 mW [6-8]. Anisotropic magnetoresistance (AMR) and giant magnetoresistance (GMR) sensors are also used as magnetic current sensors, where the electrical resistance varies as a function of the magnetic field. They are much more sensitive than Hall effect sensor, in particular the GMR sensors, but need to be configured within a Wheatstone bridge configuration [3]. The main problems of AMR sensors are related to high thermal drift and non-linearity. GMR sensors also exhibit a non-linear behaviour, high dependence with temperature and no stable hysteresis. However, for GMR sensor there

is no "geometric trick" to reduce the non-linearity, such as for AMR sensors, which can be arranged in a barber-pole configuration to overcome this problem. Furthermore a very strong magnetic field can permanently modify the sensor behaviour and damage the GMR sensor [1, 9].

With the potential to solve the abovementioned sensing problems, magnetoelectric (ME) composites have drawn increasing interest in the development of innovative current sensors [10, 11].

Among the different ME composite structures, laminated composites, comprising bonded piezoelectric and magnetostrictive layers, are the ones with the highest ME response, thus being the most suitable materials for sensor development [12]. In such ME laminates, the ME effect results from the cross interaction between the piezoelectric and magnetostrictive phases. It is an extrinsic effect, which depends on the composite microstructure and occur via the elastic coupling of the phases [13, 14]. ME current sensors are based on the Ampère's law: when an electric current is applied to an electrical conductor, a magnetic field (equation 7.1) is induced given by [15]:

$$\vec{H} = \frac{\mu \vec{I}}{2\pi r}$$
(7.1)

where $\vec{H}$ is the magnetic field, $\vec{I}$ is the electric current and r the distance.

As these current sensors are based on magnetic sensing, they possess the advantages such as non-contact measurement aptitude and the ability to measure ac and dc currents [14, 16]. Some pioneering work in ME current sensors have been carried out based on ME composites [4, 16], however, until now, all those reports use a ceramic piezoelectric phase, which is rigid, fragile and shows high dielectric losses, hindering applicability [10, 13]. Actual industry demands for flexible, non-brittle and cheap materials with low temperature fabrication process, can be met by polymer-based ME composites [13].

In this way, this work reports on the development of a current sensor fabricated from a polymer-based ME laminate based on Metglas and poly(vinylidenefluoride) (PVDF), combined with an electronic circuit to process the acquired signal. The latter is composed by a charge amplifier, a precision ac/dc converter and a microcontroller. The selection of the Metglas/PVDF composite is related to the fact that this combination provide the highest ME response and magnetic sensitivity among polymer-based ME materials [13]. Furthermore, Metglas shows high sensitivity, low noise, high magnetic permeability and high piezomagnetic coefficient [17] and PVDF shows the highest piezoelectric coefficient among polymers, chemical stability, flexibility, large electrical resistivity and low

dielectric losses [18, 19]. As the signal generated by the ME composite is in the form of a charge variation, and susceptible to noise, a charge amplifier was used to decrease such noise and convert the signal into a voltage signal, amplifying the initial amplitude and filtering lower frequency noise [20, 21].

7.2 Experimental

7.2.1 Magnetoelectric composite fabrication

The polymer-based ME laminate was produced by bonding both PVDF and Metglas layers with M-Bond 600 epoxy (Vishay Precision Group) under vacuum, using the vacuum bagging technique [22], during 3 hours at 50 ºC [23]. The ME laminate structure was composed by a piezoelectric layer of a commercial β-PVDF (Measurement Specialties, USA) with dimensions of 10 mm × 30 mm × 52 μm, poled along the thickness direction (piezoelectric coefficient d_{33} = −33 pC·N^{-1}), and a magnetostrictive layer of Metglas (2605SA1, Hitachi Metals Europe GmbH, Germany) with dimensions of 5 mm × 27 mm × 25 μm, magnetized along the longitudinal direction (magnetostrictive coefficient λ = 30 ppm).

7.2.2 Characterization

Magnetoelectric response characterization was performed in a system composed by two Helmholtz coils in order to generate a dc magnetic field (H_{dc}) ranging from 0 Oe to 22 Oe, via a dc input current (Keithley 2400), and a superimposed ac magnetic field (H_{ac}) of 0.3 Oe produced via an ac current (Agilent 33220A signal generator). Samples were characterized by measuring the induced voltage in the piezoelectric layer as a result of the magnetic field variation. Since the ME laminates are susceptible to electromagnetic noise, a lock-in amplifier (Stanford Research SR530) was used to filter the ME signal through a narrow band-pass filter.

To find the electromechanical resonance frequency of the sample, H_{dc} and H_{ac} values were kept constant (3.45 Oe and 0.3 Oe, respectively) and the frequency was varied from 1 kHz to 60 kHz. The optimum H_{dc} was achieved by maintaining the H_{ac} and frequency values constant (0.3 Oe and 28.4 kHz, respectively). The ME coefficient (α_{33}) was calculated based on equation 7.2:

$$\alpha_{33} = \frac{\Delta V}{t \cdot H_{ac}} \tag{7.2}$$

where ΔV, t and H_{ac} are the induced ME voltage, the PVDF thickness and the applied ac magnetic field value, respectively.

The device current sensing experiments were performed in a system composed by the ME laminate, a sample holder with a solenoid in order to generate a H_{ac} of 1 Oe, and the electronic readout system (Figure 7.1a). In order to simulate real conditions, a copper wire was used in which a dc current (I_{dc}) was applied ranging from 0 A to 5 A (Figure 7.1b), the induced field being calculated by equation 7.1. The system also allows the control of the distance between current sensor and the current wire.
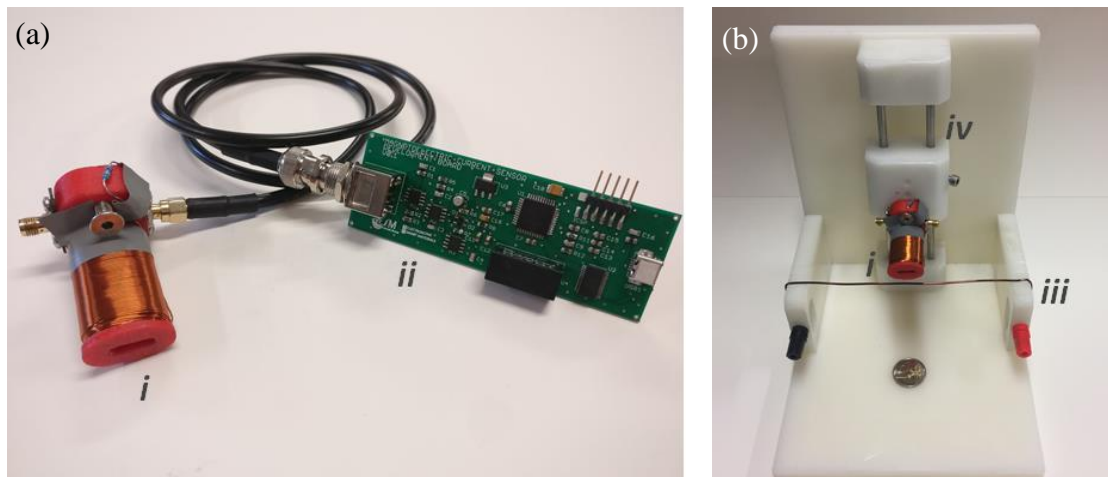
Figure 7.1. (a) ME laminate inside a sample holder with a solenoid (*i*) and electronic readout circuit of the sensing device (*ii*). (b) Sensor testing bench composed by a copper wire (*iii*) used to apply the testing current and a moving system (*iv*) allowing the precise control of distance between current sensor and the copper wire.

The purpose of the sensor is to measure the I_{dc} in the conductor wire. Having a charge response signal from the piezoelectric layer, the implemented electronic instrumentation solution (Figure 7.2) has three conversion stages, a charge amplifier, a precision ac–dc converter, and an analog-to-digital converter (ADC) and communication module, based on the readout circuit presented in [24] (see also chapters 6.2.2 and 6.2.3).
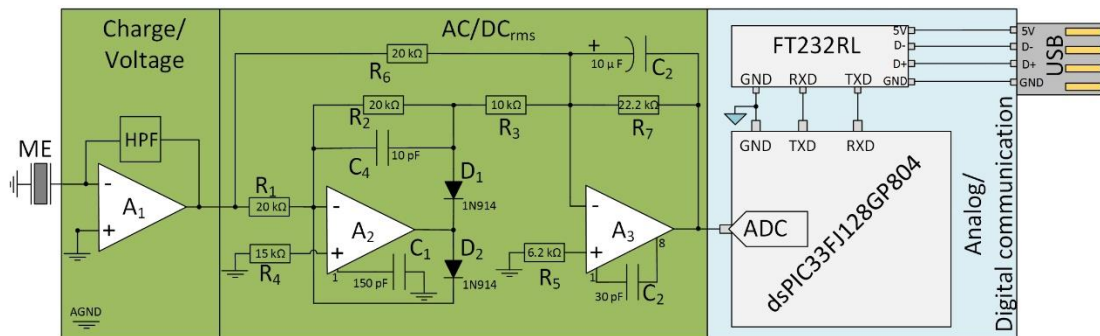
Figure 7.2. Analog and digital components of the developed electronic circuit composed by an charge to voltage converter, a precision ac to dc converter, an analog to digital converter and serial communication.

Initially the ME composite is connected to the circuit through a bayonet Neill–Concelman (BNC) connection in order to be solid grounded and for noise attenuation improvement [25]. The composite piezoelectric response requires a charge amplification step, where the charge is converted to voltage, with a gain given by equation 7.3, and filtered, with a cut-off frequency given by equation 7.4, in order to attenuate the mains frequency. The HPF (high pass filter) component, in the feedback loop of A1 (MCP6021) as shown in Figure 7.2, is composed by a resistor (R_f) and capacitor (C_f) in parallel. The values selected for C_f and R_f were 4.7 pF and 2 MΩ, respectively.

$$Gain = \frac{1}{C_f} (mV/C) \tag{7.3}$$

$$f_{HPF} = \frac{1}{2\pi R_f C_f} \tag{7.4}$$

In the second, stage a precision full-wave rectifier was used to convert the ac ME amplified signal to its rms value. Precision rectifiers are important circuits for signal processing, conditioning and instrumentation of low-level signals, resolving the problems of diode-only rectifiers, which are limited by the threshold voltages of diodes, approximately 0.3 V for germanium diodes and 0.7 V for silicon ones [26]. The incorporation of the diode in the feedback loop of an operational amplifier is extremely effective and can rectify signals having amplitudes of a few millivolts [27]. The circuit was implemented as it is suggested in [24] using for A2 and A3 LM301 amplifiers.

The third stage represents the ADC to serial port conversion, with the use of a dsPIC33FJ128GP804 microcontroller and a FT232RL – universal asynchronous receiver/transmitter (UART) to universal serial bus (USB) – to send the data to a computational terminal, where it is treated and properly presented [24].

In order to avoid high frequency digital transitions noise the analog ground (AGND) and digital ground (GND) were used to improve signal stability, as it is displayed in Figure 7.2.

The sensitivity was determined through the ratio between the minimum voltage variation divided by the electric current value at the minimum voltage variation.

7.3 Results and Discussion

The ME composite sample was characterized in terms of resonant frequency, signal amplitude and magnetic field range. Figure 7.3 illustrates the ME sample response to H_{dc} and H_{ac} variations.
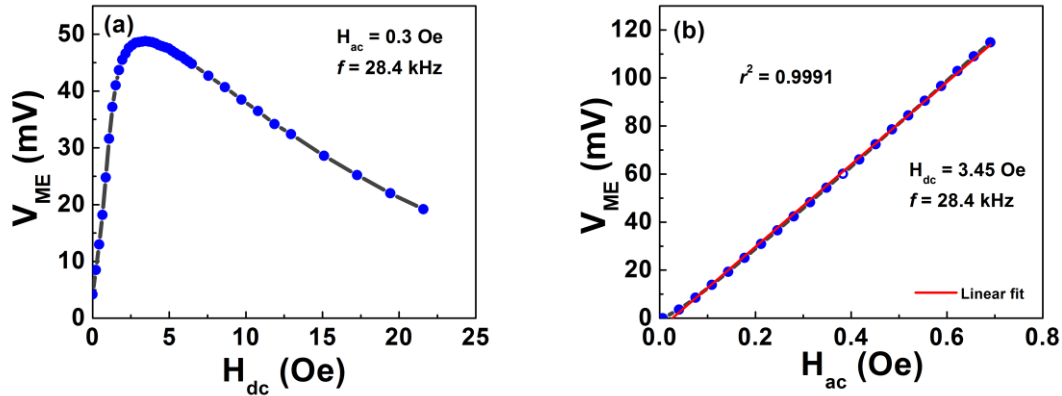
Figure 7.3. (a) ME sample output response as a function of the H_{dc}, setting the H_{ac} to 0.3 Oe at resonance frequency of 28.4 kHz; (b) ME sample output response as a function of the H_{ac}, setting the H_{dc} to 3.45 Oe and a frequency of 28.4 kHz.

Figure 7.3a shows that the ME voltage increases with increasing applied H_{dc} until 3.45 Oe when a maximum ME output voltage of 48.8 mV is reached. A maximum ME coefficient (α_{33} – determined from equation 7.1) of 31.28 $V \cdot cm^{-1} \cdot Oe^{-1}$ is obtained for such dc magnetic field. This behaviour is related with the increase of the piezomagnetic coefficient until the optimum dc magnetic field is reached [23]. With further increase of the dc magnetic field, a decrease of the induced voltage is observed, resulting from the saturation of the magnetostrictive response. Figure 7.3b shows that the ME output voltage increases linearly with increasing applied H_{ac} until 0.7 Oe when a maximum ME output voltage of 114.8 mV is reached. This linearity (r^2=0.9991) is a suitable advantage for the use of these composites for sensor devices.

In order to obtain the sample signal to be read by an ADC, the charge signal generated by the PVDF/Metglas sample will be converted to voltage by the use of a charge amplifier. Once the signal variations over time are small and the motivation of the present work is a dc current sensor, the ac voltage signal will be coupled to an ac–rms converter, establishing a ME dc signal and reducing the sampling speed requirements. After that, the response of the ME device sensor (sample + electronic components) as a function of the I_{dc} can be evaluated (Figure 7.4), in order to validate the ME current sensor based on

the ME effect. The results will be compared with the ones obtained for the composite samples.
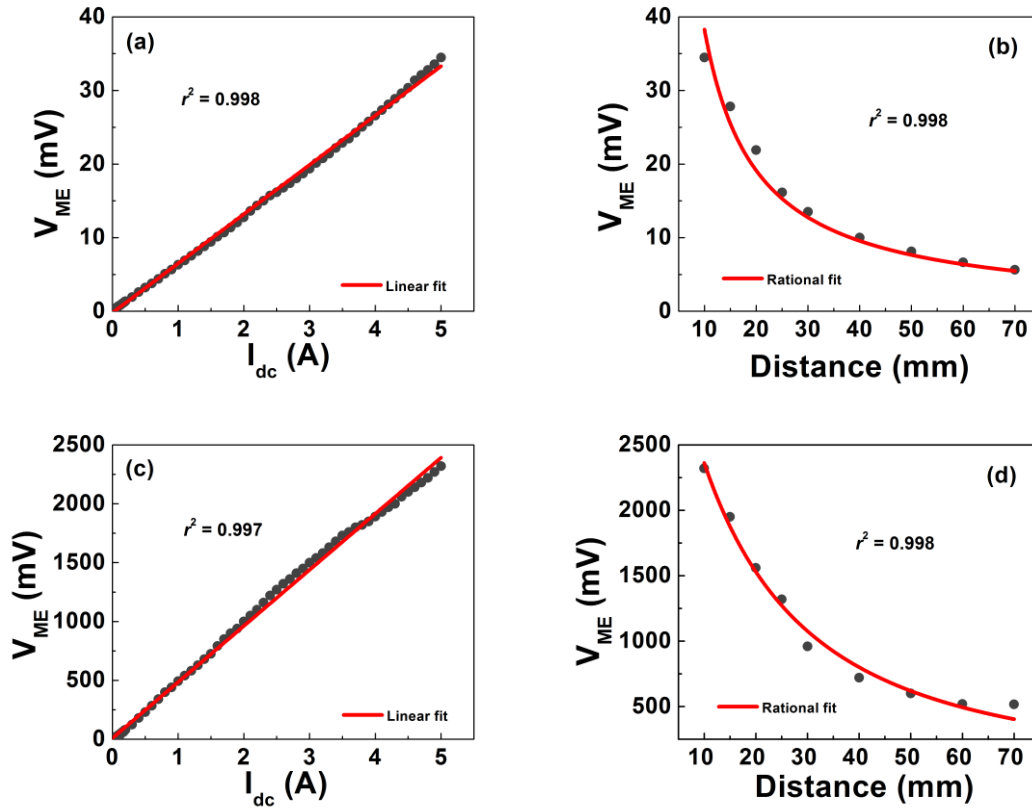
Figure 7.4. (a) ME voltage response of the composite in the range $0 < I_{dc} < 5$ A, applying a H_{ac} of 1 Oe at 26.1 kHz; (b) ME voltage response of the composite as a function of the distance between the wire and the sensor device (from 10 mm to 70 mm); (c) ME voltage response of the final device in the range $0 < I_{DC} < 5$ A, applying a H_{ac} of 1 Oe at 26.1 kHz; (d) ME voltage response of the final device as a function of the distance between the wire and the sensor device (from 10 mm to 70 mm). The fittings on the left correspond to $f(x) = 1/x$.

Figure 7.4a demonstrates that the ME response of the composite sample increases with increasing I_{dc} current up to 5 A, at which the maximum ME voltage is reached (34.48 mV). Such low current range was chosen to test the device sensor in the worst magnetic field conditions, once for higher electric currents the induced magnetic field will be more intense (equation 7.1). The sample exhibits a sensitivity of 6.7 mV·A^{-1} and a linear behaviour between 0 and 5 A (r^2=0.998). Figure 7.4b reveals that the ME voltage decreases with the distance from the wire (34.48 mV to 5.63 mV).

Figure 7.4c and Figure 7.4d reveal an increase of the ME voltage response to a maximum of 2320 mV after the electronic amplification and the signal conditioning circuit has been implemented. By fitting a function ($f(x)=1/x$) to the voltage *vs* distance curves, explained by the relation between H_{dc} and I_{dc} (equation 7.1), it is observed a good

correlation squared coefficient (r^2=0.998). After the electronic amplification, the linearity is maintained (r^2=0.997), and the sensitivity increased two orders of magnitude (476.5 mV·A^{-1}), being among the best reported in the literature and the highest values reported on ME materials (Table 7.1).

Table 7.1. Current sensor characteristics as obtained in this work, and a comparison with other recent related sensors using different technologies.

Technology	Materials	Linearity (r^2)	Sensitivity (mV·A^{-1})	Ref.
AMR	Permalloy	0.99	13.3	[28]
GMR	GMR chip	0.993	285	[29]
		0.9997	28	[30]
Hall	Hall chip	0.988	45	[31]
Shear transducer	Cymbal transducer	0.995	7	[32]
ME (ceramic)	Metglas/PZT	-	114	[33]
		-	340	[34]
ME (polymer)	Metglas/PVDF	0.997	476.5	Ours

In this way, the implementation of an amplifier with an optimized power supply rejection ratio does not influences the good linearity and increases the sensitivity of the original signal produced by the ME composite sample. Thereby it is concluded that, for this current range, the developed ME sensor has a large potential for actual current sensing due to its linearity and sensitivity.

7.4   Conclusions

The development of a dc current sensor composed by a Metglas/PVDF ME composite as an active sensing element is reported. An electronic instrumentation solution was also employed through the use of three conversion stages, a charge amplifier, a precision ac–dc converter, and an ADC and communication module.

It was found that the maximum V_{ME} occurs at 3.45 H_{dc} and a maximum α_{33} of 31.28 V·cm^{-1}·Oe^{-1} has been found for such H_{dc}.

After the incorporation of the electronic amplification circuit, the linearity is maintained (r^2=0.997) and the sensitivity increased from 6.7 mV·A^{-1} to 476.5 mV·A^{-1}. It is also found that the V_{ME} response decreases with increasing distance from 10 mm to 70 mm: from 34.48 mV to 5.63 mV and from 2320 mV to 517 mV for the sensor without electronic instrumentation and with electronic instrumentation, respectively.

It is concluded that, for this current range, the fabricated ME sensor device shows suitable characteristics to be applied in current sensing applications, in particular in multifunctional flexible devices once it has a good output linearity and the highest sensitivity reported in the literature for polymer-based composites

7.5 References

[1]   P. Ripka, "Electric current sensors: A review," *Measurement Science and Technology,* vol. 21, 2010.

[2]   C. Xiao, L. Zhao, T. Asada, W. G. Odendaal, and J. D. Van Wyk, "An Overview of Integratable Current Sensor Technologies," in *Conference Record - IAS Annual Meeting (IEEE Industry Applications Society)*, 2003, pp. 1251-1258.

[3]   S. Ziegler, R. C. Woodward, H. H. C. Iu, and L. J. Borle, "Current sensing techniques: A review," *IEEE Sensors Journal,* vol. 9, pp. 354-376, 2009.

[4]   S. Dong, J. F. Li, and D. Viehland, "Vortex magnetic field sensor based on ring-type magnetoelectric laminate," *Applied Physics Letters,* vol. 85, pp. 2307-2309, 2004.

[5]   J. Zhang, P. Li, Y. Wen, W. He, A. Yang, C. Lu*, et al.*, "High-resolution current sensor utilizing nanocrystalline alloy and magnetoelectric laminate composite," *Review of Scientific Instruments,* vol. 83, 2012.

[6]   R. S. Popovic, Z. Randjelovic, and D. Manic, "Integrated Hall-effect magnetic sensors," *Sensors and Actuators, A: Physical,* vol. 91, pp. 46-50, 2001.

[7]   A. L. Herrera-May, L. A. Aguilera-Cortés, P. J. García-Ramírez, and E. Manjarrez, "Resonant magnetic field sensors based on MEMS technology," *Sensors,* vol. 9, pp. 7785-7813, 2009.

[8]   S. Reis, M. P. Silva, N. Castro, V. Correia, J. Gutierrez, A. Lasheras*, et al.*, "Optimized anisotropic magnetoelectric response of Fe61.6Co16.4Si10.8B11.2/PVDF/Fe61.6Co16.4Si10.8B11.2 laminates for AC/DC magnetic field sensing," *Smart Materials and Structures,* vol. 25, 2016.

[9]   A. Bernieri, G. Betta, L. Ferrigno, and M. Laracca, "Improving performance of gmr sensors," *IEEE Sensors Journal,* vol. 13, pp. 4513-4521, 2013.

[10]   M. Q. Le, F. Belhora, A. Cornogolub, P. J. Cottinet, L. Lebrun, and A. Hajjaji, "Enhanced magnetoelectric effect for flexible current sensor applications," *Journal of Applied Physics,* vol. 115, 2014.

[11]   R. V. Petrov, N. V. Yegerev, G. A. Semenov, V. M. Petrov, M. I. Bichurin, and S. Aleksic, "Current sensor based on magnetoelectric effect," in *2014 18th International Symposium on Electrical Apparatus and Technologies, SIELA 2014 - Proceedings*, 2014.

[12]   S. Reis, M. P. Silva, N. Castro, V. Correia, P. Martins, A. Lasheras*, et al.*, "Characterization of Metglas/poly(vinylidene fluoride)/Metglas magnetoelectric laminates for AC/DC magnetic sensor applications," *Materials and Design,* vol. 92, pp. 906-910, 2016.

[13]   P. Martins and S. Lanceros-Méndez, "Polymer-based magnetoelectric materials," *Advanced Functional Materials,* vol. 23, pp. 3371-3385, 2013.

[14]   C. W. Nan, M. I. Bichurin, S. Dong, D. Viehland, and G. Srinivasan, "Multiferroic magnetoelectric composites: Historical perspective, status, and future directions," *Journal of Applied Physics,* vol. 103, 2008.

[15] J. T. Zhang, Y. M. Wen, and P. Li, "A passive current sensor employing self-biased magnetoelectric transducer and high-permeability nanocrystalline flux concentrator," *Rare Metals,* 2015.

[16] S. Dong, J. G. Bai, J. Zhai, J. F. Li, G. Q. Lu, D. Viehland*, et al.*, "Circumferential-mode, quasi-ring-type, magnetoelectric laminate composite-a highly sensitive electric current andor vortex magnetic field sensor," *Applied Physics Letters,* vol. 86, pp. 1-3, 2005.

[17] J. Zhai, S. Dong, Z. Xing, J. Li, and D. Viehland, "Giant magnetoelectric effect in Metglas/polyvinylidene-fluoride laminates," *Applied Physics Letters,* vol. 89, 2006.

[18] P. Martins, A. C. Lopes, and S. Lanceros-Mendez, "Electroactive phases of poly(vinylidene fluoride): Determination, processing and applications," *Progress in Polymer Science,* vol. 39, pp. 683-706, 2014.

[19] M. P. Silva, G. Botelho, J. G. Rocha, and S. Lanceros-Mendez, "Stability of the electroactive response of β-poly(vinylidene fluoride) for applications in the petrochemical industry," *Polymer Testing,* vol. 29, pp. 613-615, 2010.

[20] Z. P. Xing, J. Y. Zhai, S. X. Dong, J. F. Li, D. Viehland, and W. G. Odendaal, "Modeling and detection of quasi-static nanotesla magnetic field variations using magnetoelectric laminate sensors," *Measurement Science and Technology,* vol. 19, 2008.

[21] X. Zhuang, M. T. Yang, M. L. C. Sing, C. Dolabdjian, P. Finkel, J. Li*, et al.*, "Tunable Magnetoelectric Bending Resonance for Sensing Static Magnetic Fields," *IEEE Sensors Journal,* vol. 16, pp. 662-669, 2016.

[22] Y. Shen, J. Gao, Y. Wang, J. Li, and D. Viehland, "High non-linear magnetoelectric coefficient in Metglas/PMN-PT laminate composites under zero direct current magnetic bias," *Journal of Applied Physics,* vol. 115, 2014.

[23] M. Silva, S. Reis, C. S. Lehmann, P. Martins, S. Lanceros-Mendez, A. Lasheras*, et al.*, "Optimization of the magnetoelectric response of poly(vinylidene fluoride)/epoxy/vitrovac laminates," *ACS Applied Materials and Interfaces,* vol. 5, pp. 10912-10919, 2013.

[24] S. Reis, N. Castro, M. P. Silva, V. Correia, J. G. Rocha, P. Martins*, et al.*, "Fabrication and characterization of high-performance polymer-based magnetoelectric DC Magnetic Field sensors devices," *IEEE Transactions on Industrial Electronics,* 2017.

[25] W. Zahlit, M. Schwartz, and D. Reed, "The BNC's continuing evolution - It just keeps getting better," *Connector Specifier,* vol. 20, pp. 16-18, 2004.

[26] S. Djukić, M. Vesković, and A. Vulović, "An improved precision full-wave rectifier for low-level signal," in *2010 9th International Symposium on Electronics and Telecommunications, ISETC'10 - Conference Proceedings*, 2010, pp. 33-38.

[27] S. J. G. Gift, "New precision rectifier circuits with high accuracy and wide bandwidth," *International Journal of Electronics,* vol. 92, pp. 601-617, 2005.

[28] Z. Zhenhong, O. Syuji, A. Osamu, and K. Hideto, "Development of the highly precise magnetic current sensor module of +/-300 a utilizing AMR element with bias-magnet," *IEEE Transactions on Magnetics,* vol. 51, 2015.

[29] X. Yang, H. Liu, Y. Wang, Y. Wang, G. Dong, and Z. Zhao, "A giant magneto resistive (GMR) effect based current sensor with a toroidal magnetic core as flux concentrator and closed-loop configuration," *IEEE Transactions on Applied Superconductivity,* vol. 24, 2014.

[30]   Y. Ouyang, J. He, J. Hu, and S. X. Wang, "A current sensor based on the giant magnetoresistance effect: Design and potential smart grid applications," *Sensors (Switzerland),* vol. 12, pp. 15520-15541, 2012.

[31]   X. Cheng, Z. Sun, X. Wang, and S. Liu, "Open-loop linear differential current sensor based on dual-mode Hall effect," *Measurement: Journal of the International Measurement Confederation,* vol. 50, pp. 29-33, 2014.

[32]   W. He, Y. Lu, C. Qu, and J. Peng, "A non-invasive electric current sensor employing a modified shear-mode cymbal transducer," *Sensors and Actuators, A: Physical,* vol. 241, pp. 120-123, 2016.

[33]   C. Lu, P. Li, Y. Wen, A. Yang, C. Yang, D. Wang, *et al.*, "Magnetoelectric composite metglas/PZT-based current sensor," *IEEE Transactions on Magnetics,* vol. 50, 2014.

[34]   R. V. Petrov, I. N. Solovyev, A. N. Soloviev, and M. I. Bichurin, "Magnetoelectric current sensor," in *Progress in Electromagnetics Research Symposium*, 2013, pp. 105-108.
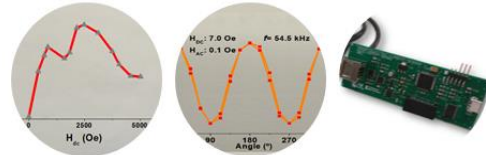
8   Final considerations, conclusions and future work

This chapter presents the final considerations of polymer-based ME sensors and materials upscaling, summarizes the main conclusions and provides some suggestions for future work.
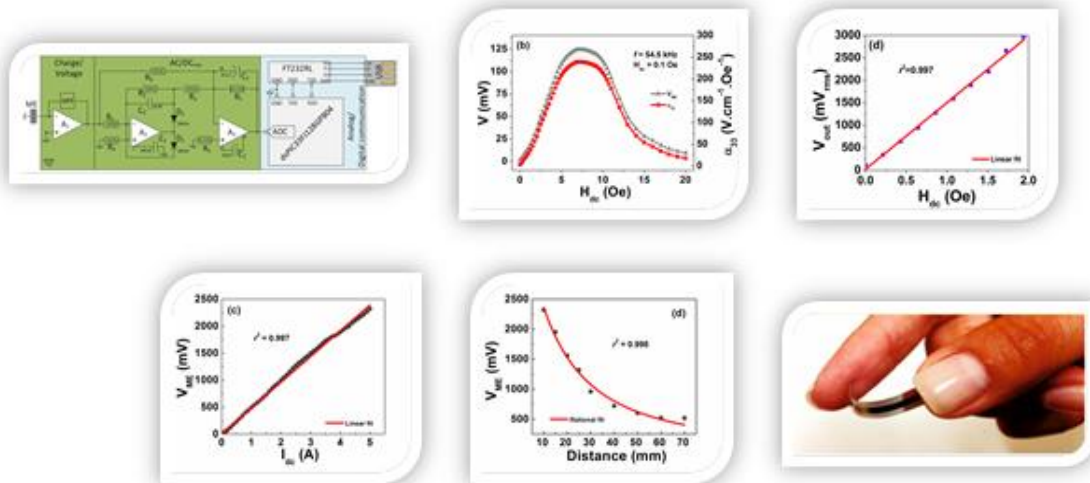
8.1 Final considerations

Magnetoelectric (ME) materials continue to be a scientific research topic with increasing interest. In particular, polymer-based ME materials are expected to make a difference in the area of smart materials. When compared to single-phase or ceramic ME materials, polymer-based ME materials are easier to integrate on a chip and typically involve a low-temperature fabrication process, moreover, they are flexible, able to be processed in complex shapes, and their interfaces can be controlled to enhance ME coupling or to add new functionalities [1, 2].

The work developed in this thesis demonstrate the viability of these materials as magnetic field and current sensors. Further, due to the simplicity of the sensors fabrication and working principle, it is possible to think about developing new sensors or applications. The viability for device applications of laminate composites and nanocomposites has been proven. Both configurations, each one with their qualities and limitations, are now ready for the challenges of technological applications. Laminate ME composites exhibit the higher ME response, within polymer-based ME materials, nonetheless, particulate nanocomposites provide other advantages such as cost effectiveness, easy fabrication process, better process parameters control, and fabrication of large volumes with a good reproducibility [2]. A poly(vinylidene fluoride) (PVDF)/Metglas ME laminate composite shows a ME coefficient $\alpha_{31} = 238$ V·O^{-1}·cm^{-1}, for a unimorph configuration, and $\alpha_{31} = 310$ V·O^{-1}·cm^{-1}, for a three-layer configuration, both at a resonance frequency of 50 kHz and with $H_{dc–max} = 8$ Oe. For lower frequencies a value of $\alpha_{31} = 7.2$ V·O^{-1}·cm^{-1} was obtained on both geometries and for the same $H_{dc–max}$. A ME nanocomposite of poly(vinylidene fluoride-trifluoroethylene) (P(VDF-TrFE)) and CoFe$_2$O$_4$ shows $\alpha_{33} = 43.1$ mV·O^{-1}·cm^{-1} at the resonance frequency and $\alpha_{33} = 4.1$ mV·O^{-1}·cm^{-1} at non-resonance for a $H_{dc–max} = 2500$ Oe [3].

There is a wide range of potential applications, where polymer-based ME materials can be used: sensors, actuators, filters, antennas, multiple-state memories, and energy harvesting devices. In some of those applications, particulate nanocomposites seem to be more suitable, whereas in other applications laminate composites will be more appropriate. The higher ME response of laminate composites, make them appropriate for sensors and energy harvesting applications. Nanocomposites allow a better process

parameters control, allowing fabricate antennas, memories and high magnetic field sensors with suitably tailored characteristics.

Laminate ME composites allow the development of ac and dc magnetic field sensors, and their anisotropic properties allow to measure both magnitude and direction of the magnetic field vector. As the optimum dc magnetic field of these materials is typically low, they become ideal for geomagnetic field measurements or applications that use the earth magnetic field as reference, such as vehicle detection, navigation, geophysical and archaeological prospection, and magnetic anomaly detectors, among others. The main disadvantage of dc ME field sensors is that they are active sensors, unlike the ac ME field sensors, which are passive.

Current sensors can also be developed using laminate ME composites. These sensors ensure electrical isolation and have the ability to measure ac and dc currents, without the need to disconnect the current conducting wire. This last advantage is particularly relevant, as it eliminates the need of powering-off the system, even in the installation and maintenance of the sensor.

It is expected that laminate ME composites can be useful also in position sensors applications [4]. Linear or angular position of an object, with a linear or an angular movement, can be determined by placing a permanent magnet on it. Likewise, linear or angular speed can be calculated by taking the first derivative of that signal. The level of a liquid is expected that can be measured based on the magnetostrictive delay line (MDL) technique. The sensor should be formed by a magnetoelectric wire and a float with a magnet inside. Appling a current pulse to the ME composite, a vortex magnetic field is created along the wire. When the current pulse reaches the point where the buoy stays, the two magnetic fields interact, resulting in a torsional mechanical wave throughout the conductor, which will be converted into a voltage. The phase shift between the current impulse and the voltage generated indicates the position of the float and, consequently, the liquid level.

Energy harvesting devices are other main application area of polymer-based laminate ME composites. Here the generated ME voltage is the main property, so using a piezoelectric–magnetostrictive–piezoelectric (PMP) configuration [5], or even an array of ME materials connected in series or parallel – to generate more voltage or current, respectively – it is possible to increase the generated ME voltage produced by the ME composite.

Polymer-based ME nanocomposites can take an important role in the miniaturization of antennas, as they allow increase the permittivity and permeability of the materials, which are critical parameter to antennas miniaturization.

Polymer-based ME materials are also playing an important role in biomedical applications. A ME actuator has proven to be useful in tissue engineering, enhancing the cell proliferation by remote stimulation of the tissues, through the application of an external magnetic field. It is also expected that these materials, in the form of new nanostructures, such as spheres, emerge to address targeted and controlled anticancer drug delivery and release [2].

In this work, two distinct types of polymer-based ME materials were studied, characterized and produced. Different materials lead to different applications and methods to produce the desired sensors. The industrial production of a particulate ME nanocomposite is very common and widely used, the technique underlying to this production can be extrusion or injection moulding [6, 7].

A laminate ME composite, which is constituted by two or three active layers, as explained before, can be easily produced in large scale by lamination [8, 9]. This technique consists in successively bounding of multiple layers, and finishes with the cut to obtain the final laminate composite geometry and dimension. This technique is widely used in industry and it is easily adapted to the materials that are used in this type of sensors.

8.2 Conclusions

Polymer-based ME composites proved to be suitable for magnetic field and current sensors applications.

Two magnetoelectric characterization systems, one for being used with high optimum dc magnetic fields and another for low optimum dc magnetic fields, were successfully developed and validated.

Nanocomposite films based on highly magnetostrictive $CoFe_2O_4$ nanoparticles and Terfenol-D microparticles dispersed in a piezoelectric P(VDF-TrFE) matrix, with an overall filler content $\approx$40 wt %, were investigated in order to develop materials that react to a wide range of magnetic field. The developed ME composite showed a double-peak wide-range ME response and a strong ME coupling at room temperature with the ME

coefficient increasing with Terfenol-D content up to 42.3 mV·cm^{-1}·Oe^{-1}, for the sample with 30 wt %.

A magnetic field sensor based on $Fe_{61.6}Co_{16.4}Si_{10.8}B_{11.2}$ (FCSB)/PVDF/FCSB laminates proved to be able to detect both ac and dc magnetic field magnitude and direction, based on the anisotropic ME effect.

The anisotropic ME sensor achieved an accuracy, linearity and sensitivity values for both dc (99% FSO, 92% FSO and 15 mV·Oe^{-1}) and ac (99 %FSO, 99 %FSO and 1400 mV·Oe^{-1}) magnetic field sensing in the order, or even higher, than those of ME magnetic field sensing and conventional magnetic field sensors. Such features, as well as the excellent reproducibility (higher than 99%) and flexibility of the FCSB/PVDF/FCSB sensor make it very attractive for the magnetic field sensing industry.

A magnetic field sensor, formed by a PVDF/Metglas ME composite as an active sensing element, a charge amplifier, an ac–rms converter, and a microcontroller with an on-chip analog-to-digital converter (ADC), was developed. It was found a linear response (r^2=0.997) in the 0–2 Oe dc magnetic field range and a maximum output voltage of 3.3 V ($\alpha_{33effective}$=1000 V·cm^{-1}·Oe^{-1}). The developed device achieves a sensitivity of 1.5 V·Oe^{-1}, suitable for magnetic sensing devices such as digital compasses or positioning systems, among others.

A dc current sensor composed by a PVDF/Metglas ME composite as an active sensing element was reported. An electronic instrumentation solution was also employed through the use of three conversion stages, a charge amplifier, a precision ac–dc converter, and an ADC and communication module. It was found that the maximum V$_{ME}$ occurs at 3.45 H_{dc} and a maximum α_{33} of 31.28 V·cm^{-1}·Oe^{-1} has been found for such H_{dc}. After the incorporation of the electronic amplification circuit, the linearity is maintained (r^2=0.997) and the sensitivity increased from 6.7 mV·A^{-1} to 476.5 mV·A^{-1}. It is also found that the V$_{ME}$ response decreases with increasing distance from 10 mm to 70 mm: from 34.48 mV to 5.63 mV and from 2320 mV to 517 mV for the sensor without electronic instrumentation and with electronic instrumentation, respectively.

Therefore, sensors based on polymer-based ME materials were successfully developed.

8.3 Future work

This thesis allowed to develop two functional prototypes: a magnetic field sensor and a current sensor. Despite the successful results already obtained, several additional steps are need to bring ME sensors to the industry and the consumer.

Therefore, the ME composites production need to pass from lab to mass-produce fabrication, without losing the accurate control of nanoparticles composition, for nanocomposites, and the quality of the interface between the magnetostrictive phase and the piezoelectric polymer phase, important either in nanocomposites as in laminate composites, but which also depends on the epoxy in laminate composites. Thus, it is important to find the right parameters to mass-produce polymer-based ME materials.

In an age where maximum size reduction is desirable, sensors integration with its noise reduction advantage, is a key issue in the successful implementation of sensors.

Further, the concept of ME sensing has to be extended to other sensors such as position sensors or liquid level sensors, proving their viability.

Finally, it is always good to find new materials with even better characteristics; traditional polymer-based ME composites need simultaneously dc and ac magnetic fields, which complicates the design of sensors, being the development of novel self-biased ME composites, that can be used as ME passive sensors in the absence of a dc magnetic field, a milestone in this research field.

8.4 References

[1]   M. Alnassar, A. Alfadhel, Y. P. Ivanov, and J. Kosel, "Magnetoelectric polymer nanocomposite for flexible electronics," *Journal of Applied Physics,* vol. 117, 2015.

[2]   S. Lanceros-Mendez and P. Martins, "Open questions, challenges and perspectives," in *Magnetoelectric Polymer-Based Composites: Fundamentals and Applications*, S. Lanceros-Mendez and P. Martins, Eds., ed: John Wiley & Sons, Ltd., 2017.

[3]   P. Martins and S. Lanceros-Méndez, "Polymer-based magnetoelectric materials," *Advanced Functional Materials,* vol. 23, pp. 3371-3385, 2013.

[4]   R. V. Petrov, M. I. Bichurin, V. S. Leontiev, N. A. Kolesnikov, I. K. Milenov, S. T. Bozhkov*, et al.*, "The crankshaft position sensor based on magnetoelectric materials," in *Proceedings - 2016 IEEE International Power Electronics and Motion Control Conference, PEMC 2016*, 2016, pp. 848-853.

[5]   M. P. Silva, P. Martins, A. Lasheras, J. Gutiérrez, J. M. Barandiarán, and S. Lanceros-Mendez, "Size effects on the magnetoelectric response on PVDF/Vitrovac 4040 laminate composites," *Journal of Magnetism and Magnetic Materials,* vol. 377, pp. 29-33, 2015.

[6]   R. O. Ebewele, "Unit Operations in Polymer Processing," in *Polymer Science and Technology*, ed: CRC Press, 2000.

[7]   P. G. Lafleur and B. Vergnes, *Polymer Extrusion*, 2014.

[8]   I. Gibson, D. W. Rosen, and B. Stucker, *Additive manufacturing technologies: Rapid prototyping to direct digital manufacturing*: Springer, 2010.

[9]   T. Dunn, "Adhesive and Thermal Lamination," in *Handbook of Troubleshooting Plastics Processes: A Practical Guide*, ed: John Wiley & Sons, Ltd., 2012, pp. 315-330.